UNIVERSIDADE FEDERAL DO CEARÁ
CENTRO DE CIÊNCIAS
PROGRAMA DE PÓS-GRADUAÇÃO EM QUÍMICA

JANEVANE SILVA DE CASTRO

SÍNTESE E APLICAÇÃO DE COMPÓSITO À BASE DE Zn_2SnO_4 NA DETECÇÃO ELETROQUÍMICA DE OFLOXACINO: UM ESTUDO EXPERIMENTAL E TEÓRICO

FORTALEZA
2023

JANEVANE SILVA DE CASTRO

SÍNTESE E APLICAÇÃO DE COMPÓSITO À BASE DE Zn_2SnO_4 NA DETECÇÃO ELETROQUÍMICA DE OFLOXACINO: UM ESTUDO EXPERIMENTAL E TEÓRICO

Tese apresentada ao Programa de Pós-Graduação em Química da Universidade Federal do Ceará, como parte dos requisitos para a obtenção do título de Doutor em Química. Área de concentração: Química Analítica.

Orientadora: Profa. Dra. Adriana Nunes Correia.

FORTALEZA

2023

Dados Internacionais de Catalogação na Publicação
Universidade Federal do Ceará
Sistema de Bibliotecas
Gerada automaticamente pelo módulo Catalog, mediante os dados fornecidos pelo(a) autor(a)

C351s Castro, Janevane Silva de.
Síntese e aplicação de compósito à base de Zn2SnO4 na detecção eletroquímica de ofloxacino: : um estudo experimental e teórico / Janevane Silva de Castro. – 2023.
115 f. : il. color.

Tese (doutorado) – Universidade Federal do Ceará, Centro de Ciências, Programa de Pós-Graduação em Química, Fortaleza, 2023.
Orientação: Profa. Dra. Adriana Nunes Correia.

1. Antibiótico. 2. Contaminante emergente. 3. Estanato de zinco. 4. Óxido de grafeno reduzido. 5. Voltametria de onda quadrada. I. Título.

CDD 540

JANEVANE SILVA DE CASTRO

SÍNTESE E APLICAÇÃO DE COMPÓSITO À BASE DE Zn_2SnO_4 NA DETECÇÃO ELETROQUÍMICA DE OFLOXACINO: UM ESTUDO EXPERIMENTAL E TEÓRICO

Tese apresentada ao Programa de Pós-Graduação em Química da Universidade Federal do Ceará, como requisito parcial à obtenção do título de Doutor em Química. Área de concentração: Química Analítica.

Aprovada em: ____/____/_____.

BANCA EXAMINADORA

_____

Profa. Dra. Adriana Nunes Correia (Orientadora)
Universidade Federal do Ceará (UFC)

_____

Profa. Dra. Andressa Galli
Universidade Estadual do Centro-Oeste (UNICENTRO)

_____

Prof. Dr. Francisco Wirley Paulino Ribeiro
Universidade da Integração Internacional da Lusofonia Afro-Brasileira (UNILAB)

_____

Prof. Dr. Norberto de Kássio Vieira Monteiro
Universidade Federal do Ceará (UFC)

_____

Prof. Dr. Paulo Naftali da Silva Casciano
Universidade Federal do Ceará (UFC)

A Deus.

Aos meus pais, Valder e Judite.

AGRADECIMENTOS

Primeiramente a Deus, por me permitir sair com vida em meio a pandemia do COVID-19, mesmo que com algumas sequelas. Sempre esteve comigo e com toda certeza sem Ele eu não teria conseguido seguir em frente. Muito obrigado pelo dom da vida, pela saúde, pelo teu infinito perdão, por tuas misericórdias, por todas as bençãos, inclusive por mais essa vitória.

Aos meus pais, Valder e Judite, por toda dedicação, amor e carinho a mim concedidos em todos os momentos da minha vida. Nunca esquecerei todos os sacrifícios realizados por ambos, visando proporcionar condições de vida digna e as melhores oportunidades. Que Deus me permita desfrutar por muitos anos de suas presenças, com bastante saúde e muitas alegrias. Minha eterna gratidão e amor a vocês.

À minha filha, Anne Camile, por me compreender em vários momentos os quais tive que abdicar de estar com você a fim de desenvolver essa pesquisa. Te amo, minha eterna filhota. Meu grande legado é você.

À minha esposa, Gabriela Petkevicius, pelo amor, reciprocidade, companheirismo, dedicação e incentivo a mim conferidos. Muito obrigado por ser essa mulher batalhadora, sábia, tranquila, paciente, inteligente, amorosa, resiliente e especialmente por ser a minha amiga mais certa nas horas incertas. Gratidão por você compartilhar a vida comigo.

Aos meus irmãos, Valber e Júnior, pois mesmo traçando caminhos distintos sempre estiveram presentes em minha vida quando se fez necessário. Que possamos cada dia mais nos unir em prol de nossos objetivos individuais e familiares.

Ao meu grande herói, Cauã Emanuel (*in memorian*), por em sua passagem ter me ensinado mesmo que de maneira dolorosa, os valores do tempo e família. Sua ausência física ainda maltrata; a dor da saudade ainda se faz presente, mas acredito que um dia vamos nos reencontrar e nessa era vindoura serão apenas alegrias, brincadeiras e risos... sem hospital, sem choro, sem dor. Te amo meu garoto.

À minha grande orientadora, Prof(a). Dra. Adriana Correia, por ter me acolhido num momento tão difícil da minha vida pessoal e acadêmica; por ter acreditado em minha recuperação e por participar intensamente da realização desse grande sonho. Carrego com muito orgulho a láurea de levar seu distinto nome junto a minha formação acadêmica. A minha "amiga Adriana" externo, imensa gratidão por toda ajuda, compreensão e conselhos pessoais; por ti tenho grande carinho e afeto. Muito obrigado também a "Profa. Dra. Adriana" por todas as

orientações, chamamentos e encaminhamentos; por esta esmerada professora e exímia pesquisadora guardo profundo respeito e admiração.

À banca examinadora, Prof(a). Dra. Andressa Galli, Prof(a). Dra. Djenaine de Souza, Prof. Dr. Francisco Wirley, Prof. Dr. Paulo Naftali, Prof. Dr. Pedro Neto, Prof. Dr. Norberto Kássio e Prof. Dr. Thiago Mielle por todo conhecimento e contribuições, vislumbrando enaltecer ainda mais a qualidade do trabalho desenvolvido.

Ainda aos Prof. Dr. Norberto Kássio, Prof. Dr. Dieric Abreu e Prof. Dr. Pierre Basílio por ter aceitado participar ativamente da execução do trabalho, contribuindo fortemente para a realização dessa conquista.

Ao Prof. Dr. Francisco Wirley, por sua preciosa amizade e pelos seus apoio, conhecimentos e esclarecimentos prestados sempre com solicitude e cordialidade.

À Prof(a). Dra. Cristiani Oliveira, por toda estrutura ofertada, atenção e auxílio nas análises cromatográficas realizadas durante esse trabalho.

Aos meus colegas do GELCORR, Ana Aline Alcanfor, Andreza Moreira, Deomar Júnior, Gisele Braga, Juliermes Carvalho, Lucas Coutinho, Lucas Lima, Marcus Vinícius, Mesaque França, Natalia Gomes, Osmar Júnior, Raíssa Costa, Renato Veríssimo, Ronnie Semedo, Valdessandro Dantas e Wanderson Crisóstomo, pela amizade e conhecimentos compartilhados.

Ao meu grande companheiro de laboratório, Luiz Bitu, por ter me acolhido desde o início do exercício de minhas funções na UFC. Com toda certeza, sem sua ajuda, certamente não teria chegado até aqui. Além da gratidão e admiração por seus ensinamentos, tenho grande orgulho de ser verdadeiramente seu amigo.

A todos os meus professores desde o ensino infantil até o ensino superior, pois através de vocês descobri minha vocação para docência e nela permaneço até os dias atuais.

À Coordenação de Aperfeiçoamento de Pessoal de Nível Superior – Brasil (CAPES) – Código de Financiamento 001, por todo apoio financeiro concedido para realização deste trabalho.

À Central Analítica-UFC/CT-INFRA/MCTI-SISNANO/Pró-Equipamentos CAPES pelas análises de microscopia eletrônica de varredura.

À UFC por toda estrutura física e recursos humanos disponibilizados desde o início da minha formação acadêmica. Foi através do ensino público, gratuito e de qualidade ofertados por esta universidade que cheguei até aqui. Muito obrigado a todos que fazem nossa universidade.

“E Deus disse: — Eu irei com você e lhe darei a vitória” (Êxodo 34:14).

RESUMO

Neste trabalho foi desenvolvida uma metodologia para detecção e quantificação do ofloxacino (OFL), usando sensor eletroquímico baseado em eletrodo de carbono vítreo modificado com compósito formado por estanato de zinco e óxido de grafeno reduzido (ECV/Zn_2SnO_4-OGr), por meio da voltametria de onda quadrada (VOQ). O Zn_2SnO_4 foi sintetizado e caracterizado por meio de difração de raios-X (DRX), espectroscopia de infravermelho por transformada de Fourier (EITF), espectroscopia Raman (ER) e microscopia eletrônica de varredura (MEV). As imagens de MEV apontaram agregação entre os componentes do compósito desenvolvido (Zn_2SnO_4-OGr) em meio à dispersão com DMF; enquanto os resultados obtidos por meio da VOQ indicaram sinergismo químico entre os mesmos frente a oxidação irreversível do OFL em sua forma protonada (OFL^+), apresentando ainda $E_p \approx 1{,}2V$, mecanismo reacional de controle misto e sugerindo a participação de dois elétrons. O sinergismo químico entre Zn_2SnO_4 e OGr também foi observado por meio da espectroscopia de impedância eletroquímica (EIE), onde obteve-se a menor resistência à transferência de carga (R_{tc}) para o ECV/Zn_2SnO_4-OGr. As condições voltamétricas otimizadas foram H_2SO_4 $5{,}0 \times 10^{-1}$ mol L^{-1} pH 0, f = 60 s^{-1}, a = 30 mV e ΔE_s = 3 mV. A curva analítica obtida apresentou faixa de linearidade de $9{,}99 \times 10^{-8}$ a $6{,}62 \times 10^{-6}$ mol L^{-1} com r = 0,998; e limites de detecção (LD) e de quantificação (LQ) do OFL iguais a $8{,}28 \times 10^{-8}$ mol L^{-1} e $2{,}76 \times 10^{-7}$ mol L^{-1}, respectivamente, sendo ainda comparados aos obtidos por meio da cromatografia líquida de alta eficiência (CLAE). O sensor desenvolvido foi aplicado com sucesso na determinação de OFL em amostras de formulação farmacêutica comercial, apresentando taxas de recuperação médias de 100,58%; (DPR = 2,65%) e estabilidade para repetibilidade (DPR = 3,20%, n = 12); além de ter demonstrado eficiência mesmo ante à presença de vários interferentes. Os estudos químico-computacionais avaliaram teoricamente a adsorção do OFL em duas superfícies distintas (Zn_2SnO_4 e OGr) e indicaram maior eficiência do processo com o Zn_2SnO_4 (E_{ads} = –21,03 eV) ante o OGr (E_{ads} = –1,90 eV); evidenciando a relevância do óxido metálico misto no compósito proposto, para o sensor eletroquímico.

Palavras-chave: antibiótico; contaminante emergente; estanato de zinco; óxido de grafeno reduzido; voltametria de onda quadrada.

ABSTRACT

In this work, a methodology was developed for the detection and quantification of ofloxacin (OFL), using an electrochemical sensor based on a glassy carbon electrode modified with a composite formed by zinc stannate and reduced graphene oxide (ECV/Zn_2SnO_4-rGO), through square wave voltammetry (SWV). Zn_2SnO_4 was synthesized and characterized using X-ray diffraction (XRD), Fourier transform infrared spectroscopy (FTIR), Raman spectroscopy (RS) and scanning electron microscopy (SEM). The SEM images showed aggregation between the components of the developed composite (Zn_2SnO_4-rGO) amid dispersion with DMF; while the results obtained through SWV indicated chemical synergism between them against the irreversible oxidation of OFL in its protonated form (OFL^+), still presenting Ep ≈ 1.2V, reaction mechanism of mixed control and suggesting the participation of two electrons. The chemical synergism between Zn_2SnO_4 and rGO was also observed by means of electrochemical impedance spectroscopy (EIS), where the lowest resistance to charge transfer (R_{tc}) was obtained for GCE/Zn_2SnO_4-rGO. The optimized voltammetric conditions were H_2SO_4 5.0×10^{-1} mol L^{-1} pH 0, $f = 60\ s^{-1}$, $a = 30$ mV e $\Delta E_s = 3$ mV. The analytical curve obtained showed a linearity range from 9.99×10^{-8} to 6.62×10^{-6} mol L^{-1} with r = 0.998; and limits of detection (LD) and quantification (LQ) of the OFL equal to 8.28×10^{-8} mol L^{-1} and 2.76×10^{-7} mol L^{-1}, respectively, being still compared to those obtained through high performance liquid chromatography (HPLC). The developed sensor was successfully applied to determine OFL in commercial pharmaceutical formulation samples, showing average recovery rates of 100.58%; (DPR = 2.65%) and stability for repeatability (DPR = 3.20%, n = 12); in addition to having demonstrated efficiency even in the presence of several interferers. The chemical-computational studies theoretically evaluated the adsorption of OFL on two different surfaces (Zn_2SnO_4 and OGr) and indicated greater process efficiency with Zn_2SnO_4 ($E_{ads} = -21.03$ eV) compared to OGr ($E_{ads} = -1.90$ eV); highlighting the relevance of mixed metal oxide in the proposed composite for the electrochemical sensor.

Keywords: antibiotic; emerging contaminant; zinc stannate; reduced graphene oxide; square wave voltammetry.

SUMÁRIO

1 INTRODUÇÃO

É fato que a água é um recurso natural indispensável a manutenção das condições de existência e equilíbrio ambiental de todas as espécies de seres vivos em nosso planeta. Partindo desse princípio, torna-se imperioso manter os recursos hídricos globais com as mínimas condições de potabilidade e usos humano e industriais em geral; visando salvaguardar uma das condições básicas para a existência da vida em nosso planeta.

Todavia, o descarte indiscriminado de fármacos nos corpos hídricos em geral ou ainda no solo, seja de maneira direta ou indireta, tornou-se um sério problema em razão da forma alarmante com a qual estas substâncias têm sido cada vez mais detectadas nessas matrizes; analgésicos, anti-histamínicos, anti-inflamatórios, antipiréticos, antibióticos, antidepressivos e hormônios, figuram entre os fármacos mais detectados (1, 2).

Esses resíduos permanecem presentes na água mesmo após estes passarem por técnicas clássicas de tratamentos, evidenciando que tal situação poderá se tornar um grave problema de saúde pública (3, 4). Tais substâncias, ao serem descartadas em matrizes hídricas podem tornar prejudicial por exemplo, o consumo de variados tipos de carnes de pescados em razão de possuir resíduos desses fármacos, além de limitar ou mesmo impedir o uso do solo e efluentes envolvidos; são os chamados contaminantes emergentes (5).

Portanto, é imprescindível desenvolver metodologias analíticas simples, rápidas e de baixo custo que facilitem o controle e fiscalização desses contaminantes. Nesse sentido, as metodologias eletroanalíticas desenvolvidas por meio de sensores eletroquímicos têm se apresentado como meios alternativos de análise devidamente plausíveis em função de suas facilidades de operação, sensibilidade e baixo custo de instrumentação; especialmente quando comparadas a outras técnicas tradicionais como a cromatografia que além de envidar muitos custos, utiliza quantidades elevadas dos mais variados solventes orgânicos (muitos deles extremamente nocivos à saúde e meio ambiente) gerando assim um elevado volume de resíduos químicos nas análises (6, 7, 8).

O uso de compósitos como agente modificante das superfícies eletródicas de sensores eletroquímicos têm sido se difundido em razão de promoverem aumento do número de sítios de ligações, podendo melhorar ainda mais a eficiência na detecção e quantificação de inúmeras substâncias, justificando assim sua exploração e aplicações (7, 8).

Dentro do contexto dos contaminantes emergentes, os antibióticos figuram como um dos grupos que mais preocupa a comunidade científica em razão de sua acumulação no meio ambiente potencializar o surgimento de superbactérias. O ofloxacino (OFL) é um

antibiótico que possui grande eficácia no tratamento de infecções oculares e dos tratos gastrointestinal, respiratório e urinário. Ao administrar o OFL em seres humanos e animais em geral, os resíduos do fármaco são excretados por meio das fezes e/ou da urina, majoritariamente sob a forma inalterada (9, 10).

Ademais, outras aplicações e usos do referido fármaco em diversas atividades aquícolas, além de descartes da indústria farmacêutica em geral e de resíduos de lixos doméstico e hospitalar, surgem como mecanismos significativos de disseminação no meio ambiente (11, 12).

Outrossim, o OFL não é facilmente degradado e/ou ainda removido completamente nas estações de tratamento de água e esgoto por meio de técnicas usuais, gerando sua bioacumulação no meio e promovendo o aumento da resistência bacteriana em meios aquáticos (13, 14, 15); de maneira que tal problema tem se tornado uma preocupação recorrente das autoridades de saúde, especialmente em razão da insegurança e incertezas sobre quais danos eles podem ocasionar a saúde humana à curto, médio e longo prazo.

Recentemente, algumas pesquisas se dedicaram a avaliar e delimitar possíveis danos causados pela contaminação com OFL em ecossistemas microbiológicos de água doce, apontando inúmeras consequências que vão desde a inibição do crescimento de alguns microrganismos, redução na interação entre espécies diferentes da microbiota e diminuição da capacidade de fixação de nitrogênio e da capacidade fotossintética e metabólica das comunidades procariontes, infertilidade em espécies eucariontes (crustáceos aquáticos); sugerindo que o OFL residual na água é capaz de perturbar o equilíbrio da microecologia aquática (16, 17).

Nessa perspectiva, o presente estudo consistiu em desenvolver uma metodologia eletroanalítica que auxilie de maneira alternativa na detecção e quantificação rápida e eficiente do OFL em amostras de formulações farmacêuticas, usando um eletrodo de carbono vítreo (ECV) modificado com um compósito de elevada estabilidade à base de estanato de zinco (Zn_2SnO_4) e óxido de grafeno reduzido (OGr), aliado ainda a uma técnica eletroquímica prática e sensível; a voltametria de onda quadrada. A metodologia proposta também vislumbra possibilidade futura de testes e aplicações em amostras mais complexas, como matrizes hídricas.

1.1 Contaminantes emergentes

Como resultado do desenvolvimento das indústrias química, farmacêutica e agrícola, muitos compostos químicos como pesticidas, hormônios esteróides, antibióticos, aceleradores de crescimento, inibidores de microrganismos patogênicos, antidepressivos, corticoides, corantes, dentre outros, dispersam-se facilmente no meio ambiente (18, 19).

As excretas humana e animal (urina e fezes) contendo resíduos de diversos fármacos advindos dos mais variados usos e indicações, bem como o descarte irresponsável de medicamentos pela população e indústrias farmacêuticas, e ainda o uso indiscriminado e desregrado de fármacos em atividades agropecuárias e aquícolas, figuram como grande fonte de contaminação de efluentes e solo (5). Essas substâncias são conhecidas como contaminantes emergentes (CE) e quando encontradas em concentrações específicas no solo, na água, no ar ou em alimentos, advindas de efeitos antrópicos, podem vir a limitar ou ainda impedir o uso/consumo do recurso (5).

Existem muitos relatos na literatura sobre a presença de compostos químicos, como pesticidas, hormônios esteróides e antibióticos no ambiente aquático (20, 21, 22, 23, 24, 25, 26, 27). Os CE não são comumente monitorados, muito embora apresentem o elevado potencial de causar efeitos adversos ao meio ambiente e aos seres humanos (20).

A Figura 1 ilustra os resultados de uma busca sistemática na base de dados Web of Science®, refinada por meio das palavras-chave "contaminantes emergentes" e pela simultaneidade do referido termo adicionado individualmente a "fármacos", "pesticidas", "solventes", "corantes" e "cosméticos"; e considerando apenas artigos científicos publicados entre os anos de 2013 e 2023.

Analisando a Figura 1 é possível observar que há grande interesse da comunidade científica internacional em torno da questão dos CE, face a elevada quantidade de artigos publicados na última década (2013-2023). Evidencia-se ainda que dentre os principais grupos dos CE, os fármacos e os pesticidas são distintamente os mais estudados denotando maior preocupação dos pesquisadores.

Utilizando a mesma metodologia de busca (base de dados Web of Science®), averiguou-se ainda os principais tipos de fármacos mais estudados (dentre os CE) pela comunidade científica internacional, refinada por meio das palavras-chave "contaminantes emergentes", "fármacos"; e pela simultaneidade da palavra-chave "contaminantes emergentes" adicionada individualmente a "analgésicos", "antibióticos", "antidepressivos", "anti-

inflamatórios", "anti-histamínicos" e "hormônios"; considerando apenas os artigos científicos publicados entre os anos de 2013 e 2023, com os dados apresentados por meio da Figura 2.

Figura 1 – Análise quantitativa da produção científica internacional relativa aos contaminantes emergentes e seus principais grupos. Os dados foram obtidos por meio da base de dados científicos Web of Science®, utilizando simultaneamente o refinamento por: palavras-chave, interstício de 2013 a 2023 e apenas artigos científicos

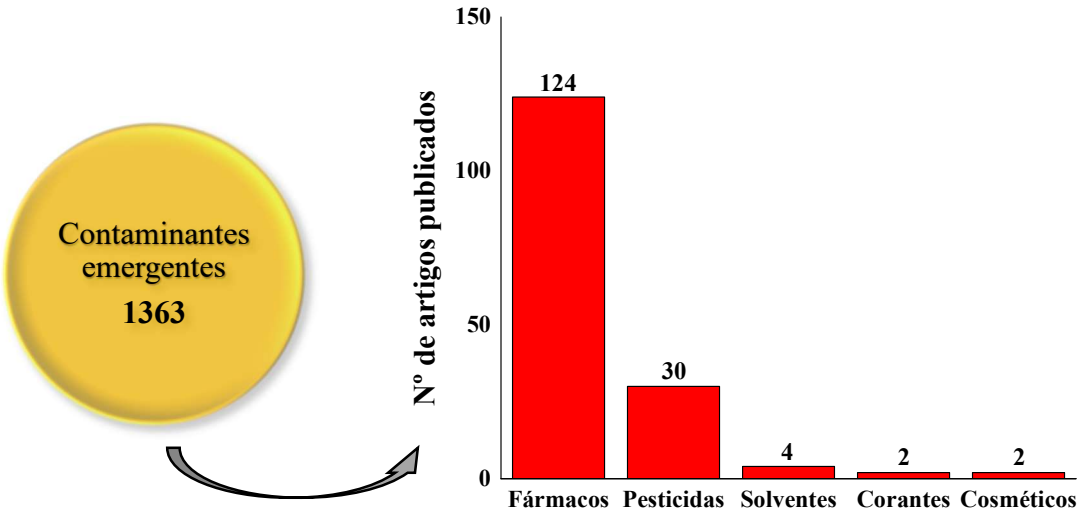

Fonte: Elaborada pelo autor (2023).

Figura 2 – Análise quantitativa da produção científica internacional relativa aos contaminantes emergentes e os grupos majoritários de fármacos. Os dados foram obtidos por meio da base de dados científicos Web of Science®, utilizando simultaneamente o refinamento por: palavras-chave, interstício de 2013 a 2023 e apenas artigos científicos

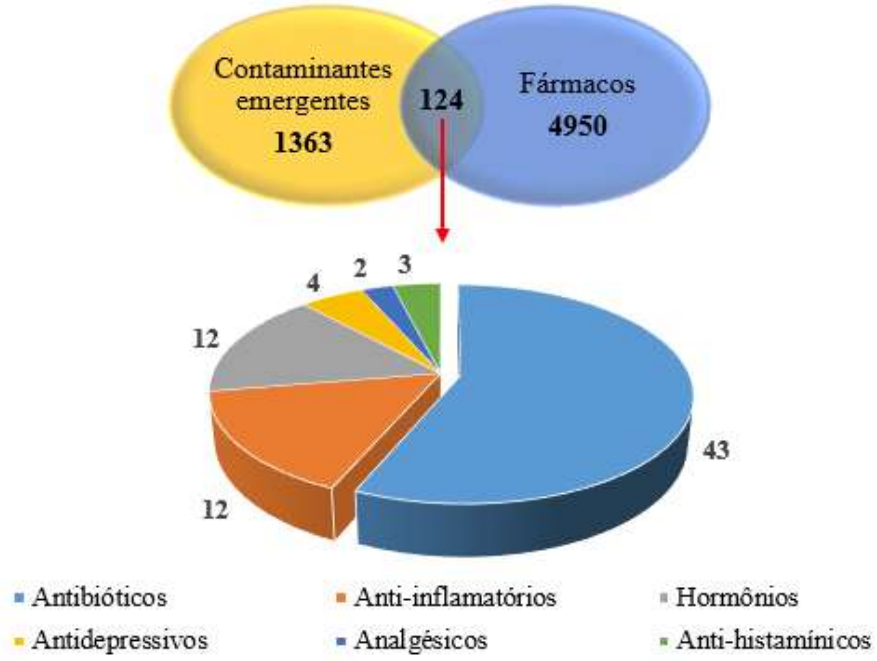

Fonte: Elaborada pelo autor (2023).

A considerar os fármacos como o grupo de CE mais pesquisado (ver Figura 1) e, por conseguinte, observando a Figura 2, é possível notar que os antibióticos figuram como o tipo de fármaco mais estudado pela comunidade científica, denotando preocupação em torno dos mesmos enquanto CE durante a última década (2013-2023).

Os padrões de ocorrência dos CE são variados e de complexo rastreio em razão das inúmeras fontes de dispersão, além do elevado potencial de bioacumulação, persistência e bioatividade de vários destes compostos, especialmente os fármacos. No caso dos antibióticos, o aumento da resistência bacteriana e a obscuridade em relação aos efeitos nocivos à espécie humana e aos ecossistemas em geral, figuram como os principais problemas (21, 22).

Diante disso, os CE têm recebido atenção crescente por parte dos governos, das organizações não governamentais (ONG) e de autoridades reguladoras, já que são substâncias químicas que atualmente não estão incluídas nos programas de monitoramento de rotina e podem ser candidatos à regulamentação futura, dependendo de sua toxicidade, efeitos danosos à saúde e frequência de ocorrência em matrizes ambientais e alimentares (28, 29, 30).

Considerando os potenciais riscos para a saúde humana e para os ecossistemas em geral, torna-se imprescindível desenvolver mecanismos de determinação e quantificação destas

substâncias, a fim de melhorar as condições de monitoramento, controle e fiscalização em variadas matrizes.

1.2 Ofloxacino: características químico-farmacológicas e meio ambiente

Segundo relatórios apresentados em 2018 tanto pela Organização Mundial de Saúde (OMS) como pelo Centro de Controle e Prevenção de Doenças (CCPD), a amoxicilina é antibiótico mais utilizado pela população no mundo inteiro; porém, outros antibióticos figuram entre os mais utilizados como o metronidazol, a azitromicina, a trimetroprima, o sulfametoxazol, o levofloxacino, o ciprofloxacino, o norfloxacino e o ofloxacino (31, 32).

O relatório da OMS (2018) expressa ainda preocupação em relação ao uso de antibióticos quinolônicos (considerados de mais amplo espectro), categorizados como “antibióticos de alerta", afirmando que os mesmos devem ser utilizados com o máximo de cautela devido ao seu alto potencial em promover resistência antimicrobiana e/ou seus efeitos colaterais (31).

A fim de correlacionar os antibióticos mais utilizados mundialmente com a temática dos CE, realizou-se uma busca utilizando mais uma vez a base de dados Web of Science®, refinada por meio das palavras-chave “contaminantes emergentes”, “antibióticos”; e pela simultaneidade da palavra-chave “contaminantes emergentes” adicionada individualmente a “amoxicilina”, “metronidazol”, “azitromicina”, “trimetroprima”, “sulfametoxazol”, “levofloxacino”, “ciprofloxacino”, “norfloxacino” e “ofloxacino”; considerando apenas os artigos científicos publicados entre os anos de 2013 e 2023, com os dados apresentados por meio da Figura 3.

Analisando a compilação dos dados ilustrados na Figura 3 é possível inferir a existência de muitas pesquisas científicas voltadas para o estudo de antibióticos, muito embora quando avaliadas conjuntamente com a palavra-chave “contaminantes emergentes” observa-se número menor de trabalhos publicados nessa perspectiva.

Figura 3 – Análise quantitativa da produção científica internacional relativa aos contaminantes emergentes e os principais antibióticos mais utilizados mundialmente. Os dados foram obtidos por meio da base de dados científicos Web of Science®, utilizando simultaneamente o refinamento por: palavras-chave, interstício de 2013 a 2023 e apenas artigos científicos

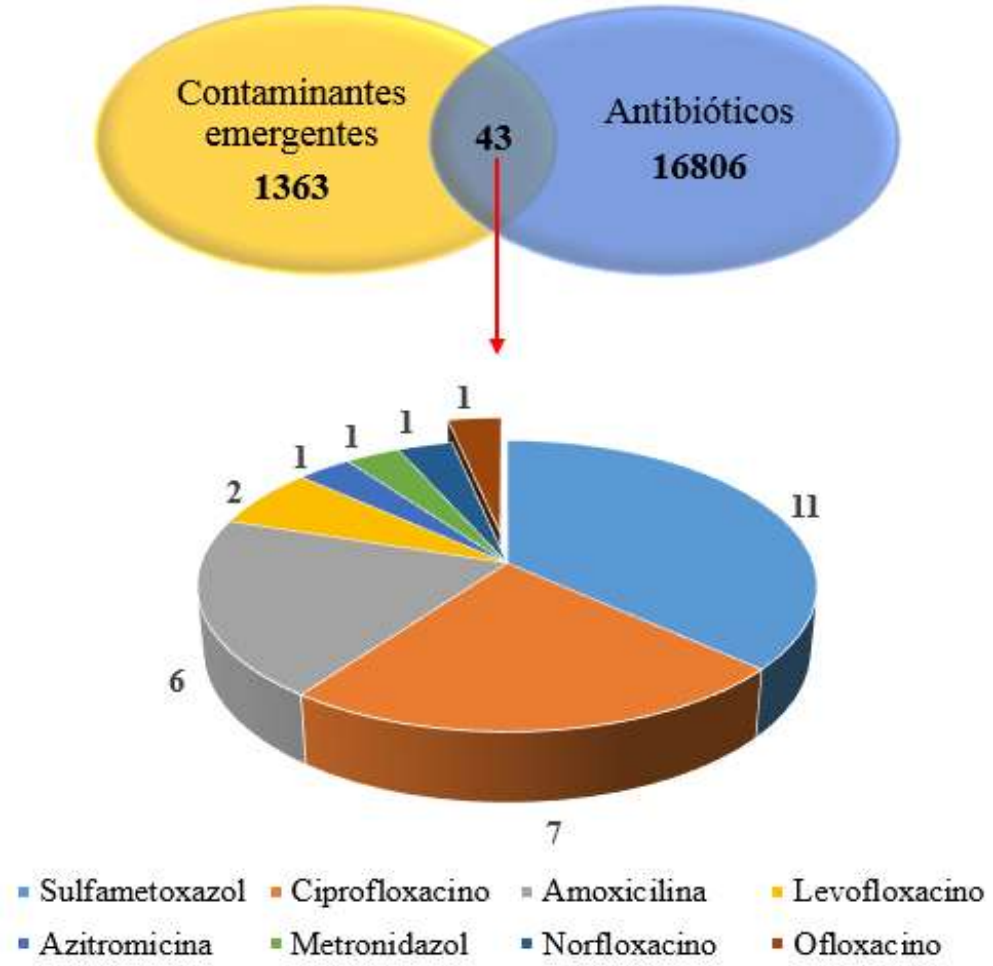

Fonte: Elaborada pelo autor (2023).

Ainda avaliando a Figura 3, observa-se que o sulfametoxazol é contaminante emergente mais citado em pesquisas publicadas dentre os antibióticos mundialmente mais utilizados. Evidencia-se também que os antibióticos quinolônicos figuram entre os menos estudados (como é o caso do OFL), considerando as condições de refinamento da busca apresentadas anteriormente.

O OFL ($C_{18}H_{20}FN_3O_4$) é um antibiótico quinolônico de amplo espectro pertencente à segunda geração da classe das fluoroquinolonas, que possui massa molar de 361,37 g mol^{-1} e baixo coeficiente de solubilidade em água (1,44 g L^{-1}); apresentando ainda eficiência antimicrobiana ante a bactérias gram-negativas e gram-positivas, possuindo indicações clínicas humanas e veterinárias (como bovinos, equinos, caninos e felinos) sendo especialmente

utilizado no combate a infecções oftálmicas e urinárias, muito embora também demonstre eficácia no combate a infecções dos tratos gastrointestinal e respiratório (33, 34).

No organismo humano o OFL possui um tempo de meia-vida de eliminação no plasma sanguíneo de 4 a 5 horas em pacientes adultos e de 6,4 a 7,4 horas em pacientes idosos e biodisponibilidade elevada (entre 85 a 95% da dosagem administrada) (9, 10).

A Figura 4 apresenta a seguir, a fórmula estrutural plana do OFL.

Figura 4 – Fórmula estrutural plana do OFL

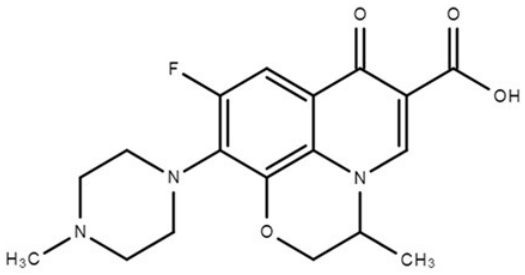

Fonte: Elaborada pelo autor (2023).

O mecanismo de ação das fluoroquinolonas (incluindo o OFL) no organismo humano é bastante afetado por suas propriedades físico-químicas, especialmente pela ionização sofrida pelas mesmas em função do pH do meio e pela capacidade que elas possuem de formar complexos com íons metálicos (35-41). OFL possui dois grupos funcionais ionizáveis, correspondentes respectivamente ao grupo carboxila (pKa_1 de 5,89 a 6,05) e ao grupo amino (pKa_2 de 7,9 a 8,2); salientando ainda que a protonação do analito é dependente da relação entre o pH do meio de solvatação e dos valores de pKa da molécula. (42-44) De maneira geral, a literatura aponta que a molécula de OFL tende a sofrer reação de oxidação bieletrônica, de caráter irreversível, com potencial de pico (E_p) variando entre 1,0 e 1,3 V. (45, 46, 47).

Considerando que OFL é um antibiótico já classificado como um CE orgânico tóxico (48) e ponderando ainda as problemáticas ambientais já elencadas relativas ao mesmo tais como: a não degradação no meio ambiente, a incompleta remoção nas estações de tratamento de água e esgoto, a bioacumulação e as incertezas em relação aos danos e efeitos nocivos à espécie humana e aos ecossistemas aquáticos e terrestres, resistência bacteriana e surgimento de superbactérias, e colocar fim a ausência de informações e dados na literatura acerca da quantidade do medicamento produzido pelas indústrias farmacêuticas humana e veterinária (44, 49, 50); torna-se imperioso desenvolver metodologias que visem detectar e mensurar esse fármaco.

1.3 Técnicas de análises químicas instrumentais quantitativas

As técnicas de análises químicas instrumentais quantitativas são utilizadas na química analítica para determinar a quantidade de um analito específico em uma dada amostra por meio de equipamentos sofisticados. De maneira geral, as principais técnicas de análises químicas instrumentais são as espectroscópicas, as cromatográficas e as eletroanalíticas (51).

As técnicas espectroscópicas são baseadas nas propriedades ópticas do analito, avaliando a interação (absorção, emissão ou dispersão de energia) entre a substância analisada e a radiação eletromagnética aplicada em diversas faixas de frequência, como por exemplo: a espectroscopia ultravioleta visível (UV-Vis) e a espectroscopia de infravermelho (IV). Apesar de muito utilizadas, as técnicas espectroscópicas possuem como desvantagens o alto custo dos equipamentos, além de apresentarem dificuldades quando aplicadas diretamente em amostras não tratadas e/ou complexas (52, 53).

As técnicas cromatográficas por sua vez são baseadas na separação dos componentes de uma amostra com base nas diferentes interações com as duas fases do sistema (estacionária e móvel), em função de variadas propriedades dos componentes como a adsorção e a polaridade. Por suas características analíticas, as técnicas cromatográficas foram amplamente aceitas pela grande comunidade científica, além de órgãos reguladores, fiscalizadores e investigativos (perícia forense); especialmente a cromatografia líquida de alta eficiência (CLAE) e a cromatografia gasosa (CG). Apesar das numerosas aplicações, as técnicas cromatográficas também possuem desvantagens tais como: equipamentos, manutenção e consumíveis (colunas e solventes específicos) de alto custo, complexidade de operação, processo demorado e minucioso de preparação das amostras envidando elevado tempo de análise, limitações na separação de substâncias com propriedades físicas e químicas semelhantes, além da elevada geração de resíduos químicos (52, 53, 54).

Já as técnicas eletroanalíticas são baseadas nas interações elétricas ocorridas entre o analito em solução e uma superfície eletródica, sendo atualmente bastante utilizadas para estudar processos reacionais eletroquímicos e quantificar espécies eletroativas; especialmente em razão da praticidade experimental, sensibilidade, custo operacional reduzido (quando comparado as técnicas cromatográficas) e baixa geração de resíduos químicos de análise. A voltametria, a amperometria, a coulometria e a potenciometria, figuram entre as mais conhecidas técnicas eletroanalíticas (55, 56, 57). O uso das técnicas eletroanalíticas voltamétricas têm sido muito utilizadas na detecção e quantificação de substâncias, sobretudo a voltametria de onda quadrada (VOQ) e a voltametria de pulso diferencial (VPD). De maneira

geral, as técnicas voltamétricas consistem em aplicar um potencial elétrico controlado a um eletrodo presente numa solução eletrolítica contendo o analito, e logo após, aferir a magnitude da corrente elétrica obtida. A superfície de resposta da corrente elétrica é diretamente proporcional a concentração do analito na matriz analisada (58, 59, 60, 61, 62).

Conceitualmente na VOQ aplica-se um potencial elétrico ao eletrodo de trabalho, promovendo uma varredura voltamétrica nos dois sentidos (direto e reverso) repetidamente em uma frequência fixa. Durante cada ciclo a corrente elétrica resultante é medida em resposta ao potencial aplicado, e a diferença entre a corrente aferida durante o pulso de subida e o pulso de descida é registrada como um processo ("pico") no perfil voltamétrico. A altura e a posição do "pico" obtido são usadas para determinar a concentração do analito em estudo e fornecer informações eletroquímicas sobre o analito e o processo eletródico ocorrido (60, 61, 62).

Buscando averiguar a utilização das principais técnicas de análises químicas instrumentais quantitativas em pesquisas acadêmicas envolvendo fármacos, realizou-se uma busca na base de dados Web of Science®, refinada por meio das palavras-chave "cromatografia gasosa", "cromatografia líquida de alta eficiência", "cromatografia de camada delgada", "espectroscopia de infravermelho", "espectroscopia de ultravioleta e visível", "voltametria", "amperometria", "coulometria", "potenciometria", "voltametria de onda quadrada", "voltametria de pulso diferencial"; e pela simultaneidade dos termos acima adicionados individualmente a "fármacos" e "ofloxacino"; considerando apenas os artigos científicos publicados entre os anos de 2013 e 2023, com os dados apresentados por meio da Figura 5.

Figura 5 – Análise quantitativa da produção científica internacional relativa as principais técnicas de análises químicas instrumentais quantitativas aplicadas para fármacos em geral e em especial para o OFL. Os dados foram obtidos por meio da base de dados científicos Web of Science®, utilizando simultaneamente o refinamento por: palavras-chave, interstício de 2013 a 2023 e apenas artigos científicos

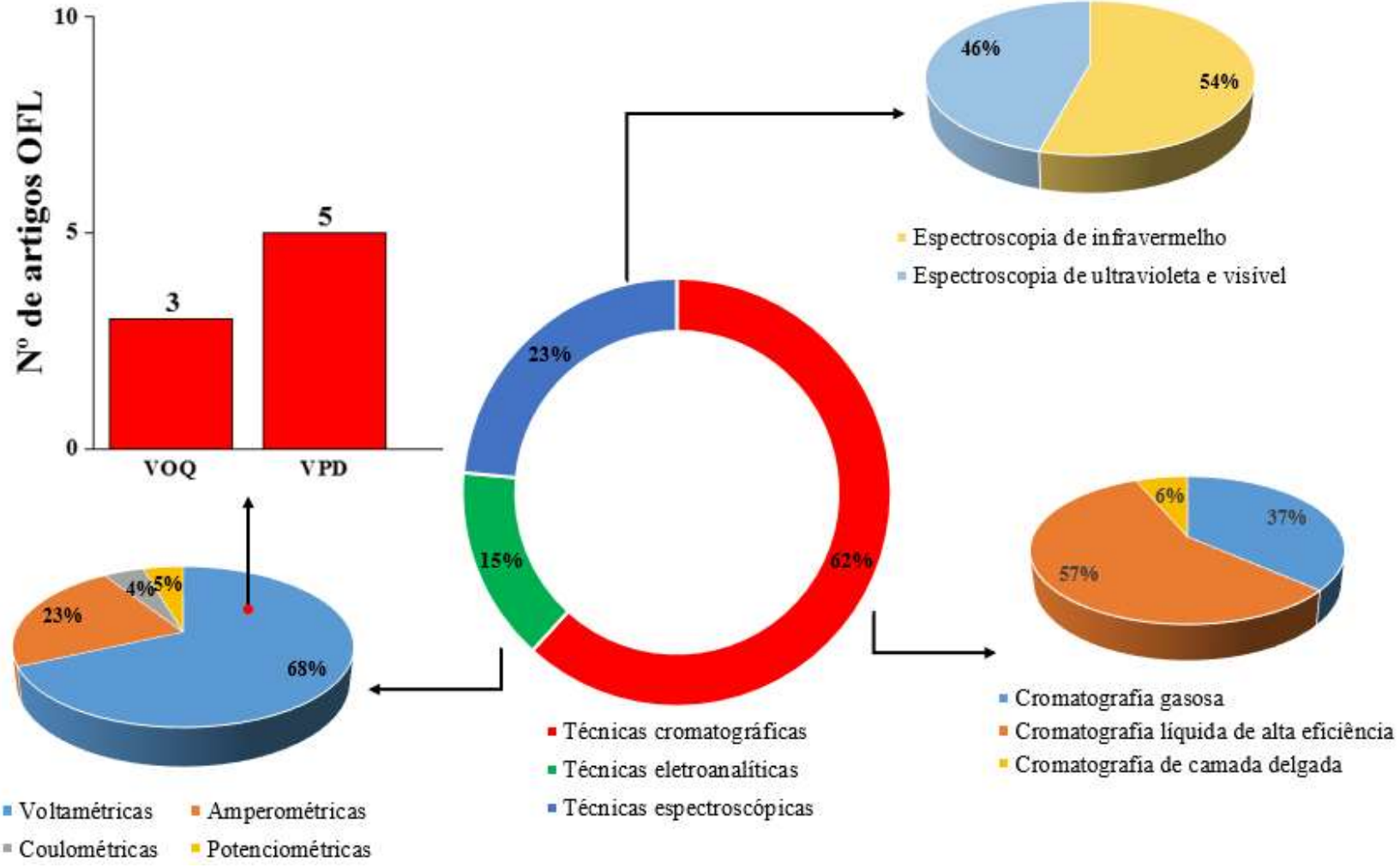

Fonte: Elaborada pelo autor (2023).

Observando a Figura 5 é possível notar claramente que a maioria dos artigos científicos publicados na última década (2013-2023) utilizou técnicas cromatográficas na detecção e quantificação de fármacos. A Figura 5 aponta ainda o uso minoritário das técnicas eletroanalíticas na determinação de tais substâncias, evidenciando que ainda há muito a ser explorado através delas; muito embora as técnicas voltamétricas sejam preferencialmente as mais utilizadas. Com base na pesquisa realizada, foram ainda encontrados 8 artigos científicos que fizeram uso da VPD e da VOQ para detecção e quantificação do OFL.

A VOQ é uma das técnicas voltamétricas de pulso mais rápidas e sensíveis, com obtenção de limites de detecção comparáveis aos das técnicas cromatográficas e espectroscópicas, razão pelas quais tem sido bastante utilizada na determinação e quantificação de muitos fármacos. Ademais, a análise dos parâmetros característicos desta técnica também possibilita os estudos cinético e mecanísticos do processo eletródico ocorrido no sistema avaliado (60, 61, 62).

1.4 Sensores eletroquímicos

A determinação de fármacos em variadas amostras ainda é uma tarefa desafiadora; no entanto, com o advento de técnicas instrumentais sensíveis, rápidas e de fácil aplicação, como a VOQ, surgiu uma nova tecnologia baseada em sensores eletroquímicos. Partindo desse pressuposto, a eletroanalítica se apresenta como um caminho alternativo na busca por novas metodologias analíticas por meio do desenvolvimento e aplicação de sensores eletroquímicos. Apresentando elevada eficiência na detecção e quantificação de substâncias, a utilização de sensores eletroquímicos tem sido bastante difundida na comunidade acadêmica internacional (63, 64, 65, 66, 67, 68).

De maneira geral, um sensor eletroquímico é um dispositivo que detecta e mede a concentração de um analito em uma solução por meio de reações eletroquímicas ocorridas na superfície eletródica. O sinal elétrico produzido mantém relação de proporcionalidade em magnitude, intensidade ou frequência com a concentração do analito. O tipo de material constituinte da superfície eletródica dos sensores eletroquímicos desempenha papel fundamental na interação eletroquímica com o analito avaliado (63, 64).

Após uma busca sistemática na base de dados Web of Science®, refinada por meio das palavras-chave “sensor”, “sensor eletroquímico”, “biossensor eletroquímico”, “eletrodo de pasta de carbono”, “eletrodo de carbono vítreo”, “eletrodo de grafite”, “eletrodo de gota pendente de mercúrio”; e pela simultaneidade da palavra-chave “sensor eletroquímico”

adicionada individualmente a “fármaco”, “antibiótico”, “ofloxacino”; e considerando apenas artigos científicos publicados entre os anos de 2013 e 2023, com os devidos resultados ilustrados na Figura 6.

Os dados presentes na Figura 6 apontam que as pesquisas envolvendo o desenvolvimento de sensores eletroquímicos correspondem a aproximadamente 6,1% de todos os trabalhos que de maneira geral envolvem sensores, e destes a maioria utiliza como base da superfície eletródica materiais carbonáceos, especialmente pasta de carbono e carbono vítreo; verificou-se ainda na última década (2013-2023) a publicação de 87 trabalhos utilizando simultaneamente as palavras-chave “sensores eletroquímicos” e “fármacos”, com 23 deles se referindo a detecção e quantificação de algum tipo de antibiótico e 5 deles aplicados ao OFL, evidenciando a carência de metodologias desenvolvidas para determinação de OFL.

É possível ainda amplificar a resposta analítica de um sensor eletroquímico por meio da adição de agentes modificadores em sua superfície como o grafeno e seus derivados, nanomateriais (partículas de metais e óxidos de metais, carbonáceos etc.), surfactantes, compósitos, dentre outros; garantindo um melhor desempenho em termos de sensibilidade, seletividade, limite de detecção, limite de quantificação e tempo de resposta. (63-66) A exemplo, a literatura descreve inúmeros trabalhos exitosos envolvendo o uso de agentes modificantes na superfície eletródica de variados sensores eletroquímicos, vislumbrando detecções mais sensíveis a substâncias específicas como por exemplo: OG-$NiSe_2$ na determinação de carbamazepina (69), OGr-$BiVO_4$ na detecção de dopamina (70) e nanotubos de carbono paredes múltiplas funcionalizado e fósforo preto (NTCPM*f*-PB) na identificação de carbendazim (71).

Figura 6 – Análise quantitativa da produção científica internacional relativa aos tipos de sensores eletroquímicos e aplicações em fármacos. Os dados foram obtidos por meio da base de dados científicos Web of Science®, utilizando simultaneamente o refinamento por: palavras-chave, interstício de 2013 a 2023 e apenas artigos científicos

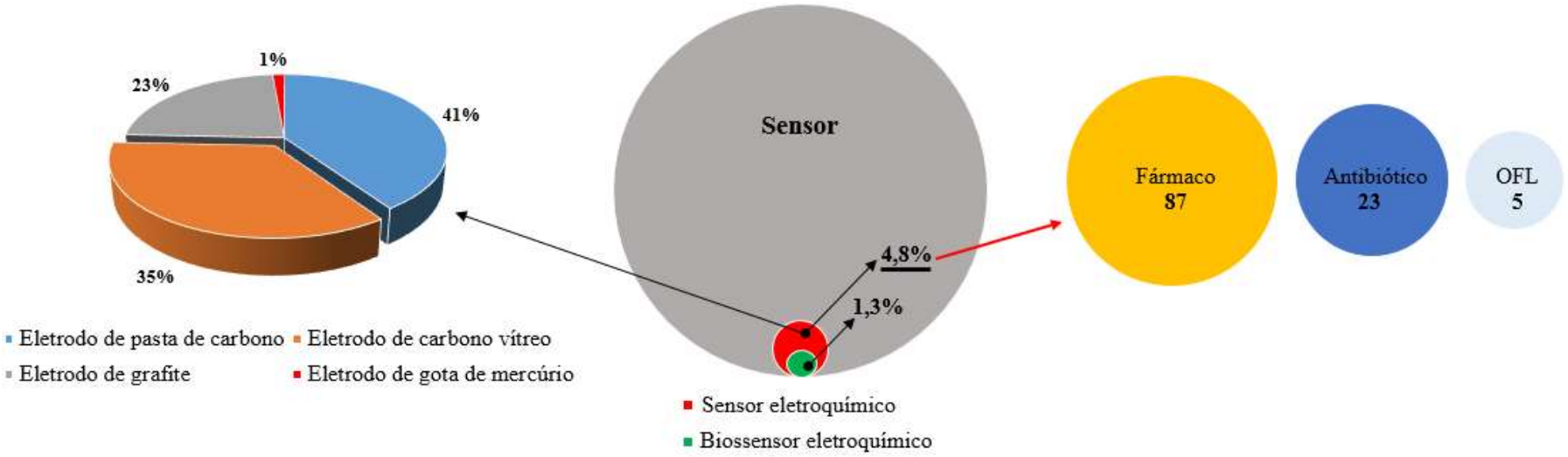

Fonte: Elaborada pelo autor (2023).

Compósitos ou ainda materiais compósitos, são produzidos pela junção de dois ou mais materiais (quer estejam no mesmo estado físico ou não) com o objetivo de se obter um produto com melhores características e propriedades físicas e/ou químicas que os componentes iniciais isoladamente. A depender das qualidades e características dos compósitos desenvolvidos, eles têm sido utilizados nas mais diversas aplicações tecnológicas que vão desde capacitores até sensores eletroquímicos.

A considerar o uso de compósitos à base de óxidos simples no desenvolvimento de sensores eletroquímicos para detecção de CE, a literatura descreve inúmeras aplicações exitosas tais como: uso de Fe_3O_4 e OGr aplicado na detecção de catecol e hidroquinona (72), uso de CuO e TiO_2 aplicada na detecção de metil paration (73), uso de MnO_2 e óxido de grafeno (OG) para determinação de guaiacol e vanilina (74), microcompósito de pasta de carbono com La_2O_3 e TiO_2 aplicado na detecção de corantes (tartrazina e amarelo crepúsculo) (75), microcompósito de pasta de carbono com MoO_3 e aplicado na detecção de paracetamol e vermelho de allura (76), uso de ZnO_2 e OG aplicado na detecção de ofloxacino (77), dentre outros.

Há ainda os óxidos mistos, que por sua vez tem despertado cada vez mais o interesse da comunidade científica em razão de uma gama de possibilidades de aplicações tecnológicas. Dentre eles, existem os óxidos ternários de estanho e zinco; chamados de estanato de zinco tais como: Zn_2SnO_4, $ZnSnO_2$ e $ZnSnO_3$ (76, 77, 78, 79)

O Zn_2SnO_4 possui propriedades diamagnéticas e semicondutoras (80, 81, 82), além de demonstrar ser um material de uso importante em inúmeras tecnologias avançadas, especialmente no desenvolvimento de sensores de gases tóxicos (79, 83, 84, 85, 86). Embora o Zn_2SnO_4 possua inúmeras utilidades, não encontrou-se na literatura quaisquer aplicações do mesmo em sensores eletroquímicos para detecção do ofloxacino ou ainda de qualquer outro CE; todavia, são relatadas inúmeras aplicações exitosas de compósitos contendo óxidos simples e/ou mistos juntamente com OGr, no desenvolvimento de sensores eletroquímicos para determinação de inúmeros CE (87, 88, 89, 90, 91), principalmente em função do OGr apresentar boa dispersão em meios polares e de possuir inúmeros sítios reativos (grupos epóxi, hidroxila e carboxila) presentes na sua estrutura basal (92, 93, 94, 95, 96).

Adicionalmente, as notáveis características de materais como OG, OGr, óxidos metálicos em geral, dentre outros, garantem um melhor desempenho dos sensores em termos de sensibilidade, limite de detecção e limite de quantificação (97, 98).

Sendo assim, o desempenho de um sensor eletroquímico depende significativamente da presença de uma superfície estruturada (modificada) e projetada com precisão para uma

interação com o analito alvo e para amplificação de sinal, como por exemplo, uma modificação à base de compósito.

2 OBJETIVOS

2.1 Objetivo geral

Desenvolver uma metodologia eletroanalítica simples para detecção e quantificação de OFL em amostras de formulação farmacêutica comercial, utilizando um sensor eletroquímico baseado em eletrodo de carbono vítreo (ECV) modificado com compósito (Zn_2SnO_4-OGr), por meio da técnica de voltametria de onda quadrada (VOQ).

2.2 Objetivos específicos

Como objetivos específicos temos:

a) caracterizar o Zn_2SnO_4 sintetizado por meio das técnicas de difração de raios-X (DRX), espectroscopia de infravermelho por transformada de Fourier (EITF), espectroscopia Raman (ER) e microscopia eletrônica de varredura (MEV).

b) caracterizar o compósito Zn_2SnO_4-OGr desenvolvido por meio das técnicas de espectroscopia Raman (ER) e microscopia eletrônica de varredura (MEV).

c) avaliar a resistência à transferência de carga das superfícies do ECV modificado individualmente com as composições Zn_2SnO_4, OGr e com o compósito (Zn_2SnO_4-OGr) por meio da técnica de espectroscopia de impedância eletroquímica (EIE).

d) estudar o comportamento eletroquímico do OFL sobre ECV/Zn_2SnO_4-OGr por meio da técnica de voltametria cíclica (VC).

e) estudar o comportamento eletroquímico e realizar testes de eletroatividade do OFL sobre ECV/Zn_2SnO_4-OGr em variados eletrólitos de suporte e diferentes valores de pH, bem como otimizar os parâmetros experimentais e voltamétricos, por meio da técnica de voltametria de onda quadrada (VOQ).

f) detectar e quantificar o OFL em formulação farmacêutica comercial, comparando os resultados obtidos por meio dos estudos de recuperação com a metodologia oficial para o fármaco, a cromatografia líquida de alta eficiência (CLAE).

g) avaliar por meio de estudo teórico o processo de adsorção do ofloxacino (OFL) individualmente nas superfícies de Zn_2SnO_4 e OGr por meio da Teoria do Funcional da Densidade (TFD) e da Aproximação do Gradiente Generalizado (AGG), estimando as energias de adsorção, estruturas de bandas e densidade total de estados.

REFERÊNCIAS

1 BILAL, M. *et al*. Hydrogen-based catalyst assisted advanced oxidation processes to mitigate emerging pharmaceutical contaminants. **International Journal Hydrogen Energy**, [*s. l.*], v. 47, n. 45, p. 19555-19569, 2022.

2 KRASUCKA, P. *et al.* Adsorption and desorption of antiviral drugs (ritonavir and lopinavir) on sewage sludges as a potential environmental risk. **Journal of Hazardous Materials**, [*s. l.],* v. 425, p. 1-10, 2022.

3 HANSEN, M. *et al.* Fate and antibacterial potency of anticoccidial drugs and their main abiotic degradation products. **Environmental Pollution**, [*s. l.*], v. 157, n. 2, p. 474-480, 2009.

4 XI, C. *et al.* Prevalence of antibiotic resistance in drinking water treatment and distribution system. **Applied and Environmental Microbiology Journal**, [*s. l.*], v. 75, p. 5714-5722, 2009.

5 PURI, M.; GANDHI, K.; KUMAR, M. S. Emerging environmental contaminants: a global perspective on policies and regulations. **Journal of Environmental Management**, [*s. l.*], v. 332, p. 1-13, 2023.

6 ZHU, C. *et al.* A flexible electrochemical biosensor based on functionalized poly (3,4-ethylenedioxythiophene) film to detect lactate in sweat of the human body. **Journal of Colloid and Interface Science**, [*s. l.*], v. 617, p. 454-462, 2022.

7 GOMES, R. N. *et al*. Understanding the dipyrone oxidation allying electrochemical and computational approaches. **Analytica Chimica Acta**, [*s. l.*], v. 105, p. 49-57, 2019.

8 TUAN LE, H. *et al*. Mo and Zn-Dual doped Cu x O nanocrystals confined High-Conductive Cu arrays as novel sensitive sensor for neurotransmitter detection. **Journal of Colloid and Interface Science**, [*s. l.*], v. 606, p. 1031-1041, 2022.

9 ZANCHETTA, P. G.; PENA, A.; GONÇALVES, R. Development and validation of an analytical method for the simultaneous quantification of ofloxacin, norfloxacin and ciprofloxacin in human urine. **Sanitary and Environmental Engineering**, Rio de Janeiro, v. 20, p. 307-314, 2015.

10 ABRAMS, A. C. **Clinical Pharmacotherapy**: principles for nursing practice. 7th ed. [*S. l.*]: Guanabara Publisher, 2006.

11 DIAZ-CRUZ, M. S.; ALDA, M. J. L.; BARCELÓ, D. Environmental behavior and analysis of veterinary and human drugs in soils, sediments and sludge. **TrAC Trends in Analytical Chemistry**, [*s. l.*], v. 22, p. 340-351, 2003.

12 ANDREU, V.; BLASCO, C.; PICO, Y. Analytical strategies to determine quinolone residues in food and the environment. **TrAC Trends in Analytical Chemistry**, [*s. l.*], v. 26, p. 534-556, 2007.

13 FENT, K.; WESTON, A. A.; CAMINADA, D. Ecotoxicology of human pharmaceuticals. **Aquatic Toxicology**, [*s. l.*], v. 76, n. 2, p. 122-159, 2006.

14 NIETO, J. *et al*. Photocatalyzed degradation of flumequine by doped TiO 2 and simulated solar light. **Journal of Hazardous Materials**, [*s. l.*], v. 155, p. 45-50, 2008.

15 WANG, P.; HE, Y.-L.; HUANG, C.-H. Oxidation of fluoroquinolone antibiotics and structurally related amines by chlorine dioxide: reaction kinetics, product and pathway evaluation. **Water Research**, [*s. l.*], v. 44, p. 5989-5998, 2010.

16 DENG, Y. *et al*. Effects of ofloxacin on the structure and function of freshwater microbial communities. **Aquatic Toxicology**, [*s. l.*], v. 244, p. 1-9, 2022.

17 NGUYEN, T.-D. *et al*. Chronic ecotoxicology and statistical investigation of ciprofloxacin and ofloxacin to Daphnia magna under extendedly long-term exposure. **Environmental Pollution**, [*s. l.*], v. 291, 118095, 2021.

18 ZUCCATO, E.; CASTIGLIONI, S.; FANELLI, R. Identification of the pharmaceuticals forhuman use contaminating the Italian aquatic environment. **Journal of Hazardous Materials**, [*s. l.*], v. 122, n. 3, p. 205-209, 2005.

19 LANANAN, F. *et al*. Symbiotic bioremediation of aquaculture wastewater in reducing ammonia and phosphorus utilizing effective microorganism (EM-1) and microalgae (Chlorella sp.). **International Biodeterioration and Biodegradation**, [*s. l.*], v. 95, p. 127-134, 2014.

20 GEISSEN, V. *et al.* Emerging pollutants in the environment: a challenge for water resource management. **International Soil and Water Conservation Research**, [*s. l.*], v. 3, p. 57-65, 2015.

21 U. S. EPA. **Aquatic life criteria for contaminants of emerging concern**: Part I: General guidelines and recommendations. [*S. l.*]: EPA, 2008.

22 VANDERMEERSCH, G. *et al*. Environmental contaminants of emerging concern in seafood–European database on contaminant levels. **Environmental Research**, [*s. l.*], v. 143, part. B, p. 29-45, 2015.

23 TKACZYK, A.; MITROWSKA, K.; POSYNIAK, A. Synthetic organic dyes as contaminants of the aquatic environment and their implications for ecosystems: a review. **Science of The Total Environment**, [*s. l.*], v. 717, p. 1-19, 2020.

24 BAYABIL, H. K.; TESHOME, F. T.; YUNCONG, C. L. Emerging contaminants in soil and water. **Frontiers in Environmental Science**, [*s. l.*], v. 10, p. 1-8, 2022.

25 MORIN-CRINI, N. *et al.* Worldwide cases of water pollution by emerging contaminants: a review. **Environmental Chemistry Letters**, [*s. l.*], v. 20, p. 2311-2338, 2022.

26 OVERTON, O. C. *et al*. Wetland removal mechanisms for emerging contaminants. **Land**, [*s. l.*], v. 12, n. 2, p. 472, 2023.

27 PRAJAPATI, D. *et al*. A critical review on emerging contaminants: origin, discernment, and remedies. **Sustainable Water Resources Management**, [*s. l.*], v. 9, p. 1-11, 2023.

28 ECR. Commission Regulation (EU) nº 37/2019 of 22 December 2009 on pharmacologically active substances and their classification regarding maximum residue limits in foodstuffs of animal origin. **Official Journal of the European Union**, [*s. l.*], 20 January, 2010.

29 EFSA. Perfluoroalkylated substances in food: occurrence and dietary exposure. **EFSA Journal**, [*s. l.*], v. 10, 2012.

30 EFSA. Scientific opinion on the risks to public health related to the presence of bisphenol A (BPA) in foodstuffs. **EFSA Journal**, [*s. l.*], v. 13, 2015.

31 OPAS. **Novo relatório da OMS revela diferenças no uso de antibióticos entre 65 países**. [*S. l.*], 12 nov. 2018. Disponível em: https://www.paho.org/pt/noticias/12-11-2018-novo-relatorio-da-oms-revela-diferencas-no-uso-antibioticos-entre-65-paises. Acesso em: 01 out. 2023.

32 CDC. A**ntibiotic use in the United States, 2018**. Atlanta, GA: US Department of Health and Human Services, 2019. Disponível em: https://www.cdc.gov/antibiotic-use/stewardship-report/pdf/stewardship-report-2018-508.pdf. Acesso em: 01 out. 2023.

33 IUPAC. **Nomenclature**. [*S. l.*]: IUPAC, c2023. Disponível em: https://iupac.org/what-we-do/nomenclature/. Acesso em: 04 mai. 2023.

34 INDICE.EU. **Medicamentos**: Princípios ativos: Ofloxacina. [*S. l.*]: Indice.eu, c2023. Disponível em: https://www.indice.eu/pt/medicamentos/DCI/ofloxacina/informacao-cientifica. Acesso em: 04 mai. 2023.

35 DRAKOPOULOS, A. I.; IOANNOU, P. C. Spectrofluorimetric study of the acid–base equilibria and complexation behavior of the fluoroquinolone antibiotics ofloxacin, norfloxacin, ciprofloxacin and pefloxacin in aqueous solution. **Analytica Chimica Acta**, [*s. l.*], v. 354, p. 197-204, 1997.

36 PARK, H.-R.; KIM, T. H.; BARK, K.-M. Physicochemical properties of quinolone antibiotics in various environments. **European Journal of Medicinal Chemistry**, [*s. l.*], v. 37, n. 1-3, p. 443-460, 2002.

37 ALBRECHT, R. Development of antibacterial agents of the nalidixic acid type. *In:* JUCKER, E. (ed.). **Progress in Drug Research**. [*S. l.*]: Birkhäuser Verlag Basel, 1977. v. 21, p. 11-104.

38 CHU, D. T.; FERNANDES, P. B. Structure-activity relationships of the fluoroquinolones. **Antimicrobial Agents and Chemotherapy**, [*s. l.*], v. 33, n. 2, p.131-135, 1989.

39 OHTA, M.; KOGA, H. Three-dimensional structure-activity relationships and receptor mapping of N1-substituents of quinolone antibacterials. **Journal of Medicinal Chemistry**, [*s. l.*], v. 34, p. 131-139, 1991.

40 JUNG, J. C.; BAEK, S.; PARK, O. S. Synthesis and antibacterial activity of 2-substituted 6-fluoro-1, 4-dihydro-4-oxo-3-quinolinecarboxylic acids. **II Farmaco**, [*s. l.*], v. 56, n. 9, p. 665-675, 2001.

41 MITSCHER, L. A. Bacterial topoisomerase inhibitors: quinolone and pyridine antibacterial agents. **Chemical Reviews**, [*s. l.*], v. 105, p. 559-592, 2005.

42 DAVYDOV, N. *et al*. Determination of fluoroquinolone antibiotics through the fluorescent response of Eu (III) based nanoparticles fabricated by layer-by-layer technique. **Analytica Chimica Acta**, [*s. l.*], v. 784, p. 65-71, 2013.

43 PINACHO, D. G.; SANCHEZ-BAEZA, F.; MARCO, M. P. Molecular modeling assisted hapten design to produce broad selectivity antibodies for fluoroquinolone antibiotics. **Analytical Chemistry**, [*s. l.*], v. 84, p. 4527-4534, 2012.

44 NOFFKE, A. L. *et al*. Designing organometallic compounds for catalysis and therapy. **Chemical Communications**, [*s. l.*], v. 48, p. 5219, 2012.

45 JIANG, Z. *et al.* Electrochemical sensor based on a novel Pt-Au bimetallic nanoclusters decorated on reduced graphene oxide for sensitive detection of ofloxacin. **Electroanalysis**, [*s. l.*], v. 29, p. 602-608, 2017.

46 JIANG, Z.; LI, G.; ZHANG, M. A novel electrochemical sensor based on SH-β-cyclodextrin functionalized gold nanoparticles/reduced-graphene oxide nanohybrids for ultrasensitive electrochemical sensing of acetaminophen and ofloxacin. **International Journal of Electrochemical Science**, [*s. l.*], v. 12, p. 5157-5173, 2017.

47 HAN, H.; LI, J.-Z.; PANG, X.-Z. Electrochemical sensor using glassy carbon electrode modified with HPMαFP/Ppy/GCE composite film for determination of ofloxacin. **International Journal of Electrochemical Science**, [*s. l.*], v. 8, p. 9060-9070, 2013.

48 PETRIE, B.; BARDEN, R.; KASPRZYK-HORDERN, B. A review on emerging contaminants in wastewaters and the environment: current knowledge, understudied areas and recommendations for future monitoring. **Water Research**, [*s. l.*], v. 72, p. 3-27, 2015.

49 KÜMMERER, K. Antibiotics in the aquatic environment: a review: part I. **Chemosphere**, [*s. l.*], v. 75, p. 417-434, 2009.

50 KEMPER, N. Veterinary antibiotics in the aquatic and terrestrial environment. **Ecological Indicators**, [*s. l.*], v. 8, p. 1-13, 2008.

51 MATOS, S. P. **Técnicas de análise química**: métodos clássicos e instrumentais. 1. ed. São Paulo: Saraiva, 2015.

52 SKOOG, D. A.; HOLLER, F. J.; CROUCH, S. R. **Principles of instrumental analysis**. [*S. l.*]: Cengage Learning, 2017.

53 PAVIA, D. L. *et al*. **Introduction to spectroscopy**. [*S. l.*]: Cengage Learning, 2014.

54 YOUNG, G. M.; LURIE, I. S. Recent forensic applications of enhanced chromatographic separation methods. **Journal of Separation Science**, [*s. l.*], v. 45, p. 369-381, 2022.

55 DU, H.; XIE, Y.; WANG, J. Nanomaterial-sensors for herbicides detection using electrochemical techniques and prospect applications. **Trends in Analytical Chemistry**, [*s. l.*], v. 135, p.1-9, 2021.

56 BARD, A. J.; FAULKNER, L. R.; WHITE, H. S. E**lectrochemical methods**: fundamentals and applications. 3rd ed. [*S. l.*]: John Wiley & Sons, 2022.

57 BOCKRIS, J. **Modern electrochemistry**: an introduction to an interdisciplinary area. [*S. l.*]: Springer Science, 2012.

58 PLETCHER, D. *et al.* **Instrumental methods in electrochemistry**. New York: John Wiley & Sons, 1985.

59 GOSSER JR., D. K. **Cyclic voltammetry**: simulation and analysis of reaction mechanisms. New York: UCH Publishers, 1993.

60 WANG, J. **Analytical electrochemistry**. New York: Wiley VCH, 2001.

61 MIRCESKI, V.; KOMORSKY-LOVRIC, S.; LOVRIC, M. **Square-Wave Voltammetry**: theory and application. República da Macedônia: Springer, 2007.

62 SOUZA, D.; MACHADO, S. A. S.; AVACA, L. A. **Voltametria de onda quadrada**. Primeira parte: aspectos teóricos. Química Nova, São Paulo, v. 26, p. 81-89, 2003.

63 BARANWAL J. *et al.* Electrochemical sensors and their applications: a review. Chemosensors, [*s. l.*], v. 10, p. 363-375, 2022.

64 MIRI, P. S. *et al*. MOF-biomolecule nanocomposites for electrosensing. **Nanochemistry Research**, [*s. l.*], v. 6, p. 213-222, 2021.

65 TANG, X. *et al.* Construction of rose flower-like NiCo-LDH electrode derived from bimetallic MOF for highly sensitive electrochemical sensing of hydrazine in food samples. **Food Chemistry**, [*s. l.*], v. 427, p. 1-8, 2023.

66 RAHMATI, Z.; ROUSHANI, M.; HOSSEINI, H. MOF-derived Ni-P bundle-like nanorods as high-performance substrate for design of electrochemical aptasensor toward cortisol detection. **IEEE Sensors Journal**, [*s. l.*], v. 23, p. 1770-1777, 2023.

67 WU, P. *et al*. Self-assembled multilayer Nb 2 C MXene/MnFe 2 O 4 electrochemical sensor with Schottky junctions for the detection of acetaminophen and dopamine. **Colloids and Surfaces A**: Physicochemical and Engineering Aspects, [*s. l.*], v. 667, p. 1-10, 2023.

68 LIU, N. *et al*. Gold nanoparticles-decorated peptide hydrogel for antifouling electrochemical dopamine determination. **Microchimica Acta**, [*s. l.*], v. 190, p. 2-10, 2023.

69 AGADI, N. P. *et al*. Fabrication of NiSe 2 decorated graphene oxide nanocomposite modified electrode as a high performance electrochemical sensor for carbamazepine. **Electroanalysis**, [*s. l.*], v. 35, n. 12, p. 1-12, 2023.

70 MUTHU D. *et al*. Reduced graphene oxide supported monoclinic bismuth vanadate nanoparticles as an electrocatalyst for selective determination of dopamine in human urine samples. **Materials Chemistry and Physics**, [*s. l.*], v. 297, p. 1-10, 2023.

71 LIAO, X. *et al*. An antifouling electrochemical sensor based on multiwalled carbon nanotubes functionalized black phosphorus for highly sensitive detection of carbendazim and corresponding response mechanisms analyses. **Microchemical Journal**, [*s. l.*], v. 190, p. 1-12, 2023.

72 EROGUL, S. *et al.* A new electrochemical sensor based on Fe 3 O 4 functionalized graphene oxide–gold nanoparticle composite film for simultaneous determination of catechol and hydroquinone. **Electrochimica Acta**, [*s. l.*], v. 186, p. 302–313, 2015.

73 TIAN, X. *et al.* Nonenzymatic electrochemical sensor based on CuO–TiO 2 for sensitive and selective detection of methyl parathion pesticide in ground water. **Sensors and Actuators B**: Chemical, [*s. l.*], v. 256, p. 135-142, 2018.

74 GAN, T. *et al*. Morphology-dependent electrochemical sensing properties of manganese dioxide-graphene oxide hybrid for guaiacol and vanillin. **Electrochimica Acta**, [*s. l.*], v. 147, p. 157–166, 2014.

75 NAGLES, E.; CERONI, M.; HURTADO, J. Simultaneous etection of tartrazine-sunset yellow in food samples using bioxide/carbon paste microcomposite with lanthanum and titanium. **Journal of Electrochemical Science and Technology**, [*s. l.*], v. 11, p. 421-429, 2020.

76 NAGLES, E. *et al*. Simultaneous electrochemical determination of paracetamol and allura red in pharmaceutical doses and food using a Mo(VI) oxide-carbon paste microcomposite. **Electroanalysis**, [*s. l.*], v. 33, n. 11, p. 2335-2344, 2021.

77 SI, X. *et al.* A sensitive electrochemical sensor for ofloxacin based on a graphene/zinc oxide composite film. **Analytical Methods**, [*s. l.*], v. 17, p. 1961-1967, 2018.

78 XIE, J. *et al*. Synthesis of zincn stannate and zinc stannate coated ano-CaCO 3 by homogeneous precipitation. **Journal of Chemical Research**, [*s. l.*], v. 35, p. 109-111, 2011.

79 SHOMAKHOV, Z. V. *et al.* Zinc stannate nanostructures for fast response gas sensors. **Russian Reviewed Scientific Edition**, [*s. l.*], v. 14, p. 726-735, 2022.

80 BARTH, T. F. W.; POSNJAK, E. Spinel structures: with and without variate atom equipoints. **Zeitschrift fur Kristallographie**: Crystalline Materials, [*s. l.*], v. 82, p. 325-341, 1932.

81 POIX, P. On some crystallographic and magnetic determinations of oxygen. Compounds having spinel structure, containing tin, titanium, magnesium, zinc and cobalt. **Annali di Chimica**, [*s. l.*], v. 10, p. 49-79, 1965.

82 COFFEEN, W. W. Ceramic and dielectric properties of the stannates. **Journal of the American Ceramic Society**, [*s. l.*], v. 36, p. 207-214, 1953.

83 YU, J. H.; CHOI, G. M. Selective CO gas detection of Zn 2 SnO 4 gas sensor. **Journal of Electroceramics**, [*s. l.*], v. 8, p. 249-255, 2002.

84 ARAFAT, M. M.; ONG, J. Y.; HASEEB, A. S. M. A. Selectivity shifting behavior of Pd nanoparticles loaded zinc stannate/zinc oxide (Zn 2 SnO 4 /ZnO) nanowires sensors. **Applied Surface Science**, [*s. l.*], v. 435, p. 928-936, 2018.

85 BELLIARD, F.; CONNOR, P. A.; IRVINE, J. T. S. Novel tin oxide-based anodes for Li-íon batteries. **Solid State Ionics**, [*s. l.*], v. 135, p. 163-167, 2000.

86 ZHANG, Y. *et al*. Crystal growth of undoped ZnO films on Si substrates under different sputtering conditions. **Journal of Crystal Growth**, [*s. l.*], v. 243, p. 439-443, 2002.

87 AKKAPINYO, C. *et al*. Disposable electrochemical sensor for food colorants detection by reduced graphene oxide and methionine film modified screen printed carbon electrode. **Molecules**, [*s. l.*], v. 26, p. 1-18, 2021.

88 BAGHERI, H. *et al*. Composite of Cu metal nanoparticles-multiwall carbon nanotubes-reduced graphene oxide as a novel and high performance platform of the electrochemical sensor for simultaneous determination of nitrite and nitrate. **Journal of Hazardous Materials**, [*s. l.*], v. 324, p. 762-772, 2017.

89 FARIA, L. V. D. *et al*. Adsorptive stripping voltammetric determination of chloramphenicol residues in milk samples using reduced graphene oxide sensor. **Analytical Methods**, [*s. l.*], v. 13, p. 5711-5718, 2021.

90 GHANBARI, M. H. *et al*. An electrochemical sensor based on poly (l-cysteine)-AuNPs reduced graphene oxide nanocomposite for determination of levofloxacin. **Microchemical Journal**, [*s. l.*], v. 147, p. 198-206, 2019.

91 LIU, G. *et al*. Electrochemical approach toward reduced graphene oxide-based electrodes for environmental applications: a review. **Science of the Total Environment**, [*s. l.*], v. 778, p. 1-14, 2021.

92 CHABOT, V. *et al*. A review of graphene and graphene oxide sponge: material synthesis and applications to energy and the environment. **Energy & Environment Science**, [*s. l.*], v. 5, p. 1564-1596, 2014.

93 RAZAQ, A. *et al*. Review on graphene, graphene oxide, reduced graphene oxide-based flexible composites: from fabrication to applications. **Materials**, [*s. l.*], v. 15, n. 3, p. 1-17, 2022.

94 GEIM, A. K.; NOVOSELOV, K. S. The rise of graphene, nanoscience and technology: a collection of reviews from nature journals. **Nanoscience and Technology**, [*s. l.*], p. 11–19, 2009.

95 KHAN, Z. U. *et al*. A review of graphene oxide, graphene buckypaper, and polymer/graphene composites: properties and fabrication techniques. **Journal of Plastic Film and Sheeting**, [*s. l.*], v. 32, p. 336-379, 2016.

96 EDA, G.; CHHOWALLA, M. Chemically derived graphene oxide: Towards large-area thin-film electronics and optoelectronics. **Advanced Materials**, [*s. l.*], v. 22, n. 22, p. 2392-2415, 2010.

97 MADURAIVEERAN, G.; JIN, W. Nanomaterials based electrochemical sensor and biosensor platforms for environmental applications. **Trends in Environmental Analytical Chemistry**, [*s. l.*], v. 13, p. 10-23, 2017.

98 KIMMEL, D. W. *et al*. Electrochemical sensors and biosensors. **Analytical Chemistry**, [*s. l.*], v. 84, n. 2, p. 685-707, 2012.

3 MANUSCRITO 1: ELECTROCATALYTIC AMPLIFIED SENSOR FOR DETERMINATION OF OFLOXACIN USING Zn_2SnO_4/REDUCED GRAPHENE OXIDE COMPOSITE AS SURFACE-MODIFYING AGENT[1]

ABSTRACT

This study describes an electroanalytical approach for the quantification of ofloxacin (OFL) through an electrochemical sensor based on a glassy carbon electrode modified with composite material (Zn_2SnO_4-rGO/GCE) using square wave voltammetry. Zn_2SnO_4 was synthesized by hydrothermal treatment and characterized by X-ray diffraction, Fourier-transform infrared and Raman spectroscopy and scanning electron microscopy. The analysis suggests a synergistic effect between the composite material, indicating irreversible oxidation of OFL in its protonated form (OFL^+), involving two electrons. The electroanalytical methodology was successfully applied to determine OFL in ophthalmic solutions samples, achieving recovery rates ranging from 98.03% to 104.91%. Furthermore, it demonstrated high stability in both repeatability (RSD = 3.20%, n = 12) and reproducibility (RSD = 4.64%, n = 7), with no observed interference when additional substances were added. These results suggest the potential electroanalytical application of Zn_2SnO_4 and recommend the developed methodology as an alternative tool for OFL determination in commercial pharmaceutical samples.

Keywords: ofloxacin; antibiotic; reduced graphene oxide; square-wave voltammetry.

---

[1] Artigo publicado no *Journal of The Electrochemical Society* e adaptado quanto à formatação para inclusão nesta tese.
Título: Electrocatalytic amplified sensor for determination of ofloxacin using Zn_2SnO_4/reduced graphene oxide composite as surface-modifying agent.
Autores: Janevane S. de Castro[*,**], Anderson V. Chaves[**], Pierre B. A. Fechine[**], Raíssa C. de Oliveira[**], Francisco W. P. Ribeiro[***], Pedro de Lima-Neto[**], Dieric S. Abreu[****], Cristiani L. C. G. de Oliveira[*****], Adriana N. Correia[**,*]
[*]Departamento de Engenharia de Alimentos, Universidade Federal do Ceará, Campus do Pici, 60440-900, Fortaleza, CE, Brazil
[**]Departamento de Química Analítica e Físico-Química, Universidade Federal do Ceará, Campus do Pici, 60440-900, Fortaleza, CE, Brazil
[***]Instituto de Ciências Exatas e da Natureza, Universidade da Integração Internacional da Lusofonia Afro-Brasileira, Campus das Auroras, 62790-970, Redenção, CE, Brazil
[****]Laboratório de Materiais e Dispositivos, Departamento de Química Analítica e Físico-Química, Centro de Ciências, Universidade Federal do Ceará, Campus do Pici, Fortaleza, CE
60440-900, Brazil
[*****]Departamento de Farmácia, Universidade Federal do Ceará, Campus do Porangabussu, 60430-372, Fortaleza, CE, Brazil
Corresponding author: Prof. Adriana Nunes Correia: E-mail address: adriana@ufc.br

1 Introduction

Ofloxacin (OFL, IUPAC name: (RS)-7-fluoro-2-methyl-6-(4-methylpiperazin-1-yl)-10-oxo-4-oxa-1-azatricyclo[7.3.1.$0^{5,13}$]trideca-5(13),6,8,11-tetraene-11-carboxylic acid (1) is a broad spectrum quinolone antibiotic, belonging to the second generation of fluoroquinolones (2). Fluoroquinolones possess at least one fluorine substituent group (–F) in its quinoline ring, promoting higher efficiency in the antimicrobial activity of the drug against gram-negative and gram-positive bacteria. This class of bactericides also possess clinical applications in both humans and veterinary medicine (cattle, equines, canines, and felines), being specially used in ophthalmic and urinary tract infections, while it also shows efficacy against respiratory and gastrointestinal tract infections (2).

Fluoroquinolone's mechanism of action is highly affected by its physicochemical properties, especially due to its ionization in the function of the medium pH and its capacity for complexation with metallic ions (3). OFL has two ionizable functional groups, which confers to it two dissociation constants, corresponding to the carboxyl (pKa_1 of 5.89 to 6.05) and amino group (pKa_2 of 7.9 to 8.2) (4, 5). Therefore, it is highlighted that the protonation of the analyte is dependent on the relation between the medium pH and the values of pKa, as shown in Figure 1A.

Figure 1 – (A) Species present in the OFL acid-base balance. (B) Distribution (α') of the OFL species with the pH using the acid-base equilibrium and mass-balance equations

(A)

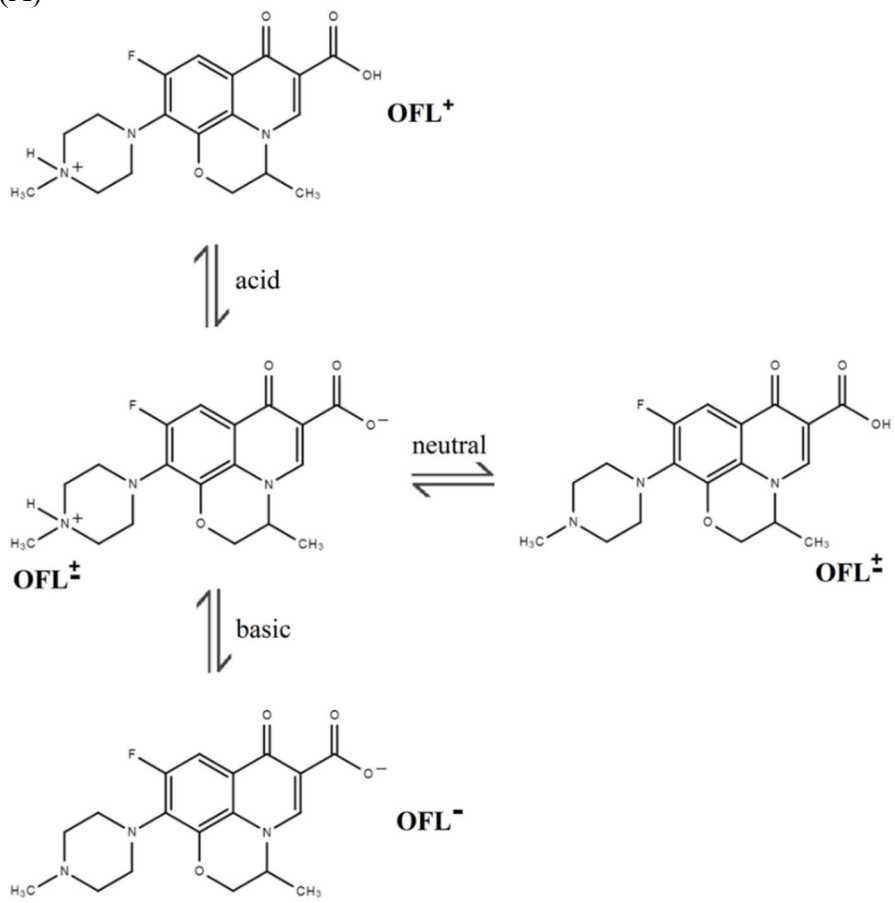

(B)

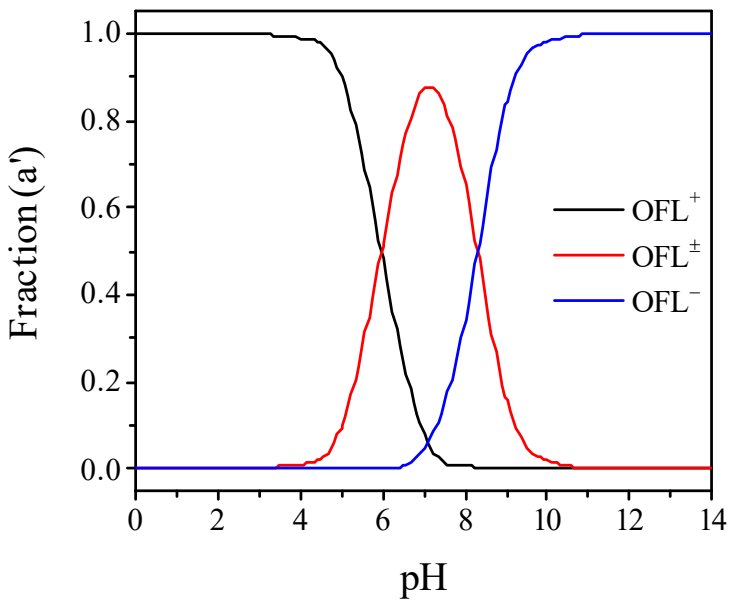

Fonte: (6).

Literature describes numerous successful applications of simple oxide-based composites on development of electrochemical sensors, such as Fe_3O_4 and rGO applied in catechol and hydroquinone detection (7), CuO and TiO_2 in methyl parathion detection (8), MnO_2 and graphene oxide (GO) to determine guaiacol and vaniline (9), usage of ZnO and Gr to detect OFL (10), and other applications.

Despite records of the use of the ZnO-Gr nanocomposite in the development of an electrochemical sensor for OFL detection, the linearity range obtained was at relatively high concentrations (1-100 μmol L^{-1}), presenting a value of LOD equal to 0.33 μmol L^{-1} and very low sensitivity to the drug (0.089 A mol^{-1} L); compromising its use in samples with low concentrations of OFL (10).

Mixed oxides have raised much of the scientific community´s interest due to their numerous technological applications. Some oxides are based on zinc and tin (Zn_2SnO_4, $ZnSnO_2$ e $ZnSnO_3$), known generically as zinc stannates (11). Its majority is synthesized from ZnO and SnO_2 reactions at high temperatures (above 1000 ºC) or from reactions between $Zn(CH_3COO)_2$ and $SnCl_4$ in alkaline medium, although the synthesis cannot promote complete conversion of ZnO and SnO_2 in zinc stannate (11). The literature reports the development of the Zn_2SnO_4/graphene composite, prepared using a hydrothermal route, where the octahedral Zn_2SnO_4 crystals remained firmly confined by the graphene sheets, forming a unique hybrid structure, enhancing Li storage performance (12).

Zn_2SnO_4 has diamagnetic and semiconductor properties (13) and is specially applied in toxic gas sensing (14). However, no records were found in the literature of applications of Zn_2SnO_4 in developing electrochemical sensors for any drugs, making its use for such purposes unprecedented. Some studies are reported in the literature concerning using simple/mixed oxide-based composites and rGO in the development of electrochemical sensors (15, 16, 17). rGO presents good dispersion in polar mediums and possesses numerous reactive sites (epoxy, hydroxyl, and carboxyl) in its basal structure, qualifying this material as an excellent material for electrochemical sensors, considering sensibility, limit of detection (LOD) and limit of quantification (LOQ) (17, 18).

Most of the drugs (among them the OFL) have official methodologies of detection based on chromatographic techniques, which often make the determination process more difficult due to the high cost of analysis. In that regard, electroanalytical methodologies have been presented as an alternative for drug detection, especially due to their ease of operation, high sensitivity, selectivity, low cost of instrumentation and absence of organic solvents (19).

Therefore, the objective of this investigation is to propose a simple electroanalytical methodology to determine and quantify OFL in pharmaceutical samples using an electrochemical sensor based on the modification of the glassy carbon surface with the composite Zn_2SnO_4-rGO (Zn_2SnO_4-rGO/GCE) and using square-wave voltammetry (SWV) as an electroanalytical technique; also envisioning the possibility of tests and applications in more complex samples (such as water matrices), which could become an alternative tool for controlling and supervising the drug in waters. The study also addresses the relevant relationship between the OFL speciation diagram and the electrostatic nature of the modified electrode surface.

2 Material and methods

2.1 Chemicals and reagents

OFL (≥ 99.9%), Nafion® (≥ 95.0%), and rGO were acquired from Sigma-Aldrich®. Pharmaceutical samples containing OFL (sterile ophthalmic solution, OFLOX®) were purchased from Allergan (Brazil). OFL standards were produced by dissolving a determined quantity in ethanol (96%). Zn_2SnO_4 was synthesized using $SnCl_2.2H_2O$ (≥ 98.0%) and $Zn(CH_3COO)_2.2H_2O$ (≥ 98.0%), both acquired from Dinâmica®. H_2SO_4 solutions in 5.0×10^{-3} mol L^{-1}, 5.0×10^{-2} mol L^{-1} and 5.0×10^{-1} mol L^{-1} were prepared. Britton-Robinson (BR), Sörensen, and Clark-Lubs buffer solutions were prepared with an adjusted pH of 2.0, and phosphate buffer solution (PBS) was prepared with an adjusted pH of 7.4. $K_4[Fe(CN)_6]$ / $K_3[Fe(CN)_6]$ 1.0×10^{-3} mol L^{-1} solution was prepared in KCl 1.0×10^{-1} mol L^{-1}. All reagents were of analytical grade. Ultra-purified water (18.2 MΩ cm) was used in the glassware cleaning and the preparation of the solutions, obtained through the Milli-Q® (Millipore, Inc.) system.

2.2 Apparatus

A Micronal® pHmeter (model B474A) was used to measure the solutions' pH. A Quimis® (model Q335D) ultrasonic bath was used to homogenize the composite suspension and perform the GCE cleaning post-polishment procedure. To homogenize the solution in the electrochemical cell and to clean the procedure of the modified GCE surface, a Gehaka® (model AA-840) magnetic stirrer was used, along with a magnetic bar. A PGSTAT 101 Metrohm®

(Eco Chemie) potentiostat/galvanostat was connected to a computer with Nova software (version 2.1.3) was used. A conventional three-electrode system was carried out with a GCE (BASi®, 3mm diameter) as the working electrode, a platinum plate as the counter electrode (1.03 cm^2) and an $Ag_{(s)}/AgCl_{(s)}/Cl^-_{(aq)}$ (saturated KCl) as the reference electrode. Chromatographic analysis was performed using a Waters® (model Alliance 2695) HPLC, coupled to a UV-Vis detector (diode array adjusted at 294 nm) and a reverse phase C18 column Eclipse plus from Agilent (250 mm × 4.6 mm, 5 μm particle size), using isocratic elution with a mobile phase consisting of 60% acetonitrile and 40% acetic acid 1% (pH 7,0), injection volumes of 20 μL, 1.0 mL min^{-1} flow, while the column was kept at 35 ºC.

2.3 Synthesis of Zn_2SnO_4

Zn_2SnO_4 was synthesized using the hydrothermal method. Briefly, separate solutions of tin chloride dehydrate ($SnCl_2.2H_2O$) and zinc acetate dehydrate ($Zn(CH_3COO)_2.2H_2O$) were prepared separately with a 1:2 molar ratio, respectively. After stirring the mixture for 10 minutes, the pH was adjusted by adding 0.75 g NaOH, and the solution was left to settle for 15 min. The solution was transferred into a Teflon-lined steel autoclave and heated at 200 ºC for 22 h. After the reaction was complete, the autoclave was cooled, and the resulting precipitate was separated by centrifugation and then washed several times with deionized water and ethanol to remove any residual ions in the solution. Finally, the sample was dried at 80 ºC for 12 h. The chemical reaction that represents the formation of Zn_2SnO_4 particles in an alkaline medium via the hydrothermal route is shown in equation (1): (12)

$$2Zn^{2+}_{(aq)} + Sn^{4+}_{(aq)} + 8OH^-_{(aq)} \rightarrow Zn_2SnO_{4(s)} + 4H_2O_{(l)} \quad (1)$$

2.4 Characterization of Zn_2SnO_4

X-ray diffraction (XRD) measurements were conducted at room temperature using a Bruker diffractometer (D8 Advance) with CuKα tube (λ = 1.5418 Å), equipped with a LynxEye linear detector. The instrumental parameters were a voltage of 40 kV and a current of 40 mA, scanning in the 2θ range of 10 - 90° with a step of 0.02. For Fourier transform infrared spectroscopy (FTIR) spectra, a Perkin-Elmer (model 2000 FT-IR) spectrophotometer was used

with a scan range from 4000 to 400 cm^{-1}. To obtain the pellets, the sample was previously dried to remove water absorption and dispersed in KBr in a 1:10 ratio, which was molded with a hydraulic press. Raman spectroscopy of powder and thin film samples was conducted using the LabRam HR Raman Spectrometer (Horiba) equipped with a microscope (BX41, Nikon). A 100x objective lens (UMPlanFl, Olympus) with a numerical aperture (NA) of 0.90 was employed to focus a He-Ne laser (Melles Griot) with a wavelength of 632.8 nm on the surface of the thin film sample for excitation. The Raman scattered light was dispersed using a 600 gr/mm diffraction grating and then projected onto a Peltier cooling charge-coupled device (CCD) detector. Raman spectra were acquired at multiple points across the thin films, with an acquisition time of 10 s at each point, and each spectrum represented an average of 5 readings. The resulting Raman spectra were processed using the Fityk program (20) employing a nonlinear deconvolution algorithm known as the Levenberg-Marquardt method. Spectrum fits were performed assuming a linear baseline, and all deconvoluted curves exhibited a Lorentzian distribution shape. The micrograph images of the samples were obtained by scanning electron microscopy (SEM, Quanta® 450 FEG electron microscope and FEI Ambiental) with an acceleration of up to 20 kV. The samples were fixed onto carbon strips, air-dried, and covered with a thin gold layer to ensure good conductivity.

2.5 Sensor preparation

The individual suspensions of Zn_2SnO_4 and rGO were prepared both at 1.0 mg mL^{-1} in dimethylformamide (DMF), while the composite suspension (Zn_2SnO_4-rGO) was prepared by mixing 1.0 mg of both Zn_2SnO_4 and rGO in 1.0 mL (DMF) with 0.5% Nafion®. All prepared suspensions were homogenized in an ultrasonic bath for 120 min. Before modification, the GCE surface was polished using 3 μm diamond paste, being cleaned in an ultrasonic bath in ethanol (96%) and ultrapure water, respectively, for 3 minutes each. Afterward, the GCE was modified with Zn_2SnO_4-rGO composite suspension using a 1.5 μL aliquot, being dried shortly after in a drying oven at ± 60 °C for 15 min.

2.6 Electrochemical experiments

Electrochemical experiments were conducted at 25 ºC using 10 mL of supporting electrolyte in the electrochemical cell. Evaluations of the electrochemical properties of the

sensor were performed with cyclic voltammetry (CV) between 0.0 and 1.5 V in 5.0×10^{-1} mol L^{-1} H_2SO_4, varying the scan rate (ν) from 10 up to 200 mV s^{-1}.

To study the charge transfer process in the electrode surface, electrochemical impedance spectroscopy (EIS) was carried out in presence of 1.0×10^{-3} mol L^{-1} $K_4[Fe(CN)_6]/K_3[Fe(CN)_6]$, with a molar ratio 1:1 (Fe^{2+}/Fe^{3+}) in 1.0×10^{-1} mol L^{-1} KCl, ranging from 60 kHz to 100 mHz, with a amplitude perturbation of 5 mV.

SWV measurements were carried out from 0.0 up to 1.5 V, with experimental conditions optimization being evaluated in different buffer solutions: Britton-Robinson (BR) pH 2.0; Sörensen pH 2.0; Clark-Lubs pH 2.0; PBS pH 7.4) and H_2SO_4 (0.005 - 0.5 mol L^{-1}) and voltammetric parameters: f (10 to 150 s^{-1}), a (10 to 50 mV) and ΔE_s (1 to 5 mV). Between the consecutive SWV measurements, solutions were kept under stirring for 3 min and rested, followed by a resting time of at least 30 s. After optimizing the initial parameters, an ideal cleaning procedure was evaluated for the modified electrode surface submerged in solution through mechanical stirring for 60, 120, 180 and 240 s to assure OFL desorption out of the electrode surface.

2.7 Electroanalytical methodology

After the optimization of the voltammetric parameters, analytical curves were obtained using the standard addition method. Analytical parameters such as linearity range, LOD, LOQ, correlation coefficient (r), sensitivity, confidence intervals, precision (repeatability and reproducibility), accuracy (recovery percentage), BIAS% and relative standard deviation (RSD%) were determined according to described in the literature (21, 22, 23, 24, 25). The LOD and LOQ were calculated using equations 2 and 3 (21, 25):

$$\mathbf{LOD} = \frac{\mathbf{3.3\sigma}}{\mathbf{S}} \quad (2)$$

$$\mathbf{LOQ} = \frac{\mathbf{10\sigma}}{\mathbf{S}} \quad (3)$$

where:

σ = standard deviation of the linear coefficient (intercept) of the analytical curve;

S = the slope of the analytical curve.

Values of LOD and LOQ calculated for OFL on Zn_2SnO_4-rGO/GCE were compared with values obtained for HPLC methods.

2.8 Application of methodology in commercial pharmaceutical formulation

The efficiency of the electrochemical methodology developed to determine OFL was assessed through recovery tests in commercial pharmaceutical samples (sterile ophthalmic solution) utilizing the proposed sensor (Zn_2SnO_4-rGO/GCE). The obtained results were compared with values obtained from HPLC (official methodology recommended by the Brazilian Pharmacopoeia) (26). Comparisons between concentration averages of recovered OFL obtained from the two methodologies were conducted through *t*-test, with its variances being evaluated by *F*-test (21, 22).

3 Results and discussion

3.1 Characterization of the Zn_2SnO_4

An electrochemical sensor performance is affected by the electrode surface modifiers (27). Aspects such as its morphology, chemical bonds, molecular structure, and geometry are topics that must be known to obtain detailed information about the surface modifier material. With that in mind, synthesized Zn_2SnO_4 was characterized through XRD, FTIR, RS and SEM.

XRD was used to study the crystallinity of the material. As seen, the sample presented a single phase of zinc stannate compound (Zn_2SnO_4), which presented a cubic inverse spinel crystalline structure with a Fd3m spatial group, No. 028235, according to the crystallographic database (Inorganic Crystal Structure Database, ICSD), Fig. 2A (28, 29). The crystallite unit cell showed tetrahedral sites occupied by Zn^{2+} ions (ZnO_4) and octahedral sites occupied by zinc and tin ions (ZnO_6 and SnO_6), respectively. (Fig. 2B) The results obtained provide relevant information for a more detailed physical characterization of the spatial structure of the Zn_2SnO_4 crystallite, including presenting the basic physical measurements of the crystallite structure.

Figure 2 – (A) Diffraction pattern obtained from Zn_2SnO_4 sample (B) Crystal structure of Zn_2SnO_4

(A)

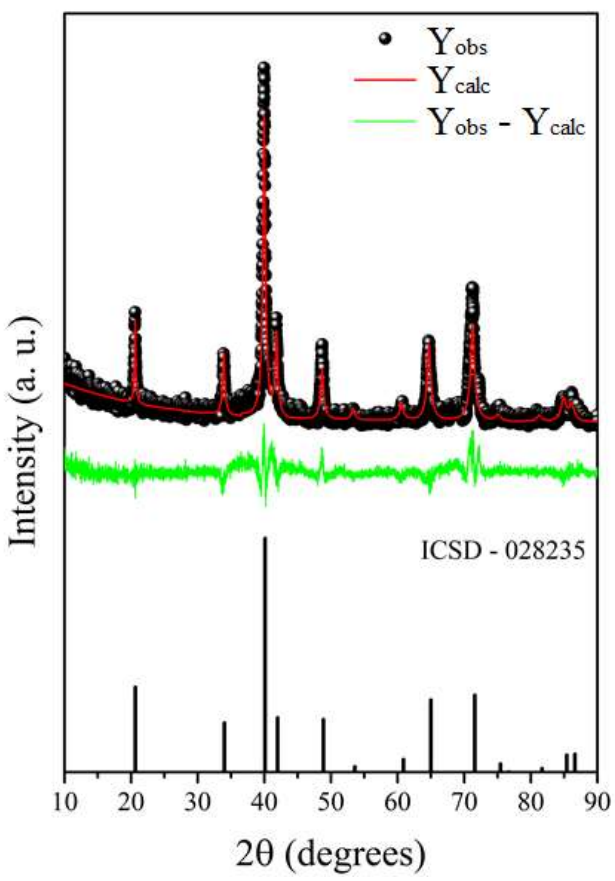

(B)

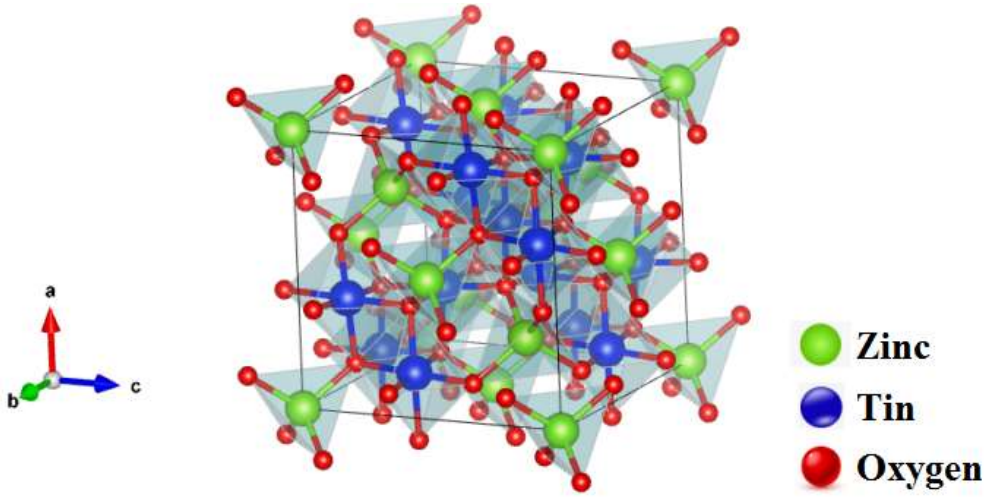

Fonte: (6).

Table 1 shows the results of the refinement and lattice parameters of the sample through Rietveld method using GSAS/EXPGUI software (30, 31), indicating a value of *S*

(goodness of fit) of 1.23 and weighted profile *R*-value (R_{wp}) of the 26.07 %, indicating a good agreement with data obtained in the literature (32). The crystallite average diameter size for the Zn_2SnO_4 sample was 22.96 (± 0.51) nm through the Scherrer equation (29, 33). Fig. 3 shows SEM image of the Zn_2SnO_4. It can be found that the material presents a truncated octahedron morphology. This geometry was also found by other authors who used the same synthetic route (hydrothermal method) used in the present work (34, 35). The average particle size of octahedrons was 1.16 (± 0.24) μm.

Table 1 – Pattern structural results refined by Rietveld method of the Zn_2SnO_4 sample

Crystalline phase	Mass (%)	Lattice parameters			Density (g cm^{-3})	Diameter (nm)
		a (Å)	b (Å)	c (Å)		
Zn_2SnO_4	100	86.93	86.93	86.93	11.08	22.96

Fonte: (6).

Figure 3 – SEM image obtained for surface with Zn_2SnO_4 at 10.000x magnification

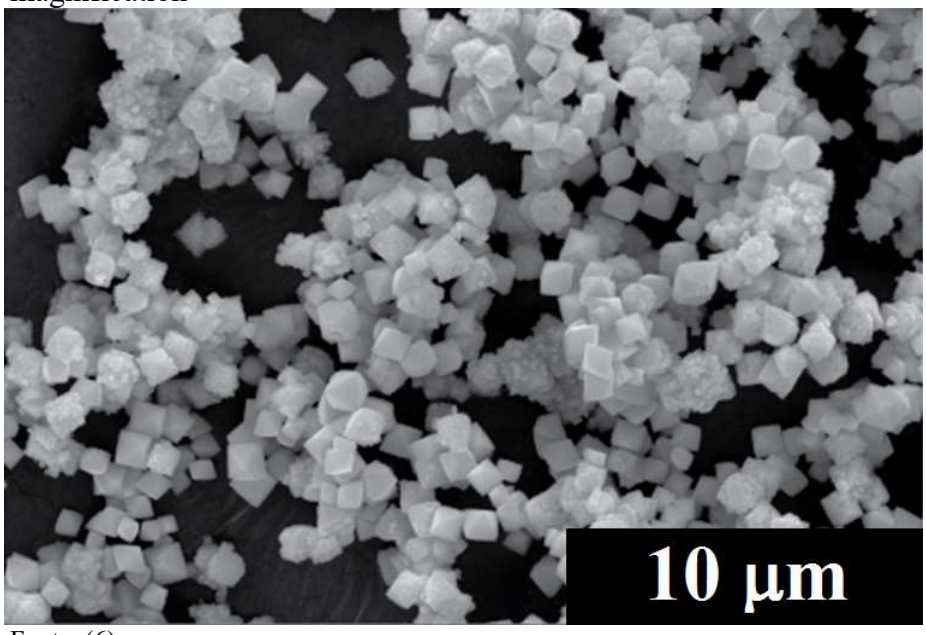

Fonte: (6).

FTIR spectrum obtained for Zn_2SnO_4 (Fig. 4) points towards 620 cm^{-1} and 578 cm^{-1} absorption band, which, according to literature, corresponds to natural oxygen bonds vibrations (Sn–O) and (Zn–O); such results back up the XRD crystallographic structure presented in this work (36). FTIR spectrum for Zn_2SnO_4 described a broad band around 3434

cm^{-1} from O–H intermolecular hydrogen bonds, 620 cm^{-1} and 578 cm^{-1} bands can be attributed to Sn–O and Zn–O vibrations, respectively, due to the occurrence of water molecules in the interlamellar space of numerous crystallite types, which are resultant of its own structural organization (36, 37).

Figure 4 – FTIR spectra for Zn_2SnO_4

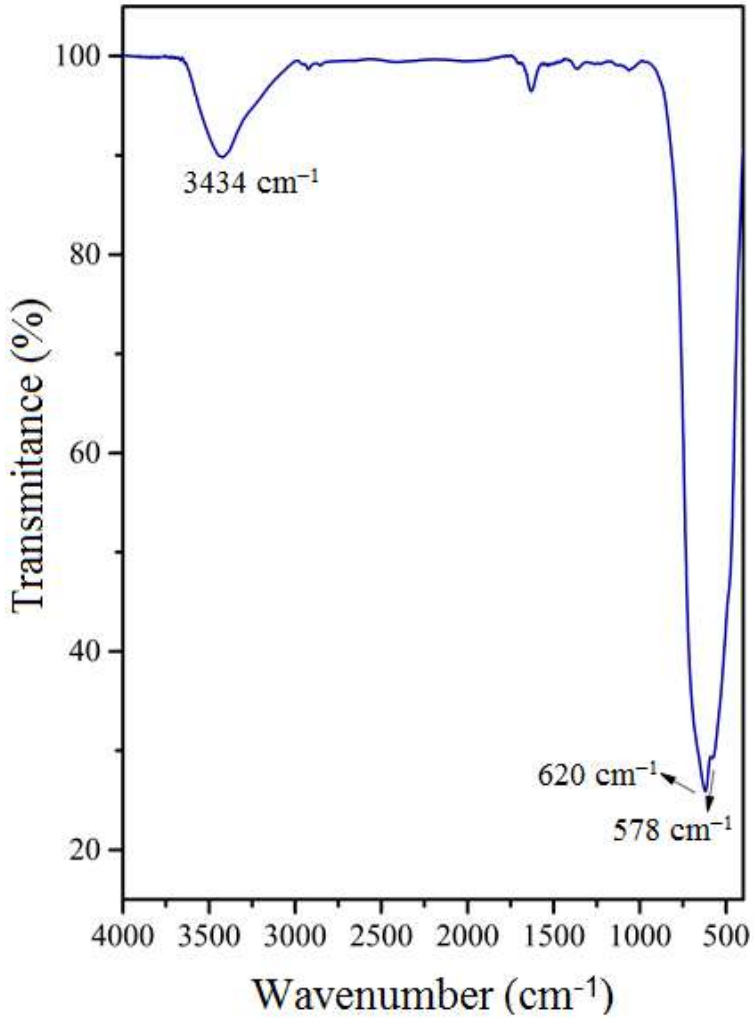

Fonte: (6).

Raman spectroscopy was utilized to assess the stretching vibrations of the chemical bonds present in the as-prepared powder of Zn_2SnO_4. Figure 1S (Supplementary Material) shows the Raman spectrum of Zn_2SnO_4 powder, displaying characteristic peaks at 667 cm^{-1}, 534 cm^{-1}, and 434 cm^{-1}. According to group theory, the inverse spinel Zn_2SnO_4 exhibits a total number of vibration modes: $\Gamma = 1A_{1g} + 1E_g + 3F_{2g} + 7F_{1u}$, where $1A_{1g}$, $1E_g$, and $3F_{2g}$ are active

Raman modes (38, 39, 40). The data obtained confirm a cubic inverse spinel crystal structure for Zn_2SnO_4, supporting the results obtained in this work using XRD and FTIR techniques.

In addition, Raman spectroscopy was used to characterize the composite thin film Zn_2SnO_4-rGO and to elucidate the role of Zn_2SnO_4 in influencing the structural and electronic properties of rGO within the composite, including defects and disorder. To eliminate the effect of the background Raman modes from the glassy carbon electrode, thin films of Zn_2SnO_4, rGO, and the composite Zn_2SnO_4-rGO were prepared on gold substrates following the procedure outlined in section 2.4. The Raman spectra of the rGO and Zn_2SnO_4-rGO (Fig. 5. (b) and (c) respectively) show the two main feature D and G bands centered at 1327 cm^{-1} and 1589 cm^{-1} respectively (41). Besides the typical D and G bands, the Raman spectrum of rGO exhibits additional bands centered at 1150 cm^{-1} (D′ band) and 1516 cm^{-1} (D″ band). Conversely, the Raman spectrum of the Zn_2SnO_4-rGO composite shows similar peaks slightly shifted to 1148 cm^{-1} (D′ band), 1519 cm^{-1} (D″ band) and 1426 cm^{-1} (D‴ band) also appeared. The appearance of new D bands in the Raman spectrum is linked to defects that interrupt the regular graphene lattice (42). These defects stem from the disordered graphitic structure induced by the presence of sp^3 bonds and are also connected to the existence of amorphous phases (41, 42, 43). The structural defects and imperfections on the nanosheet basal plane of graphene were commonly identified using the intensity ratio of the D and G bands (Tuinstra–Koenig correlation, I_D/I_G) (41, 44). In the gold-coated film of the Zn_2SnO_4-rGO composite, an I_D/I_G ratio of 1.56 shows a decrease compared to the I_D/I_G ratio of 1.75 for the gold-coated film of pristine rGO, revealing an increase in the crystallinity of the rGO in the composite (42). Although this behavior indicates an increase in crystallinity, the presence of other featured bands (observed additional D bands) exhibits an opposite trend.

Figure 5 – Raman spectra of gold-coated films for (a) Zn_2SnO_4-rGO composite, (b) rGO, and (c) Zn_2SnO_4, within the range of 300–1800 cm^{-1}. The white circles (○) represent the experimental Raman spectra, the solid red lines (—) indicate the fitted spectra, and the solid black lines (—) depict the best Lorentzian fitting curves.

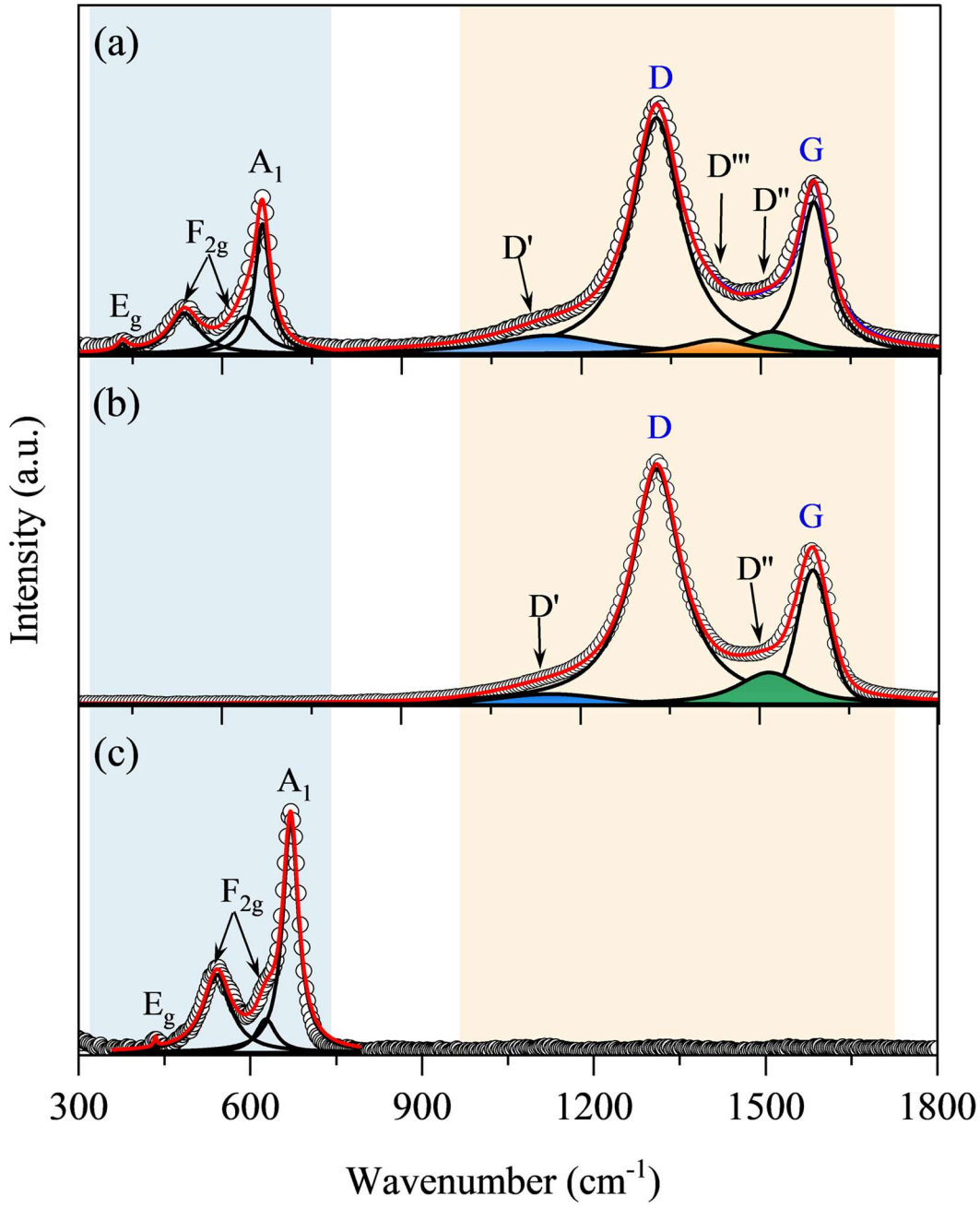

Fonte: (6).

Notably, there is an increase in the D′ band in the Raman spectrum of the Zn_2SnO_4-rGO composite (Figure 5. (a)) compared to that in rGO (Figure 5. (b)). This behavior is linked to the oxidation level of the rGO sheets, where the intensity rises, and the peak position shifts to lower wavenumber values as the oxygen content increases (42). This aligns with the presence

and interaction of oxides from Zn_2SnO_4 near rGO. A comparison between Raman spectra of gold-coated film Zn_2SnO_4 (Figure 5. (c)) and Zn_2SnO_4-rGO composite (Figure 5. (c)) show evidence of the interaction between Zn_2SnO_4 and reduced graphene oxide. The Raman spectrum of the gold-coated film of pristine Zn_2SnO_4 displays characteristic peaks at 670 cm^{-1} (A_{1g}), attributed to the symmetric stretching of the Zn–O bonds in ZnO_4 tetrahedra; 541 cm^{-1} and 627 cm^{-1} (F_{2g}), and 434 cm^{-1} (E_g) representative of the vibrations of Zn–O and Sn–O in octahedral sites (32). Meanwhile, in the gold-coated film of the Zn_2SnO_4-rGO composite (Figure 5 (c)), the Raman spectra within the Zn_2SnO_4 modes region (400-760 cm^{-1}) exhibit a slight downshift in the A_{1g} band (667 cm^{-1}) and an opposite trend in the F_{2g} bands: a slight downshift to 536 cm^{-1} and an upward shift to 640 cm^{-1}. We attribute this behavior to the anisotropic interaction of Zn–O and Sn–O in octahedral sites with the rGO, causing the shift of the F_{2g} bands towards lower and higher wavenumbers, respectively, due to changes in the chemical bond length. The shorter bond length results in a shift to higher wavenumbers, an ordinary phenomenon in vibrational spectroscopy.

3.2 Characterization of modified electrode surfaces

SEM images (Fig. 6 A-E) for GCE, Zn_2SnO_4/GCE, rGO/GCE and Zn_2SnO_4-rGO/GCE surfaces were obtained to evaluate the surface morphology.

Figure 6 – SEM images obtained for the surfaces of GCE (A), rGO/GCE (B) and Zn_2SnO_4/GCE (C) at 10.000x magnification; and Zn_2SnO_4-rGO/GCE (D) and (E) respectively with magnifications of 10.000x and 150.000x

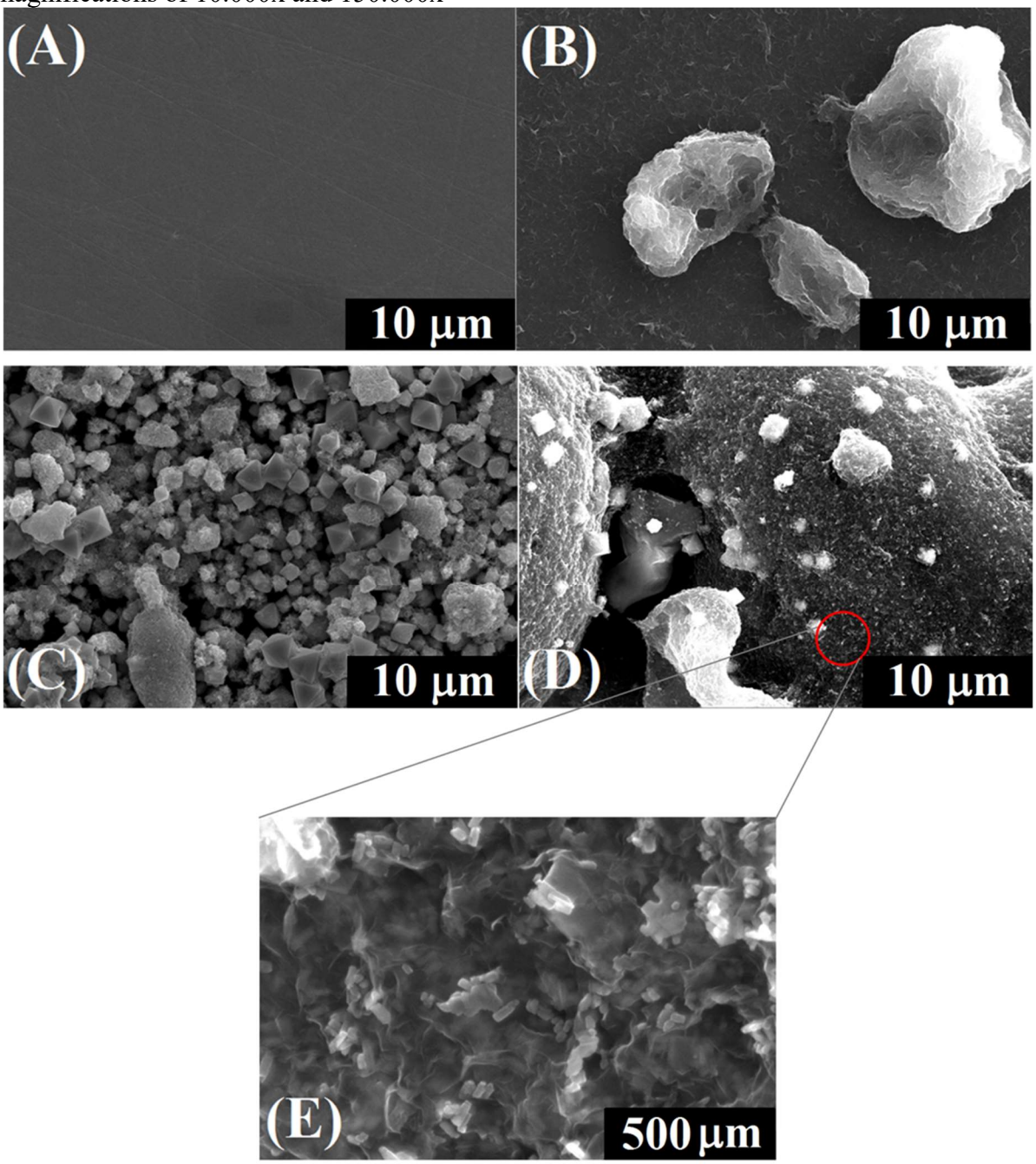

Fonte: (6).

GCE (Fig. 6A) presented a regular and uniform electrochemical surface, while in rGO/GCE (Fig. 6B) compact layers were observed, possibly explained by the stability granted by (π-π) interactions that are present in rGO structure (45, 46). Zn_2SnO_4/GCE surface (Fig. 6C) showed a structure formed primarily by isolated crystals, confirming once more the cubical structure formed by ZnO_4 tetrahedrons and ZnO_6/SnO_6 octahedrons (47). Zn_2SnO_4-rGO/GCE

image (Figs. 6D and 6E) illustrates the proposed composite's morphology, showing both the components' aggregation and synergism amidst the dispersion of the material.

3.3 Electrochemical performance of the modified GCE in the ferrocyanide/ferricyanide system

EIS provides data on electrolyte resistance (R_{Ω}), also known as solution resistance (R_S); and on the charge transfer resistance (R_{tc}). The diameter of the arc (semicircle) observed is related to the resistance that the electrode surface offers to the charge transfer process so high R_{tc} values indicate greater difficulty in the occurrence of redox processes.

Values of charge transfer resistance (R_{ct}) for GCE, Zn_2SnO_4/GCE, rGO/GCE and Zn_2SnO_4-rGO/GCE were evaluated through EIS in $K_4[Fe(CN)_6]/K_3[Fe(CN)_6]$ + KCl, as shown in the Nyquist diagrams (Fig. 7A).

Figure 7 – (A) Nyquist plots for GCE, rGO/GCE, Zn_2SnO_4/GCE and Zn_2SnO_4-rGO/GCE in 1.0×10^{-3} mol L^{-1} $K_4[Fe(CN)_6]/K_3[Fe(CN)_6]$ (1:1) and 1.0×10^{-1} mol L^{-1} KCl. The insert corresponds to the Nyquist plots in the region of high frequencies. (B) Fitting of equivalent electrical circuit obtained for Zn_2SnO_4-rGO/GCE

(A)

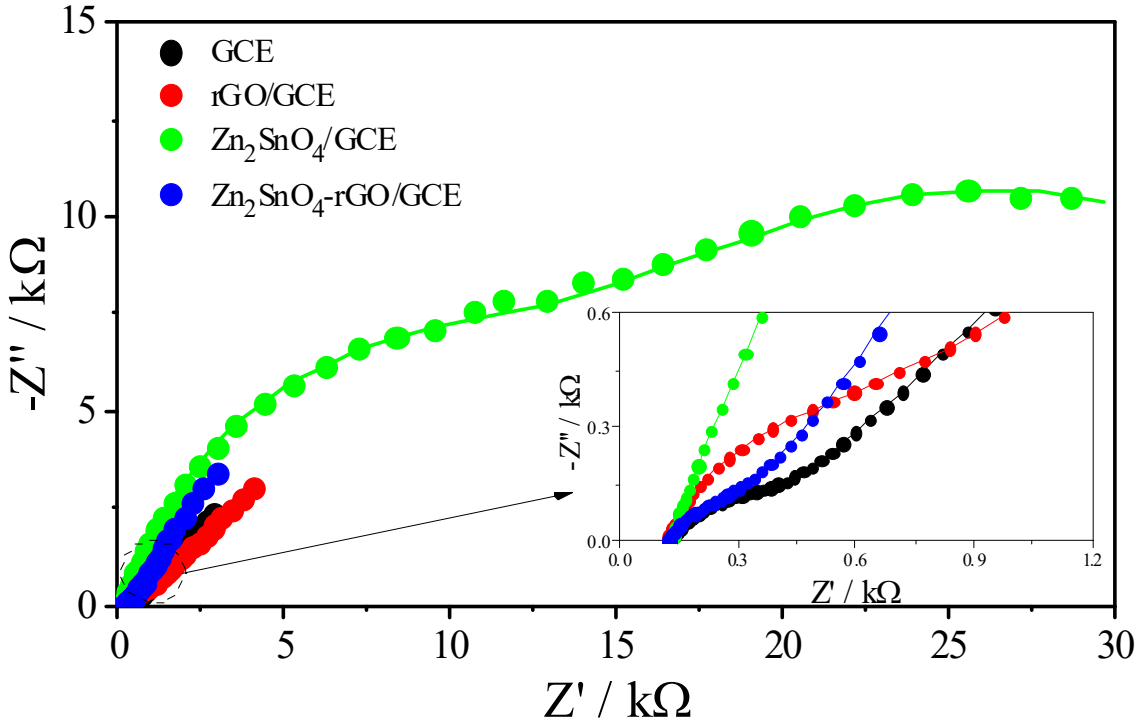

(B)

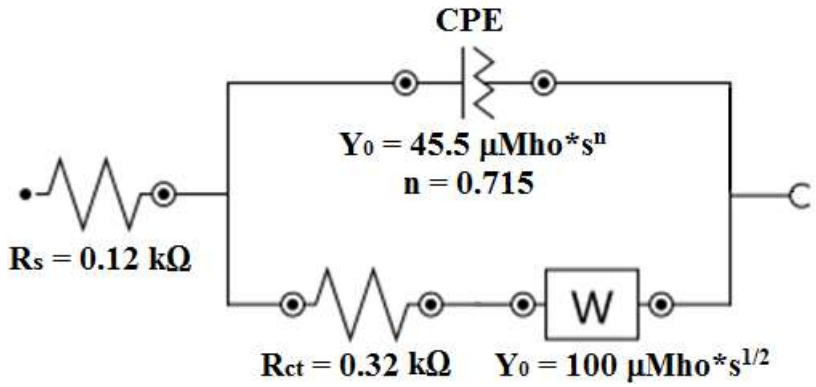

Fonte: (6).

When considering the Nyquist diagrams, it was observed that the Zn_2SnO_4/GCE surface showed two arcs in separate R_{ct} values, the highest being 23.24 kΩ and the absence of the Warburg's diffusion line. This indicates that Zn_2SnO_4 individual usage during GCE's

modification did not favor the charge transfer process in the electrode's surface. Several articles report the presence of two arcs in a Nyquist diagram and Warburg's diffusion line absence, including tin oxides (SnO_2, SnO_4 and SnO_6) (47, 48). However, there's no consensus about such behavior, which is attributed to the passivation layer formation or the rapid oxide recombination in the electrode's surface (47, 48).

Nevertheless, the Zn_2SnO_4-rGO/GCE surface presented the lowest R_{ct} value (0.32 kΩ) of those that were evaluated, inferring that there was a relevant synergism between materials (Zn_2SnO_4 and rGO) and by such, the developed composite (Zn_2SnO_4-rGO) favored the charge transfer process at the electrode surface, with an equivalent circuit represented in Fig. 7B. It was also observed that although Nafion® contributes to physical aggregation of the composite materials (Zn_2SnO_4-rGO), it also promotes relative difficulty during the charge transfer process in the electrode surface ($K_4[Fe(CN)_6]/K_3[Fe(CN)_6]$) due to its sulfonate groups ($–SO_3^-$) present in its structure, generating electrostatic repulsion (49).

3.4 Evaluation of the electrochemical behavior of OFL in GCE/Zn_2SnO_4-rGO through CV

CV experiments were carried out to evaluate scan rate influence between 10 and 200 mV s^{-1} in the presence of 2.95 × 10^{-5} mol L^{-1} OFL in 5.0 × 10^{-1} mol L^{-1} H_2SO_4 using Zn_2SnO_4-rGO/GCE between 0.0 and 1.5 V. Its electrochemical behavior is shown in Fig. 8.

Figure 8 – Cyclic voltammograms of 2.95×10^{-5} mol L^{-1} OFL in 5.0×10^{-1} mol L^{-1} H_2SO_4, using Zn_2SnO_4-rGO/GCE, with scan rates between 10 and 200 mV s^{-1}

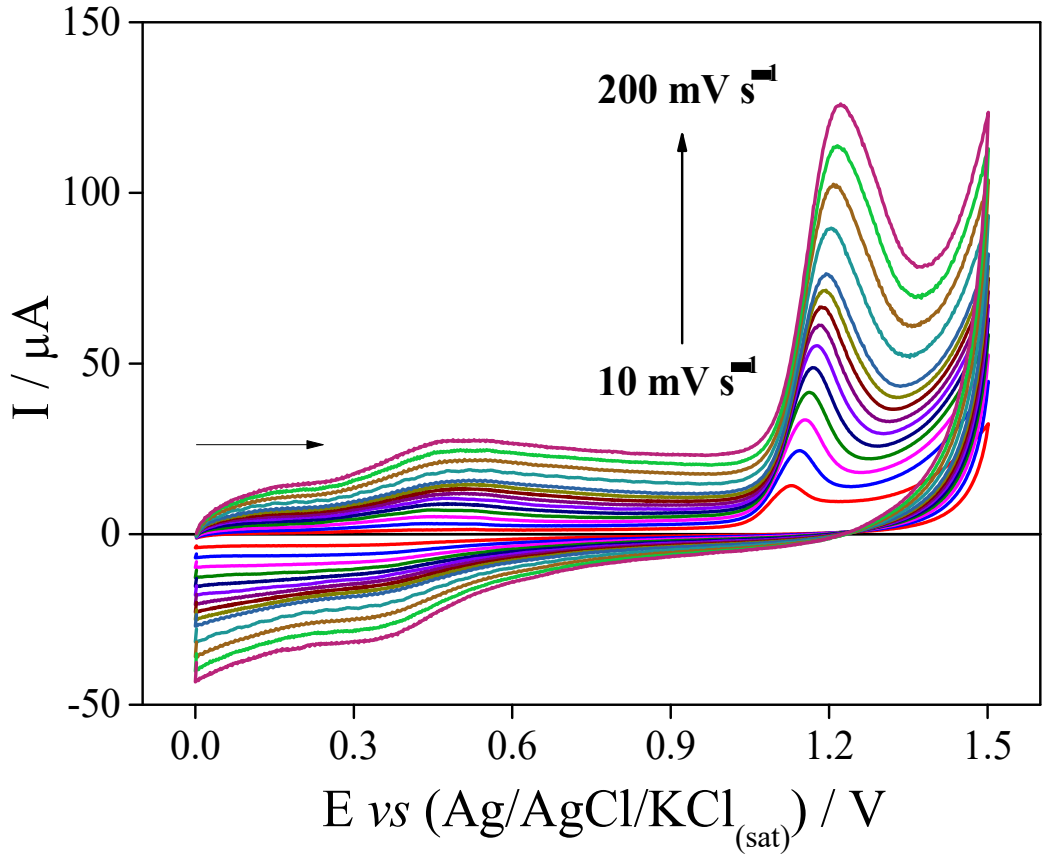

Fonte: (6).

OFL voltammetric profiles clearly indicate that OFL suffered an oxidation process when using Zn_2SnO_4-rGO/GCE. Moreover, it can be noted that the reverse peak is absent and that the increase of the scan rate (ν) promoted both the enhancement of I_p values and the dislocating peak potential (E_p) towards more positive values, confirming the irreversible process for OFL in Zn_2SnO_4-rGO/GCE (50, 51, 52). In addition, a discrete reversible process was noted in approximately 0.5 V. According to the literature, this fact can be attributed to oxide formations due to interactions between H_2SO_4 and carbonaceous materials, such as GC and rGO (53, 54, 55).

A linear relation between I_p and the scan rate square root ($\nu^{1/2}$), as expressed in the equation: I_p (µA) = $-1.09 \times 10^{-5} \pm 4.24 \times 10^{-7} + 1.90 \times 10^{-4} \pm 1.45 \times 10^{-6}$ $\nu^{1/2}$ (V s^{-1}) with r = 0.999, suggests that OFL oxidation process is primarily diffusion controlled (56). Relation between log I_p and log ν was also established: log I_p (µA) = $-5.73 \pm 0.04 + 0.71 \pm 0.02$ log ν (mV s^{-1}) with r = 0.995. Since its angular coefficient is 0.71, it was concluded that the OFL

oxidation process has mixed control (both diffusional and adsorptive), although its inclination points out that it is mostly controlled by diffusion (closer to 0.5) (56).

It was also estimated the number of electrons involved in OFL oxidation, through E_p and log ν relation, as expressed in the equation: E_p (V) = 1.05 ± 2.0 × 10^{-3} + 0.07 ± 1.0 × 10^{-3} log ν (mV s^{-1}) with r = 0.996. For irreversible and anodic reactions, there's a linear relation between E_p and log ν, which has its inclination expressed in equation 4 (56):

$$\frac{\Delta \mathbf{E_p}}{\Delta \log \boldsymbol{v}} = \frac{\mathbf{2.303RT}}{\boldsymbol{\alpha n}\mathbf{F}} \quad (4)$$

where R is the universal gas constant (J K^{-1} mol^{-1}), temperature is T (K), F is Faraday's constant (C), α is the electrons' transfer coefficient and *n* is the number of electrons transferred.

Through the line equation obtained, E_p (V) = 1.05 ± 2.0 × 10^{-3} + 0.07 ± 1.0 × 10^{-3} log ν (mV s^{-1}) with r = 0.996, and its proper substitutions (8.314 J $K^{-1}mol^{-1}$, 298.15 K and 96,480 C mol^{-1}, αn was determined to be 0.86. For systems with organic molecules in aqueous medium, α = 0.5 (57) which concludes that the number of electrons involved in the rate-determining step is 2, as previously reported in the literature (4, 5).

3.5 Electrochemical behavior of OFL in modified electrodes, through SWV

3.5.1 Evaluation of OFL species distribution and optimization of the supporting electrolyte and pH

As previously seen (Fig. 1A), OFL protonation is dependent on the solvation medium pH and pKa values, which directly influences the number of species (4, 5). To understand better the behavior of the OFL species concentrations in the function of the pH, a species distribution study was carried out through the construction of a species distribution curve, calculated by acid-base equilibrium and mass balance, as seen in Fig. 1B.

As observed, three OFL species can exist in an aqueous medium. Protonated OFL species (OFL^+) are predominant in pH values below 2.0; neutral OFL species ($OFL^{\pm}$) are common in the 6.0 to 8.5 pH range; meanwhile, deprotonated OFL species (OFL^-) predominate in pH values above 10.0. The crossover point in their distribution curves (α' = 0.5) happens when pH is equal to pKa, according to literature (pKa_1 = 5.9 and pKa_2 = 8.2) (4, 5). It is fundamental to know the analyte species in the function of pH to correlate which pH condition

favors the formation of chemical and electrostatic interactions at the modified electrode surface (58).

Zn_2SnO_4-rGO promotes the formation of a negatively charged electrode surface due to the chemical structure of its components. Zn_2SnO_4 has neutral molecular structure (13, 47); rGO has in its basal structure epoxy (-COC-), hydroxyl (-OH) and carboxyl (-COOH) functional groups, which are charged negatively and provide excellent reaction sites to a protonated analyte (such as OFL^+) (18); Nafion® has sulfonate groups ($–SO_3^–$) in its structure, also negatively charged, and equally reactive to a protonated analyte (49). With such analysis, it's been concluded that the composite-modified electrode surface (with the composite proposed in this work, Zn_2SnO_4-rGO/GCE) has great electrostatic interaction with protonated species, such as OFL^+ in this work. These results corroborate with Liu *et al.* (58) concerning OFL oxidation under different pH conditions. According to Fig. 1B, supporting electrolyte and pH optimization studies were restricted to pH conditions below 2.0 because the preferred species (OFL^+) was primarily present. Based on the discussion above, the importance of understanding the relationship between the OFL speciation diagram and the electrostatic nature of the modified electrode surface can be seen, including theoretically evaluating the possible optimized pH conditions of the studied system (58).

Due to the limited number of buffer solutions available in the determined range (0 to 2.0), it was chosen BR, Clark-Lubs and Sörensen buffers, 5.0×10^{-3} mol L^{-1} H_2SO_4; 5.0×10^{-2} mol L^{-1} H_2SO_4 and 5.0×10^{-1} mol L^{-1} H_2SO_4. To evaluate the proposed optimization procedure and verify the low electrochemical interaction between the composite-modified electrode surface (Zn_2SnO_4-rGO) and both the neutral and deprotonated analyte species ($OFL^{\pm}$ e $OFL^–$), pH 7.4 PBS was assessed to reproduce physiological medium. Supporting electrolyte and pH influence was evaluated through SWV, using 2.95×10^{-5} mol L^{-1} OFL in Zn_2SnO_4-rGO/GCE, using standard parameters $f = 100$ s^{-1}, $a = 50$ mV and $\Delta E_s = 2$ mV, as shown in Fig. 9.

Figure 9 – Square-wave voltammograms on different supporting electrolytes and pH values for 2.95×10^{-5} mol L^{-1} OFL using Zn_2SnO_4-rGO/GCE at f = 100 s^{-1}, a = 50 mV and ΔE_s = 2 mV

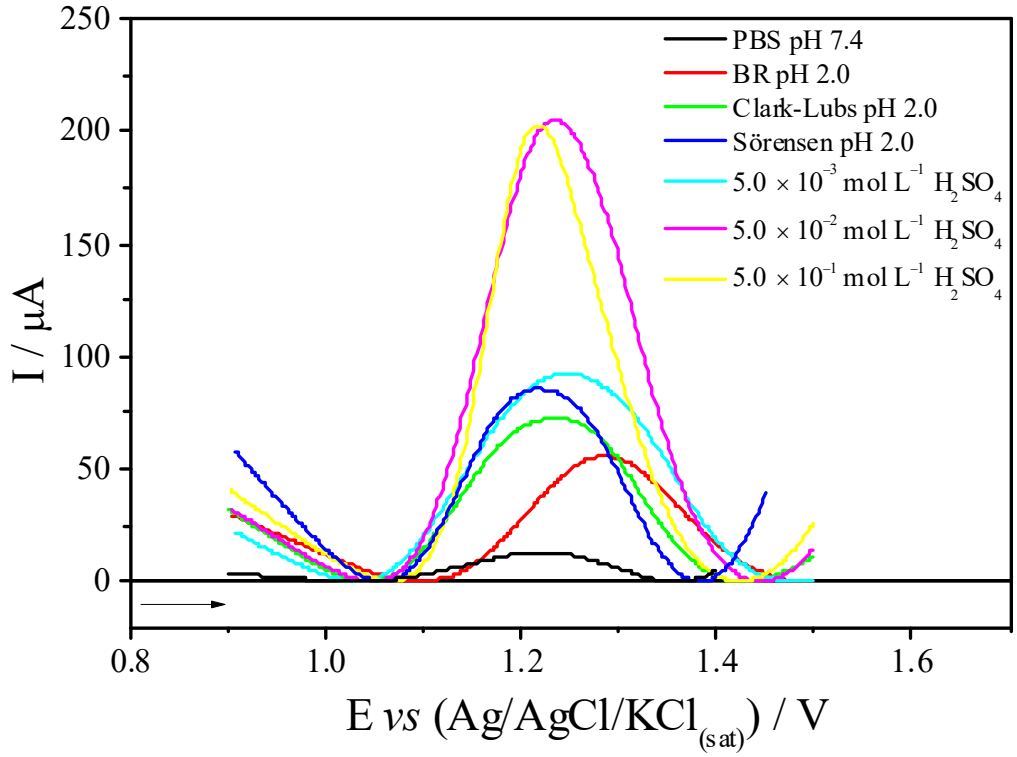

Fonte: (6).

At first, SWV experiments showed an OFL irreversible (I_{dir}/I_{rev} > 1) oxidation process (I_p > 0) in all analyzed electrolytes in the 1.0 to 1.5 V potential range (59). It was observed that the pH 7.4 PBS buffer solution was the least effective in OFL detection when using the Zn_2SnO_4-rGO/GCE sensor, confirming what was proposed based on the OFL species fraction distribution diagram (Fig. 1B) and in the general behavior of the composite components (Zn_2SnO_4, rGO and Nafion®). With the voltammetric profiles as a basis, both the supporting electrolyte and pH-optimized conditions were 5.0×10^{-1} mol L^{-1} H_2SO_4, having presented both higher sensitivity ($I_p = 2.29 \times 10^{-4}$ A) and selectivity ($\Delta E_{p/2}$ = 131 mV) to OFL.

3.5.2 Evaluation of electrochemical synergism between modifying agents and optimization of the electrode surface cleaning process and SWV parameters

Electrochemical synergism between the developed composite components (Zn_2SnO_4 and rGO) when used for OFL oxidation was evaluated using 2.39×10^{-5} mol L^{-1} OFL and optimized supporting electrolyte and pH (5.0×10^{-1} mol L^{-1} H_2SO_4) in the following

conditions: bare GCE, rGO/GCE, Zn_2SnO_4/GCE and Zn_2SnO_4-rGO/GCE; through SWV at f = 100 s^{-1}, a = 50 mV and ΔE_s = 2 mV (Fig. 10).

Figure 10 – Square-wave voltammograms on different electrode surfaces for 2.39×10^{-5} mol L^{-1} OFL in 5.0×10^{-1} mol L^{-1} H_2SO_4 at f = 100 s^{-1}, a = 50 mV e ΔE_s = 2 mV

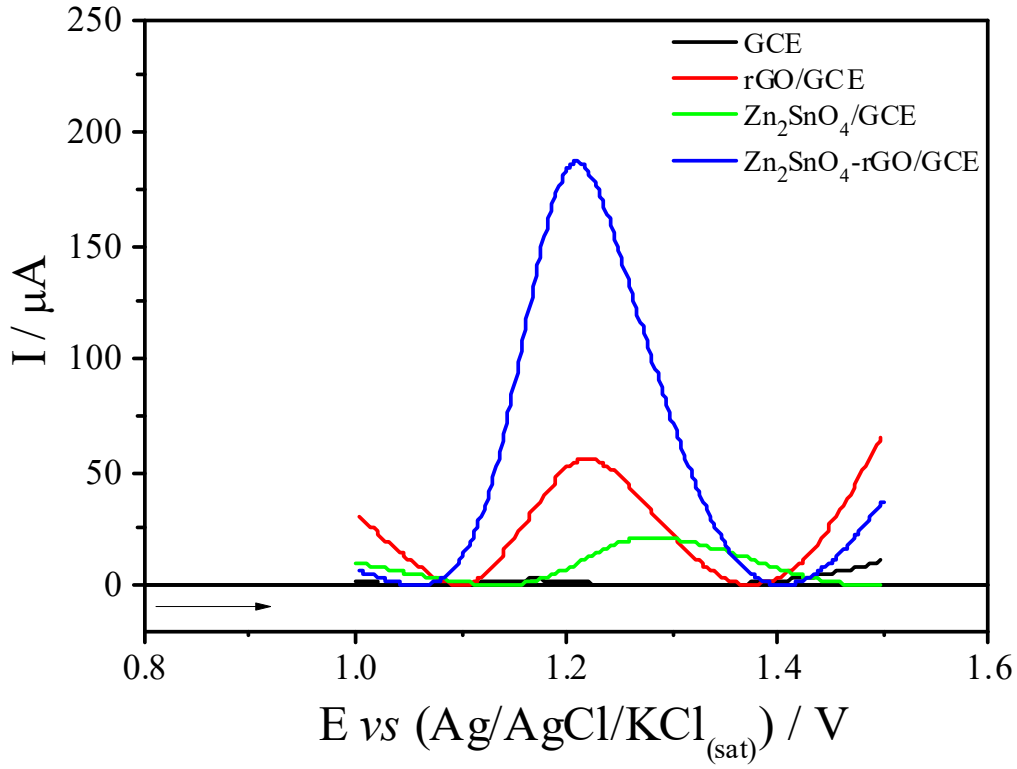

Fonte: (6).

By Fig. 10, it was observed that all modifications were more effective than bare GCE. A clear chemical synergism between Zn_2SnO_4 and rGO when used to detect OFL was noted, as it amplified significantly the I_p signal, justifying Zn_2SnO_4-rGO as the optimized modification for this work.

In sequence, an experimental cleaning procedure based on simple mechanical stirring of the solution containing OFL was tested, using 60, 120, 180 and 240 s as stirring times. The most effective sensor cleaning condition was 180 s, being chosen as the optimized procedure.

SWV optimization parameters were carried out at 2.95×10^{-5} mol L^{-1} OFL in 5.0×10^{-1} mol L^{-1} H_2SO_4, using Zn_2SnO_4-rGO/GCE. f, a and ΔE_s values were evaluated in 10 to 100 s^{-1}, 10 to 50 mV, and 1 to 5 mV ranges, respectively. Linear dependency between f and I_p values in the 10 to 60 s^{-1} was observed: I_p (μA) = $1.62 \times 10^{-5} \pm 2.45 \times 10^{-6} + 1.57 \times 10^{-6} \pm$

6.28×10^{-8} *f* (s^{-1}), with r = 0.992; it was also noted that I_p values were proportional to *f* increments, which confirmed through SWV the irreversible nature of the OFL oxidation process in the proposed system, which corroborates to the CV results obtained in this work (50, 60, 61).

Frequency optimization study was also used to estimate the value of *n*, through the relation between E_p and log *f*, according to: E_p (V) = $1.01 \pm 4.0 \times 10^{-3} + 0.08 \pm 2.0 \times 10^{-3}$ log *f* (s^{-1}); with r = 0.995. For irreversible and anodic reactions, there is a linear relation between E_p and log *f*, following equation 5 (61, 62):

$$\frac{\Delta \mathbf{E_p}}{\Delta \log \boldsymbol{f}} = \frac{\mathbf{2.303RT}}{\boldsymbol{\alpha n}\mathbf{F}} \quad (5)$$

Substituting in the equation above inclination (0.08) and other values (R, T and F), it was estimated that *n* was equal to 2, corroborating with the previously reported (4, 5, 61, 62, 63).

Values of *a* presented linear dependency with I_p from 10 up to 30 mV: I_p (μA) = $1.33 \times 10^{-5} \pm 8.64 \times 10^{-7} + 2.99 \times 10^{-6} \pm 4.65 \times 10^{-8}$ *a* (mV) with r = 0.999. The linearity range observed between I_p and *a* is in agreement with the SWV theory for the theoretical optimized amplitude determination in irreversible systems, which follows the 50/*n* ratio, where *n* is the number of electrons involved (60, 61, 62). That way, the theoretical optimized amplitude value was equal to 25 mV, which was very close to the experimentally obtained value (30 mV).

ΔE_s values presented linearity with I_p from 1 up to 3 mV: I_p (μA) = $5.03 \times 10^{-5} \pm 1.78 \times 10^{-7} + 5.13 \times 10^{-5} \pm 1.27 \times 10^{-7}$ ΔE_s (mV) with r = 0.999. As such, for the developed electrochemical methodology, the optimized parameters were *f* = 60 s^{-1}, *a* = 30 mV and ΔE_s = 3 mV.

3.6 Analytical curves for OFL and evaluation of interferents

After optimizing SWV values, OFL analytical curves were constructed using Zn_2SnO_4-rGO/GCE in 5.0×10^{-1} mol L^{-1} H_2SO_4 with *f* = 60 s^{-1}, *a* = 30 mV and ΔE_s = 3mV. Fig. 11 shows the SWV voltammetric profiles obtained, with the insertion of an average analytical curve, including error bars.

Figure 11 – Square-wave voltammograms for OFL concentrations from 9.99 × 10^{-8} to 6.62 × 10^{-6} mol L^{-1} in 5.0 × 10^{-1} mol L^{-1} H_2SO_4 using Zn_2SnO_4-rGO/GCE at f = 60 s^{-1}, a = 30 mV, and ΔE_s = 3 mV. The insert shows the mean calibration curve of three independent curves

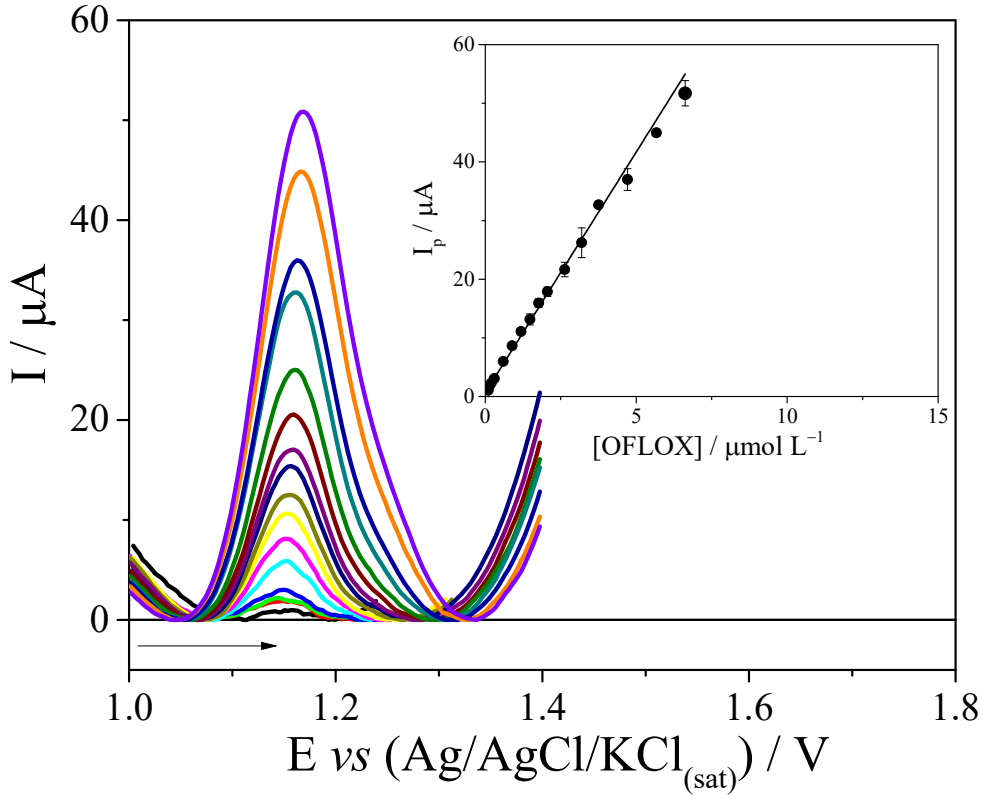

Fonte: (6).

Results show a linear relation between I_p and OFL concentration ([OFL]) from 9.99 × 10^{-8} up to 6.62 × 10^{-6} mol L^{-1}: I_p (µA) = 6.49 × 10^{-7} ± 6.48 × 10^{-8} + 8.21 ± 0.13 [OFL] (µmol L^{-1}) with r = 0.998 and n = 16. Calculated values of LOD and LOQ were 8.28 × 10^{-8} and 2.76 × 10^{-7} mol L^{-1}, respectively; these values were inferior to those obtained through HPLC (Table 2), evidencing a satisfactory sensitivity of the developed sensor.

Table 2 – Analytical parameters calculated from calibration curves for the determination of OFL at Zn_2SnO_4-rGO/GCE using SWV and HPLC

Parameter	SWV	HPLC
Linearity range (mol L^{-1})	9.99×10^{-8} a 6.62×10^{-6}	3.19×10^{-6} a 2.21×10^{-4}
Intercept	$6{,}49 \times 10^{-7}$ A	11520 (u.a.)
Slope	8.21 A mol^{-1} L	8.43×10^{9} (u.a.) mol^{-1} L
Confidence interval of intercept	$\pm 6.48 \times 10^{-8}$	± 210
Confidence interval of slope	$\pm 1.30 \times 10^{-1}$	$\pm 3.74 \times 10^{8}$
Correlation coefficient (R)	0.998	0.997
Standard deviation of intercept (S_a)	2.06×10^{-7} A	236 (u.a.)
Standard deviation of slope (S_b)	2.28×10^{-1} A mol^{-1} L	9.07×10^{7} (u.a.) mol^{-1} L
LOD (mol L^{-1})	8.28×10^{-8}	8.65×10^{-8}
LOD (µg L^{-1})	29.92	31.26
LOQ (mol L^{-1})	2.76×10^{-7}	2.88×10^{-7}
LOQ (µg L^{-1})	99.63	104.09
% RSD Repeatability (n = 12)	3.20	----------
% RSD Reproducibility (n = 7)	4.64	----------

Fonte: (6).

The precision of the methodology was confirmed through intraday (repeatability; n = 12) and interday (reproducibility; n = 7), showing in both tests RSD lower than 5%, which demonstrated the efficiency and reliability of the proposed sensor being compared to other published articles, as seen in Table 3.

Table 3 – Analytical characteristics for determination of OFL applied electrochemical devices

Electrode	Linearity range (μmol L^{-1})	LOD (μmol L^{-1})	Sensitivity (A mol^{-1} L)	Real sample	Ref.
rGO/Pt-Au/GCE	0.08 a 100	0.05	2.40	Tablets and human urine	(64)
rGO/AuNPs/SH-β-CD/GCE	0.01 a 10	0.008	0.28	Tablets and human urine	(65)
Ppy/HPMαFP/GCE	2 a 100	0.065	0.076	Ophthalmic solution	(66)
Gr/pABSA/GCE	0.1 a 40	0.03	0.2425	Ophthalmic solution	(67)
Gr/ZnO/GCE	1 a 100	0.33	0.089	Tablets and saline solution	(10)
CA/CPE	0.06 a 10	0.02	0.80	Tablets and saline solution	(68)
*f*MWCNT/GCE	0.5 a 100	0.01	0.3064	Tablets, capsules and injection	(69)
IL-rGO/GCE	0.007 a 0.7	0.00028	7.70	Ophthalmic solution and human urine	(70)
Zn_2SnO_4-rGO/GCE	0.09 a 6.62	0.0828	8.21	Ophthalmic solution	This work

Fonte: (6).

CA (Cysteic acid); AuNPs (Gold nanoparticles); GCE (Glass carbono electrode); CPE (Carbon past electrode); Gr (Graphene); HPMαFP (1-phenyl-3-methyl-4-(α-furoyl)-pyrazolone-5); IL (Ionic liquid); rGO (Reduced graphene oxide); pABSA (p-aminobenzene sulfonic acid); Ppy (Polypyrrole); Pt-Au (Platinum and gold); SH-B-CD (Beta-cyclodextrin); ZnO (Zinc oxide); Zn_2SnO_4 (Zinc stannate).

Zn_2SnO_4-rGO/GCE showed that it was the most sensitive (8,21 A mol^{-1} L) among the sensors cataloged in Table 3, presenting comparable and adequate characteristics for OFL detection. An interference study for OFL detection using Zn_2SnO_4-rGO/GCE was carried out adding various chemical species in fixed OFL quantities (Fig. 12) in the 100:1 ratio ([interferent]:[OFL]).

Figure 12 – Effect of inorganic and organic species on the reduction signal of OFL in 5.0 × 10^{-1} mol L^{-1} H_2SO_4 on Zn_2SnO_4-rGO/GCE

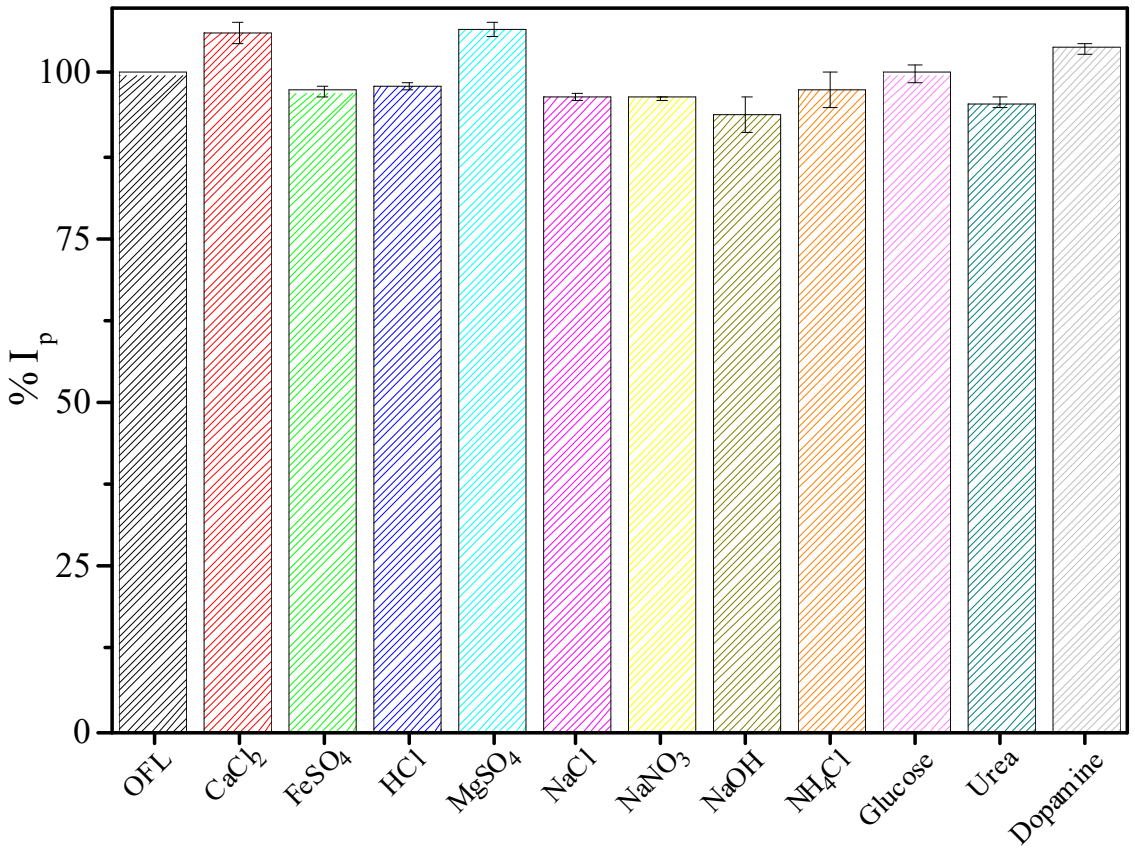

Fonte: (6).

Results pointed that Fe^{2+}, Na^+, NH_4^+, H^+, SO_4^{2-}, NO_3^-, Cl^-, glucose, urea and dopamine species in 100 times higher concentrations than OFL exhibited interferences lower than ± 5%. To compare the mean I_p obtained for each of the interferers with the mean I_p obtained for the system with only the OFL, the *t*-test was applied. For all the interferers evaluated, the $t_{calculated}$ was lower than $t_{critical}$ (4.30), indicating that none of them promoted a significant difference at the 5% level (p-value > 0.05) in the OFL detection I_p, highlighting that the developed sensor (Zn_2SnO_4-rGO/GCE) has good anti-interference capacity.

3.7 Sensor application in commercial pharmaceutical formulation

Zn_2SnO_4-rGO/GCE was applied in ophthalmic solution samples containing OFL. Recovery studies were performed through analysis of six different concentration points in triplicate, distributed in three concentration ranges (low, medium, and high) in the linearity range of the calibration curve (25), meanwhile calculating REC%, RSD% and BIAS% (Table 4) (23, 24).

Table 4 – Recovery of OFL in commercial pharmaceutical formulation (n = 3), at different concentrations, through the Zn_2SnO_4-rGO/GCE, using SWV in the optimized parameters; $f = 60\ s^{-1}$, $a = 30$ mV e $\Delta E_s = 3$ mV

		Zn_2SnO_4-rGO/GCE					
Ophthalmic solution	$[OFL]_{added}$ (mol L^{-1})	2.99×10^{-7}	5.96×10^{-7}	1.19×10^{-6}	1.48×10^{-6}	2.92×10^{-6}	3.20×10^{-6}
	$[OFL]_{found}$ (mol L^{-1})	2.98×10^{-7}	6.26×10^{-7}	1.22×10^{-6}	1.46×10^{-6}	2.90×10^{-6}	3.13×10^{-6}
	Confidence interval (mol L^{-1})	$\pm 1.12 \times 10^{-7}$	$\pm 4.07 \times 10^{-7}$	$\pm 8.59 \times 10^{-7}$	$\pm 7.71 \times 10^{-7}$	$\pm 1.37 \times 10^{-6}$	$\pm 3.46 \times 10^{-7}$
	Recovery (%)	99.74	104.91	102.77	98.88	99.18	98.03
	RSD (%)	0.89	2.54	1.49	1.63	0.81	0.53
	BIAS (%)	– 0.26	4.91	2.78	– 1.12	– 0.82	– 1.97

Fonte: (6).

The slopes of the lines obtained through linear regressions of the standard analytical curve and the analytical curve of the commercial pharmaceutical formulation (ophthalmic solution) were compared, considering the same [OFL] points in each of the conditions, presenting slope values equal to 8.21 ± 0.13 and 8.02 ± 0.08 A mol^{-1} L, respectively; making it possible to verify the parallelism between the lines (21, 25). To confirm this observation, the *F* and *t*-tests were used to evaluate a possible significant difference between the average slope values obtained for each of the curves. The $F_{calculated}$ (3.0) and $t_{calculated}$ (0.48) values found were lower than the $F_{critical}$ (19.0) and $t_{critical}$ (4.30) values, indicating that there was no significant difference (p-value > 0.05) between the slopes of the curves; and that, therefore, there was no occurrence of the matrix effect in the commercial pharmaceutical formulation samples (21, 25).

Using the International Conference for Harmonization (ICH) as a basis, it was possible to affirm that the proposed analytical method showed satisfactory REC%, with recovery percentages of 70 to 130% (21). The %REC obtained is also within the tolerance limit (80% and 110%), in accordance with the standards of the Brazilian National Health Surveillance Agency (ANVISA-Brazil) for analyte recovery studies at the concentrations evaluated in this research (25). The developed methodology presented $REC\%_{average}$ = 100.58%, while having high precision (average RSD% = 1.31%) and accuracy (BIAS% < ± 5%) for OFL determination in ophthalmic solution, demonstrating high sensitivity and selectivity in a complex matrix. Thereafter, it was possible to conclude that the proposed procedure using Zn_2SnO_4-rGO/GCE is adequate to determine OFL in pharmaceutical formulation.

SWV results were compared to those obtained through HPLC coupled to a UV-Vis detector (Table 5) to evaluate the efficiency of the proposed sensor, as suggested by the Brazilian Pharmacopoeia for OFL detection (26).

Table 5 – Recovery of OFL in commercial pharmaceutical formulation (n = 3), through SWV using Zn_2SnO_4-rGO/GCE and HPLC with UV-Vis detector

		SWQ	HPLC (UV-Vis)
Ophthalmic solution	$[OFL]_{added}$ (mol L^{-1})	3.19×10^{-6}	3.19×10^{-6}
	$[OFL]_{found}$ (mol L^{-1})	3.13×10^{-6}	3.17×10^{-6}
	Confidence interval (mol L^{-1})	$\pm 3.46 \times 10^{-7}$	$\pm 3.92 \times 10^{-7}$
	Recovery (%)	98.03	99.18
	RSD (%)	0.53	0.86
	BIAS (%)	– 1.97	– 0.81

Fonte: (6).

Recovery results found in both methods (SWV and HPLC) were evaluated through the *F*-test. A result of $F_{calculated}$ = 1.96 was obtained, below the theoretical value ($F_{critical}$ = 19.0), indicating that there was no significant difference between the obtained results, and as such, the two methodologies do not differ in precision.

4 Conclusions

A novel sensor based on metallic ternary oxides (Zn_2SnO_4) allied with rGO was successfully developed for OFL determination. The good electrochemical performance of the modified electrode was attributed to the synergistic effects between Zn_2SnO_4/rGO. OFL on Zn_2SnO_4-rGO/GCE exhibited only an irreversible oxidation process involving two electrons; OFL protonated species were responsible for higher electroactivity and a typical mixed diffusion-adsorption controlled process. The newly developed electrochemical sensor showed analytical data with excellent wide linearity, sensitivity, accuracy, precision (repeatability and reproducibility) and anti-interference ability. The LOD and LOQ values obtained with the proposed sensor were lower than the data obtained by HPLC methods. In addition, the electroanalytical methodology developed was successfully applied for OFL determination in pharmaceutical formulation. Therefore, the sensor based on Zn_2SnO_4-rGO can be considered an excellent alternative tool to OFL analysis.

ACKNOWLEDGMENTS

This study was financed in part by the Coordenação de Aperfeiçoamento de Pessoal de Nível Superior - Brasil (CAPES) – Finance Code 001 (PROEX 23038.000509/2020-82). The authors thank the financial support given by the following Brazilian funding agencies: Coordenação de Aperfeiçoamento de Pessoal de Nível Superior (CAPES), Conselho Nacional de Desenvolvimento Científico e Tecnológico (CNPq) and Fundação Cearense de Apoio ao Desenvolvimento Científico e Tecnológica (FUNCAP). P.B.A. Fechine thanks CNPq (proc. 308452/2022-4) and Funcap (proc. PNE-0112-00048.01.00/16). F.W.P. Ribeiro acknowledges the funding provided by FUNCAP-BPI (proc. BP5-0197-00017.01.00/22). P. de Lima-Neto thanks CNPq (proc. 302825/2022-3). D. S. Abreu thanks FINEP (CV. 01.22.0174.00 BIONANO SPR) and CNPq (proc. 407954/2022-8) for financial support. A.N. Correia

gratefully acknowledges the funding provided by CNPq (proc. 305136/2018-6 and proc. 305103/2022-9). The authors would like to thank the Central Analítica-UFC/CT-INFRA/MCTI-SISANO/Pró-Equipamentos CAPES for their support.

REFERENCES

1 IUPAC. **Nomenclature**. [*S. l.*]: IUPAC, c2023. Disponível em: https://iupac.org/what-we-do/nomenclature/. Acesso em: 04 mai. 2023.

2 ZANCHETTA, P. G.; PENA, A.; GONÇALVES, R. Development and validation of an analytical method for the simultaneous quantification of ofloxacin, norfloxacin and ciprofloxacin in human urine. **Sanitary and Environmental Engineering**, Rio de Janeiro, v. 20, p. 307-314, 2015.

3 DRAKOPOULOS, A. I.; IOANNOU, P. C. Spectrofluorimetric study of the acid–base equilibria and complexation behavior of the fluoroquinolone antibiotics ofloxacin, norfloxacin, ciprofloxacin and pefloxacin in aqueous solution. **Analytica Chimica Acta**, [*s. l.*], v. 354, p. 197-204, 1997.

4 DAVYDOV, N. *et al*. Determination of fluoroquinolone antibiotics through the fluorescent response of Eu (III) based nanoparticles fabricated by layer-by-layer technique. **Analytica Chimica Acta**, [*s. l.*], v. 784, p. 65-71, 2013.

5 PINACHO, D. G.; SANCHEZ-BAEZA, F.; MARCO, M. P. Molecular modeling assisted hapten design to produce broad selectivity antibodies for fluoroquinolone antibiotics. **Analytical Chemistry**, [*s. l.*], v. 84, p. 4527-4534, 2012.

6 CASTRO, J. S. *et al.* Electrocatalytic amplified sensor for determination of ofloxacin using Zn2SnO4/reduced graphene oxide composite as surface-modifying agent. **Journal of the Electrochemical Society**, [*s. l.*], v. 171, n. 1, 2024.

7 EROGUL, S. *et al.* A new electrochemical sensor based on Fe 3 O 4 functionalized graphene oxide–gold nanoparticle composite film for simultaneous determination of catechol and hydroquinone. **Electrochimica Acta**, [*s. l.*], v. 186, p. 302–313, 2015.

8 TIAN, X. *et al.* Nonenzymatic electrochemical sensor based on CuO–TiO 2 for sensitive and selective detection of methyl parathion pesticide in ground water. **Sensors and Actuators B**: Chemical, [*s. l.*], v. 256, p. 135-142, 2018.

9 GAN, T. *et al*. Morphology-dependent electrochemical sensing properties of manganese dioxide-graphene oxide hybrid for guaiacol and vanillin. **Electrochimica Acta**, [*s. l.*], v. 147, p. 157–166, 2014.

10 SI, X. *et al.* A sensitive electrochemical sensor for ofloxacin based on a graphene/zinc oxide composite film. **Analytical Methods**, [*s. l.*], v. 17, p. 1961-1967, 2018.

11 XIE, J. *et al*. Synthesis of zincn stannate and zinc stannate coated ano-CaCO 3 by homogeneous precipitation. **Journal of Chemical Research**, [*s. l.*], v. 35, p. 109-111, 2011.

12 SONG, W. *et al.* Graphene-induced confined crystal growth of octahedral Zn 2 SnO 4 and its improved Li-storage properties. **Journal of Materials Research**, [*s. l.*], v. 27, p. 3096-3102, 2012.

13 COFFEEN, W. W. Ceramic and dielectric properties of the stannates. **Journal of the American Ceramic Society**, [*s. l.*], v. 36, p. 207-214, 1953.

14 SHOMAKHOV, Z. V. *et al.* Zinc stannate nanostructures for fast response gas sensors. **Russian Reviewed Scientific Edition**, [*s. l.*], v. 14, p. 726-735, 2022.

15 AKKAPINYO, C. *et al*. Disposable electrochemical sensor for food colorants detection by reduced graphene oxide and methionine film modified screen printed carbon electrode. **Molecules**, [*s. l.*], v. 26, p. 1-18, 2021.

16 LIU, G. *et al*. Electrochemical approach toward reduced graphene oxide-based electrodes for environmental applications: a review. **Science of the Total Environment**, [*s. l.*], v. 778, p. 1-14, 2021.

17 RAZAQ, A. *et al*. Review on graphene, graphene oxide, reduced graphene oxide-based flexible composites: from fabrication to applications. **Materials**, [*s. l.*], v. 15, n. 3, p. 1-17, 2022.

18 EDA, G.; CHHOWALLA, M. Chemically derived graphene oxide: Towards large-area thin-film electronics and optoelectronics. **Advanced Materials**, [*s. l.*], v. 22, n. 22, p. 2392-2415, 2010.

19 ZHU, C. *et al.* A flexible electrochemical biosensor based on functionalized poly (3,4-ethylenedioxythiophene) film to detect lactate in sweat of the human body. **Journal of Colloid and Interface Science**, [*s. l.*], v. 617, p. 454-462, 2022.

20 WOJDYR, M. Fityk: a general-purpose peak fitting program. **Journal of Applied Crystallography**, [*s. l.*], v. 43, part 5, p. 1126-1128, 2010.

21 EMA. **ICH Guideline Q2 (R2) on Validation of Analytical Procedures**: step 2b. The Netherlands: EMA, 2022. Disponível em: ttps://pink.pharmaintelligence.informa.com/-/media/supporting-documents/pink-sheet/2022/04/p0422ema_21.pdf/, 2022. Acesso em: 01 May 2023.

22 MILLER, J. N.; MILLER, J. C. **Statistics and chemometrics for analytical chemistry**. 4th ed. England: Prentice Hall, 2005.

23 THOMPSON, M. *et al.* Harmonized guidelines for the use of recovery information in analytical measurement. **Pure and Applied Chemistry**, [*s. l.*], v. 71, n. 2, p. 337-348, 1999.

24 PRICHARD, E.; BARWICK, V. **Quality assurance in analytical chemistry**. 1st ed. New York: Wiley, 2007.

25 ANVISA. **Resolução da Diretoria Colegiada - RDC nº 166, de 24 de julho de 2017**. Dispõe sobre a validação de métodos analíticos e dá outras providências. [Brasília, DF]: Anvisa, 2017. Disponível em: http://antigo.anvisa.gov.br/documents/10181/2721567/RDC_166_2017_COMP.pdf/d5fb92b3-6c6b-4130-8670-4e3263763401. Acesso em: 14 March 2023.

26 ANVISA. **Farmacopeia brasileira**. 6. ed. Brasília, DF: Anvisa, 2019. Disponível em: https://www.gov.br/anvisa/pt-br/assuntos/farmacopeia/farmacopeia-brasileira/insumos-farmaceuticos-e-especialidades-ate-2a-errata-p-pdf-com-capa.pdf. Acesso em: 19 April 2023.

27 LUO, T. *et al.* Sub-20nm-Fe 3 O 4 square and circular nanoplates: synthesis and facet-dependent magnetic and electrochemical properties. **ChemComm**, [*s. l.*], v. 50, p. 15952-15955, 2014.

28 YOUNG, R. A.; MACKIE, P. E.; VON DREELE, R. B. Application of the pattern-fitting structure-refinement method of X-ray powder diffractometer patterns. **Journal of Applied Crystallography**, [*s. l.*], v. 10, p. 262-269, 1977.

29 YOUNG, R. A. **The Rietveld Method**. 4th ed. United States of American: Oxford University Press, 1996.

30 TOBY, B. H. EXPGUI, a graphical user interface for GSAS. **Journal of Applied Crystallography**, [*s. l.*], v. 34, p. 210-213, 2001.

31 LARSON, A. C.; VON DREELE, R. B. **GSAS**: General structure analysis system. New Mexico: Los Alamos National Laboratory Report LAUR 86-748, 2004.

32 RIETVELD, H. M. Line profiles of neutron powder-diffraction peaks for structure refinement. **Acta Crystallographica**, [*s. l.*], v. 22, p. 151-152, 1967.

33 MALI, S. S.; SHIM, C. S.; HONG, C. K. Highly porous zinc stannate (Zn 2 SnO 4) nanofibers scaffold photoelectrodes for efficient methyl ammonium halide perovskite solar cells. **Scientific Reports**, [*s. l.*], v. 5, p. 1-14, 2015.

34 JIA, T. *et al.* Synthesis, characterization and enhanced visible-light photocatalytic activity of Zn 2 SnO 4 /C nanocomposites with truncated octahedron morphology. **Ceramics International**, [*s. l.*], v. 42, p. 13893-13899, 2016.

35 DOU, J.; CHEN, Q. Zinc stannate nanostructures for energy conversion. **Chinese Journal of. Chemistry**, [*s. l.*], v. 39, n. 2, p. 367-380, 2021.

36 RAWAL, I. Facial synthesis of hexagonal metal oxide nanoparticles for low temperature ammonia gas sensing applications. **RSC Advances,** [*s. l.*], v. 5, p. 4135-4142, 2015.

37 WANG, S. *et al.* Influence of inorganic admixtures on the 11 Å-tobermorite formation prepared from steel slags: XRD and FTIR analysis. **Construction and Building Materials**, [*s. l.*], v. 60, p. 42-47, 2014.

38 NIKOLIĆ, M. V. *et al.* Far infrared properties of bulk sintered and thin film Zn 2 SnO 4, **Materials Science and Engineering**: B, [*s. l.*], v. 138, n. 1, p. 7-11, 2007.

39 WANG, Y.-F. *et al.* Nano-Zn 2 SnO 4 /reduced graphene oxide composites for enhanced photocatalytic performance. **Materials Chemistry and Physics Mater**, [*s. l.*], v. 254, p. 1-8, 2020.

40 SHEN, X. *et al.* Phase transition of Zn 2 SnO 4 nanowires under high pressure. **Journal of Applied Physics**, [*s. l.*], v. 106, n. 11, p. 1-5, 2009.

41 TUINSTRA, F.; KOENIG, J. L. Raman spectrum of graphite. **The Journal of Chemistry Physics**, [*s. l.*], v. 53, n. 3, p. 1126-1130, 1970.

42 CLARAMUNT, S. *et al.* The importance of interbands on the interpretation of the raman spectrum of graphene oxide. **Journal of Physics Chemistry C**, [*s. l.*], v. 119, p. 10123-10129, 2015.

43 MUZYKA, R. *et al.* Characterization of graphite oxide and reduced graphene oxide obtained from different graphite precursors and oxidized by different methods using raman spectroscopy. **Materials (Basel)**, [*s. l.*], v. 11, n. 7, 2018

44 LÓPEZ-DÍAZ, D. Towards understanding the raman spectrum of graphene oxide: the effect of the chemical composition. **Coatings**, [*s. l.*], v. 10, n. 6, p. 1-12, 2020.

45 KOSOWSKA, K. *et al.* Chitosan and graphene oxide/reduced graphene oxide hybrid nanocomposites: evaluation of physicochemical properties. **Materials Chemistry and Physics**, [*s. l.*], v. 216, p. 28-36, 2018.

46 CHLANDA, A. *et al.* Investigation into morphological and electromechanical surface properties of reduced-graphene-oxide-loaded composite fibers for bone tissue engineering applications: a comprehensive nanoscale study using atomic force microscopy approach. **Micron**, [*s. l.*], 146, 2021.

47 ONWUDIWE, D. C.; OYEWO, O. A. Facile synthesis and structural characterization of zinc stannate/tin oxide and zinc stannate/tin composites for the removal of methylene blue from water. **Materials Research Express**, [*s. l.*], v. 6, n. 1, 2019.

48 BREDAR, A. R. C. *et al.* Electrochemical impedance spectroscopy of metal oxide electrodes for energy applications. **ACS Applied Energy Materials**, [*s. l.*], v. 3, p. 66-88, 2020.

49 PERLES, C. E. Physicochemical properties related to the development of Nafion membranes for application in fuel cells. **Polymers**, São Carlos, v. 18, n. 4, p. 281-288, 2008.

50 BARD, A. J.; FAULKNER, L. R. **Electrochemical Methodos Fundamentals and Applications**. 1st ed. New York: Wiley, 2001.

51 PLETCHER, D. *et al.* **Instrumental methods in electrochemistry**. New York: John Wiley & Sons, 1985.

52 TOLEDO, R. A. *et al.* Estudo eletroquímico e químico-quântico da oxidação do antidepressivo tricíclico amitriptilina. **Química Nova**, São Paulo, v. 28, n. 3, p. 456-461, 2005.

53 MCCREERY, R. L. Advanced Carbon Electrode Materials for Molecular Electrochemistry. **Chemical Reviews**, [*s. l.*], v. 108, n. 7, p. 2646-2687, 2008.

54 QIAO, J. X.; LUO, H. Q.; LI, N. B. Electrochemical behavior of uric acid and epinephrine at an electrochemically activated glassy carbon electrode. **Colloids Surf B Biointerfaces**, [*s. l.*], v. 62, n. 1, p. 31-35, 2008.

55 YI, Y. *et al.* Electrochemical corrosion of a glassy carbon electrode. **Catalysis Today**, [*s. l.*], v. 295, p. 32-40, 2017.

56 GOSSER JR., D. K. **Cyclic voltammetry**: simulation and analysis of reaction mechanisms. New York: UCH Publishers, 1993.

57 WANG, J. **Analytical electrochemistry**. New York: Wiley VCH, 2001.

58 LIU, T. *et al.* New insights into the effect of pH on the mechanism of ofloxacin electrochemical detection in aqueous solution. **Physical Chemistry Chemical Physics**, [*s. l.*], v. 21, p. 16282-16287, 2019.

59 KOMORSKY-LOVRIC, S.; LOVRIC, M. Theory of square-wave stripping voltammetry with adsorptive accumulation. **Electrochemical Acta**, [*s. l.*], v. 335, p. 289-294, 1989.

60 WEBBER, A.; SHAH, M.; OSTERYOUNG, J. Electrochemical reduction and determination of cimetidine at nanomolar to micromolar levels of concentration. **Analytica Chimica Acta**, [*s. l.*], v. 154, p. 105-109, 1983.

61 MIRCESKI, V.; KOMORSKY-LOVRIC, S.; LOVRIC, M. **Square-Wave Voltammetry**: theory and application. República da Macedônia: Springer, 2007.

62 SOUZA, D.; MACHADO, S. A. S.; AVACA, L. A. **Voltametria de onda quadrada**. Primeira parte: aspectos teóricos. Química Nova, São Paulo, v. 26, p. 81-89, 2003.

63 RIBEIRO, F. W. P. *et al.* Analytical determination of nimesulide and ofloxacin in pharmaceutical preparations using square-wave voltammetry. **Journal of Analytical Chemistry**, [*s. l.*], v. 69, p. 62-71, 2014.

64 JIANG, Z. *et al.* Electrochemical sensor based on a novel Pt-Au bimetallic nanoclusters decorated on reduced graphene oxide for sensitive detection of ofloxacin. **Electroanalysis**, [*s. l.*], v. 29, p. 602-608, 2017.

65 JIANG, Z.; LI, G.; ZHANG, M. A novel electrochemical sensor based on SH-β-cyclodextrin functionalized gold nanoparticles/reduced-graphene oxide nanohybrids for ultrasensitive electrochemical sensing of acetaminophen and ofloxacin. **International Journal of Electrochemical Science**, [*s. l.*], v. 12, p. 5157-5173, 2017.

66 HAN, H.; LI, J.-Z.; PANG, X.-Z. Electrochemical sensor using glassy carbon electrode modified with HPMαFP/Ppy/GCE composite film for determination of ofloxacin. **International Journal of Electrochemical Science**, [*s. l.*], v. 8, p. 9060-9070, 2013.

67 SI, X. *et al.* Detection of ofloxacin by differential pulse voltammetry in drugs based on a novel p-aminobenzene sulfonic acid/graphene. **International Journal Electrochemical Science**, [*s. l.*], v. 15, p. 8883-8891, 2020.

68 ZHANG, F. *et al.* Simultaneous determination of ofloxacin and gatifloxacin on cysteic acid modified electrode in the presence of sodium dodecyl benzene sulfonate. **Bioelectrochemistry**, [*s. l.*], v. 89 p. 42-49, 2013.

69 HUANG, K.-J. *et al.* Voltammetric behavior of ofloxacin and its determination using a multi-walled carbon nanotubes-nafion film coated electrode. **Microchimica Acta**, [*s. l.*], v. 162 p. 227-233, 2008.

70 WONG, A. *et al.* Electrochemical sensor based on graphene oxide and ionic liquid for ofloxacin determination at nanomolar levels. **Talanta**, [*s. l.*], v. 161, p. 333-341, 2016.

ANEXO A - SUPPLEMENTARY MATERIAL

Figure S1 – Raman spectroscopy of pure phase Zn_2SnO_4 powder

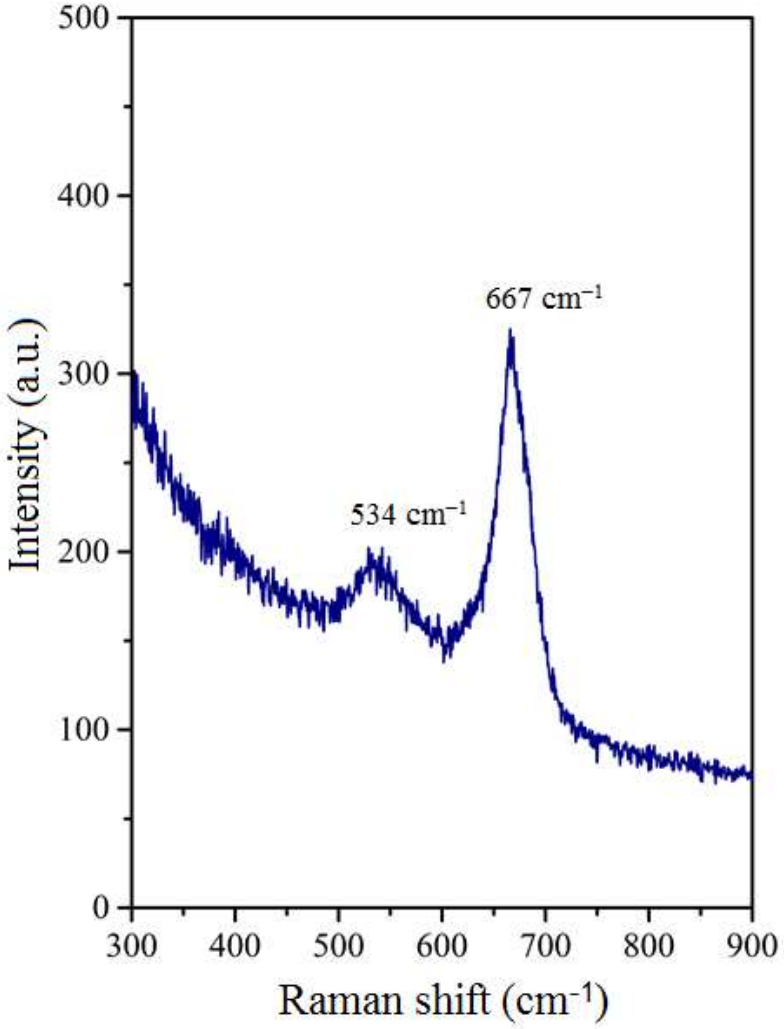

Fonte: (6).

4 MANUSCRITO 2: THEORETICAL INSIGHTS FROM ADSORPTION OF OFLOXACIN USING Zn_2SnO_4/REDUCED GRAPHENE OXIDE COMPOSITE[2]

ABSTRACT

Emerging Contaminants (EC), such as pesticides, steroid hormones, antibiotics growth accelerators, and inhibitors of pathogenic microorganisms, among others, have become an increasingly severe and worrying problem to ecosystems and human health, including the contamination of water bodies. Therefore, it is imperative to seek ways to measure and evaluate the current conditions of various environmental matrices so that urgent strategies can be planned and designed to mitigate the spread of these contaminants. Ofloxacin, a widely prescribed antibiotic, is resistant to biological degradation and promotes bacteria resistance, being considered environmentally maleficent. In this sense, this work arises to theoretically study the adsorption of ofloxacin (OFL) on two surfaces (zinc stannate (Zn_2SnO_4) and reduced graphene oxide (rGO)), considering that OFL is classified as a toxic organic EC and, therefore, it is imperative to develop analytical methodologies for their removal. Furthermore, all theoretical calculations were carried out in the CASTEP software using Density Functional Theory (DFT) and the GGA functional, obtaining results for adsorption energy, band structure and Total Density of States (TDOS). The results showed that adsorption occurs more effectively with Zn_2SnO_4 (1 0 0), with an adsorption energy of –21.03 eV, compared to –1.90 eV in the rGO surface (1 0 0), and that the metallic character of this compound did not change after OFL adsorption. However, the OFL-Zn_2SnO_4 complex had more states to be occupied. Furthermore, it was observed that the OFL-rGO complex presented a greater semiconductor character.

Keywords: emerging contaminants; ofloxacin; adsorption; in silico approach.

---

[2] Artigo submetido ao periódico: ***Chemical Papers*** e adaptado quanto à formatação para inclusão nesta tese.
Título: Theoretical insights from adsorption of ofloxacin using Zn_2SnO_4/reduced graphene oxide composite
Autores: Janevane S. de Castro[*,**], Renato V. de Oliveira[**], Lucas L. Bezerra[**], José O. de Souza-Júnior[**], Anderson V. Chaves[**], Pierre B. A. Fechine[**], P. de Lima-Neto[**], Adriana N. Correia[**], Norberto K. V. Monteiro[**]
[*]Departamento de Engenharia de Alimentos, Universidade Federal do Ceará, Campus do Pici, 60440-900, Fortaleza, CE, Brazil
[**]Departamento de Química Analítica e Físico-Química, Universidade Federal do Ceará, Campus do Pici, 60440-900, Fortaleza, CE, Brazil
Corresponding author: Prof. Norberto K. V. Monteiro. E-mail address: norbertokv@ufc.br

1 Introduction

Emerging contaminants (EC) and environmental pollutants are a class of natural or synthetic chemical compounds of extreme importance to the pharmaceutical and agricultural industries that contaminate Earth's atmosphere, lithosphere, and hydrosphere, thus affecting the terrestrial ecosystem and human health. Among these compounds and their derivatives, we can highlight pesticides, surfactants, pharmaceutical products, fertilizers, heavy metals, etc. (1, 2, 3). Therefore, developing electroanalytical techniques capable of removing the EC is extremely important for achieving the sixth goal of the United Nations Sustainable Development Goals, which guarantees clean water and sanitation for all (4, 5, 6).

It's a fact that water is an indispensable natural resource for maintaining the conditions of existence and environmental equilibrium of all species of living beings on our planet. Starting from this principle, it's imperative to maintain the global hydric resources with the minimum conditions of potability and human and industrial use to secure one of the basic conditions for life on planet Earth (2, 5, 6).

Ofloxacin (OFL) is a highly prescribed synthetic antibiotic for treating respiratory and urinary infections in humans and animals (7). As a contaminant, it not only persists in the environment due to the difficulty of biological degradation but can also contribute to developing bacteria resistance to the antibiotic (7, 8). Aiming to reduce the impact of ofloxacin on the environment, it has developed works investigating the antibiotic's capture by adsorption (7, 8, 9, 10). For example, Cu-BTC@Fe_3O_4 nanoparticles presented an adsorption capacity of 11.14 mg g^{-1} for ofloxacin, with an efficiency of 62.31% within a 3-hour contact time (9). Additionally, calcined verde-lodo (CVL) clay effectively adsorbed ofloxacin and presented potential for electrochemical-based regeneration after adsorption (10).

Computational methodologies based on Density Functional Theory (DFT) (11, 12, 13) were utilized to investigate the adsorption mechanism of emerging contaminants (14, 15, 16, 17). According to Spaolonzi *et al*. (14), compared to other contaminants, ofloxacin was found to be most reactive, as indicated by its lower hardness value, obtained from the HOMO/LUMO energy gap, considering that molecules with larger gaps are more stable and less reactive. This result suggests that ofloxacin has higher removals. Electronic properties, e.g., the density of states and charge density, of the interaction between paracetamol and different adsorbents were obtained using DFT calculations, showing a good correlation with experiments performed (17).

Due to the environmental problems related to the EC, this work pursues an alternative to detect and remove the drug ofloxacin (OFL) in a simple, fast, and inexpensive way using of two adsorbents, zinc stannate (Zn_2SnO_4) and reduced graphene oxide (rGO), because both the surfaces possess numerous applications in adsorptive process (18, 19, 20, 21).

To better understand the stability and spontaneity of the adsorption process of OFL in both compounds (zinc stannate and reduced graphene oxide), theoretical calculations involving adsorption energy were performed (19, 22, 23). Furthermore, electronic properties calculations such as band structures and total density of states were performed to understand better the energy band gap for the adsorbents (Zn_2SnO_4 and rGO) without the adsorbate and with the adsorbate (OFL), as well as analyze the conduction and valence bands of the species.

2 Computational methodology

The Density Functional Theory (DFT) was employed to analyze the ofloxacin adsorption in Zn_2SnO_4 (1 0 0) and rGO (1 0 0) surfaces through Cambridge Serial Total Energy Package (CASTEP) software (24). The optimization, single point, and electronic calculations were realized by the Generalized Gradient Approximation (GGA) parametrized through Perdew-Burke-Ernzerhof (PBE) functional as an exchange-correlation term (25). Both systems (Zn_2SnO_4-ofloxacin and rGO-ofloxacin) were simulated with an energy cutoff of 381.0 eV, and the Brillouin Zone (BZ) k-points sampling was generated by the Monkhorst–Pack (26) with a 1 × 1 × 1 grid. Furthermore, the Broyden Fletcher Goldfarb Shanno (BFGS) (27) algorithm was utilized in the optimization calculations with the convergence criteria of maximum energy change of 5.0 × 10□□ eV atom□□, maximum RMS force of 0.1 eV $Å^{-1}$, maximum RMS stress of 0.2 GPa, and maximum RMS (root mean square) displacement of 5.0 × 10^{-3} Å.

Two layers slab models were used to represent the Zn_2SnO_4 (1 0 0) surface, while one layer slab model was used to describe the rGO (1 0 0). In both systems, the layers remained relaxed during the geometry optimization. Furthermore, a vacuum region was created between the slabs of 30 Å for both systems. Fig. 1 shows the ofloxacin molecule adsorbed in (a) Zn_2SnO_4 (1 0 0) surface and (b) rGO (1 0 0) surface. The adsorption energy (E_{ads}) calculation between the ofloxacin molecule with the Zn_2SnO_4 (1 0 0) and rGO (1 0 0) surfaces were obtained through equation 1.

$$E_{ads} = E_{Zn_2SnO_4\text{-}ofloxacin/rGO\text{-}ofloxacin} - (E_{ofloxacin} + E_{Zn_2SnO_4/rGO}) \quad (1)$$

where the terms are the EZn_2SnO_4-*ofloxacin/rGO-ofloxacin* , *Eofloxacin* and EZn_2SnO_4/*rGO* terms are the total energies of the complex between the ofloxacin molecule with the Zn_2SnO_4 (1 0 0) or rGO (1 0 0) surfaces, ofloxacin molecule isolated in vacuum, and on the clean surface, respectively.

Figure 1 - (a) Zn_2SnO_4 (1 0 0) supercell adsorbed with the ofloxacin molecule. (b) rGO (1 0 0) supercell adsorbed with the ofloxacin molecule

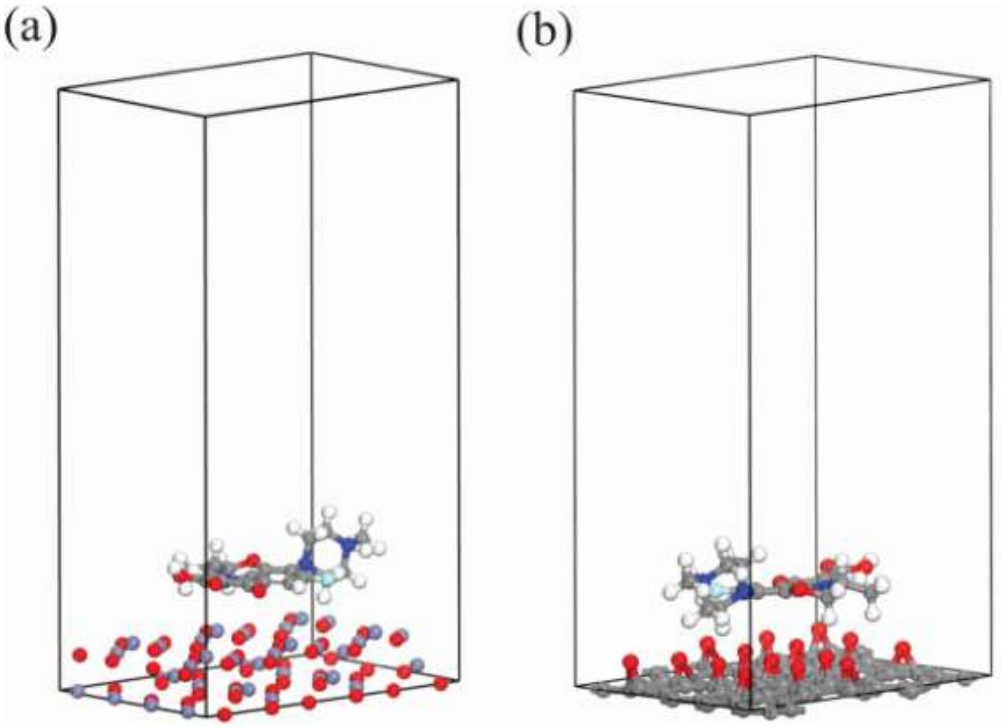

Fonte: Artigo submetido ao periódico Chemical Papers (Anexo B).

3 Results and discussion

3.1 Ofloxacin adsorption on Zn_2SnO_4 (1 0 0) surface and rGO (1 0 0) supercell

The ofloxacin molecule adsorption on both surfaces was analyzed based on adsorption energy obtained from equation 1. The Zn_2SnO_4-ofloxacin and rGO-ofloxacin systems registered adsorption energy values of −21.03 eV and −1.90 eV, respectively. Therefore, the adsorption results indicated that the ofloxacin molecule showed more favorable adsorption on the Zn_2SnO_4 (1 0 0) surface than the rGO (1 0 0) surface due to the lowest adsorption energy values.

3.2 Electronic properties

The band structures and density of states were utilized to analyze the electronic properties of systems. Figs. 2a and 2b showed the band structures only of Zn_2SnO_4 (1 0 0) and rGO (1 0 0) surfaces, while the Figs. 2c and 2d showed the same surfaces adsorbed with the ofloxacin molecule, respectively. The Fermi energy (E_F) represented by the dashed line in red color in all the graphs at 0 eV is utilized to separate the conduction and from the valence band (28).

Analyzing the system containing the Zn_2SnO_4 (1 0 0) surface (Figs. 2a and 2c), it was observed that before or after the ofloxacin adsorption, the conduction band remains overlaps the valence band, indicating that the metallic character did not change with the ofloxacin molecule adsorption. For the rGO (1 0 0) surface (Fig 2b), after the ofloxacin adsorption (Fig. 2d), it was observed an increase of 0.024 (this band gap may be seen in Fig S1 in the supplementary material through zoom of Fig. 2b) to 0.554 eV of a direct band gap in Z k-point, indicating an increase of semiconductor character.

Figure 2 – Band structure of the (a) Zn_2SnO_4 (1 0 0) surface, (b) rGO (1 0 0) surface, (c) ofloxacin adsorbed in Zn_2SnO_4 (1 0 0) surface, and (d) ofloxacin adsorbed in rGO (1 0 0) surface

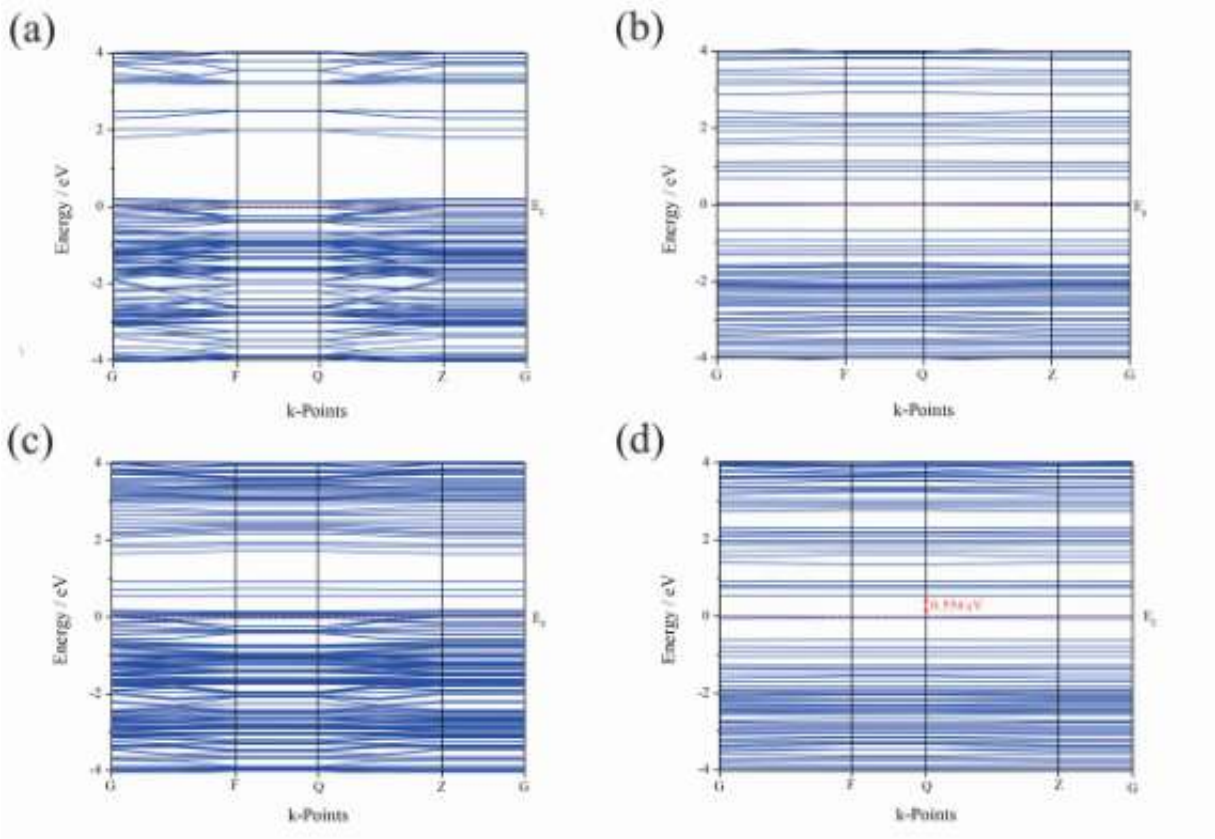

Fonte: Artigo submetido ao periódico Chemical Papers (Anexo B).

Fig. 3 shows the Total Density of States (TDOS) analysis for the Zn_2SnO_4-ofloxacin (black line) and rGO-ofloxacin (red line) systems. The energy range utilized in the TDOS analysis was −30 to 30 eV. Concerning the Zn_2SnO_4-ofloxacin system, it registered the highest peak (190 electrons eV^{-1}) in band conduction, around −10.5 eV. The second highest peak was registered at 130 electrons eV^{-1}, around 22.2 eV in the valence band. On the other hand, the rGO-ofloxacin TDOS showed the highest peak at a value of 170 electrons eV^{-1}, around 14.2 eV in the valence band.

Figure 3 – TDOS of complexes formed by the (a) Zn_2SnO_4 (1 0 0) surface with the ofloxacin molecule and (b) rGO (1 0 0) surface with the ofloxacin molecule

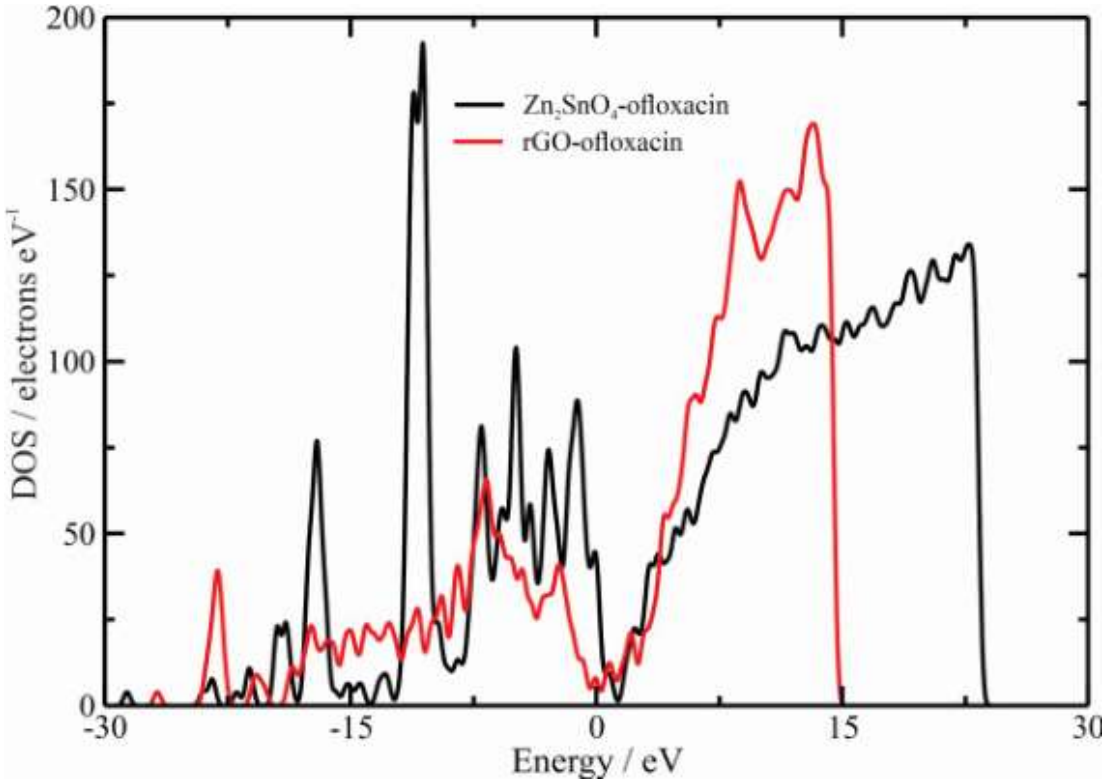

Fonte: Artigo submetido ao periódico Chemical Papers (Anexo B).

The second highest peak (65 electrons eV^{-1}) was registered in the conduction band around −7.2 eV. The other peaks with small TDOS values will not be discussed for the two systems analyzed. Therefore, the TDOS results suggest that after the ofloxacin molecule adsorption, the Zn_2SnO_4-ofloxacin system has more states to be occupied than the rGO-ofloxacin system.

4 Conclusions

The DFT calculations indicated that the OFL molecule has favorable adsorption on the Zn_2SnO_4 (1 0 0) surface than the rGO (1 0 0) surface. The electronic properties showed that after the OFL molecule adsorption, it did not change the behavior of metallic character for the Zn_2SnO_4-ofloxacin system. However, the rGO-ofloxacin system showed an increase in semiconductor character. Furthermore, the TDOS analysis indicated that the Zn_2SnO_4-ofloxacin system has more states to be occupied concerning the rGO-ofloxacin system after the ofloxacin molecule adsorption.

Supplementary Information: The online version contains supplementary material available.

ACKNOWLEDGEMENTS

This study was financed in part by the Coordenação de Aperfeiçoamento de Pessoal de Nível Superior - Brasil (CAPES) – Finance Code 001. The authors thank the financial support given by the following Brazilian funding agencies: Coordenação de Aperfeiçoamento de Pessoal de Nível Superior (CAPES), Conselho Nacional de Desenvolvimento Científico e Tecnológico (CNPq) and Fundação Cearense de Apoio ao Desenvolvimento Científico e Tecnológica (FUNCAP). R. V. de Oliveira, Lucas L. Bezerra and José O. de Souza-Júnior thank CNPq and CAPES for their grants. P.B.A. Fechine thanks CNPq(proc. 308452/2022-4) and Funcap (proc. PNE-0112-00048.01.00/16). P. de Lima-Neto thanks CNPq (proc. 302825/2022-3). A.N. Correia gratefully acknowledges funding provided by CNPq (proc. 305136/2018-6 and proc. 305103/2022-9). The authors also thanks Centro Nacional de Processamento de Alto Desempenho (CENAPAD) of the Federal University of Ceará (UFC) for providing computational resources.

Conflict of interest: The authors declare that they have no conflict of interest.

REFERENCES

1 COCCIA, M.; BONTEMPI, E. New trajectories of technologies for the removal of pollutants and emerging contaminants in the environment. **Environmental Research**, [*s. l.*], v. 229, p. 1-10, 2023.

2 RADWAN, E. K. *et al.* Recent trends in treatment technologies of emerging contaminants. **Environmental Quality Management,** [*s. l.*], v. 32, n. 3, p. 7-25, 2023.

3 PURI, M.; GANDHI, K.; KUMAR, M. S. Emerging environmental contaminants: a global perspective on policies and regulations. **Journal of Environmental Management**, [*s. l.*], v. 332, p. 1-13, 2023.

4 TUNIOLI, F. *et al*. Adsorption of emerging contaminants by graphene related materials and their alginate composite hydrogels. **Journal of Environmental Chemical Engineering**, [*s. l.*], v. 11, n. 2, p. 1-11, 2023.

5 GHAFAR, H. H. A.; RADWAN, E.K.; EL-WAKEEL S. T. Removal of Hazardous Contaminants from Water by Natural and Zwitterionic Surfactant-modified Clay. **ACS Omega**, [*s. l.*], v. 5, p. 6834-6845, 2020.

6 AL-RIFAI, J. H.; KHABBAZ, H.; SCHÄFER, A. I. Removal of pharmaceuticals and endocrine disrupting compounds in a water recycling process using reverse osmosis systems. **Separation and Purification Technology**, [*s. l.*], v. 77, p. 60–67, 2011.

7 ANTONELLI, R. *et al.* Ofloxacin adsorption by calcined Verde-lodo bentonite clay: batch and fixed bed system evaluation. **Journal of Molecular Liquids**, [*s. l.*], v. 315, p. 1-13, 2020.

8 DILXAT, D. *et al.* Insights into the interaction mechanism of ofloxacin and functionalized nano-polystyrene. **Spectrochimica Acta Part A**: Molecular and Biomolecular Spectroscopy, [*s. l.*], v. 284, p. 1-10, 2023.

9 CHANG, F. *et al.* Selective adsorption of emerging contaminants from aqueous solution using Cu-based composite by solvothermal. **International Journal of Environmental Science and Technology**, [*s. l.*], v. 19, p. 11161–11168, 2022.

10 ANTONELLI, R. *et al.* Hybrid process of adsorption and electrochemically based green regeneration of bentonite clay for ofloxacin and ciprofloxacin removal. **Environmental Science and Pollution Research**, [*s. l.*], v. 30, p. 53648-53661, 2023.

11 PARR, R. G. Density Functional Theory of Atoms and Molecules. *In*: FUKUI, K.; PULLMAN, B. (ed.). **Horizons of Quantum Chemistry**. Dordrecht: Springer Netherlands, 1980. p 5–15.

12 STEPHENS, P. J. *et al*. Ab Initio Calculation of Vibrational Absorption and Circular Dichroism Spectra Using Density Functional Force Fields. **The Journal of Physical Chemistry**, [*s. l.*], v. 98, p. 11623–11627, 1994.

13 HOHENBERG, P.; KOHN, W. Inhomogeneous Electron Gas. **Physical Review**, [*s. l.*], v. 136, p. B864–B871, 1964.

14 SPAOLONZI, M. P. *et al*. Green-functionalized carbon nanotubes as adsorbents for the removal of emerging contaminants from aqueous media. **Journal of Cleaner Production**, [*s. l.*], v. 373, p. 1-14, 2022.

15 RAO, A. *et al.* Adsorption of five emerging contaminants on activated carbon from aqueous medium: kinetic characteristics and computational modeling for plausible mechanism. **Environmental Science and Pollution Research**, [*s. l.*], v. 28, p. 21347–21358, 2021.

16 SPAOLONZI, M. P.; SILVA, M. G. C.; VIEIRA, M. G. A. Adsorption of antibiotic cefazolin in organoclay fixed-bed column: characterization, mathematical modeling, and DFT-based calculations. **Environmental Science and Pollution Research**, [*s. l.*], v. 29, p. 31646–31658, 2022.

17 SPALTRO, A. *et al.* Removal of paracetamol from aqueous solution by activated carbon and silica. Experimental and computational study. **Journal of Contaminant Hydrology**, [*s. l.*], v. 236, p. 1-10, 2021.

18 EL-SAYED, D. S. Electronic band structure and density of state modulation of amphetamine and ABW type–zeolite adsorption system: DFT-CASTEP analysis. J**ournal of Molecular Modeling**, [*s. l.*], v. 29, n. 96, p. 1-11, 2023.

19 LIANG, H. *et al.* Adsorption behavior of molecules on Zn 2 SnO 4 (1 1 1) crystal plane and its effect on electrical conductivity. **Inorganic Chemistry Communications**, [*s. l.*], v. 144, p. 1-11, 2022.

20 KASHYAP, A. *et al.* Selective and Sensitive Detection of Formaldehyde at Room Temperature by Tin Oxide Nanoparticles/Reduced Graphene Oxide Composite. **ACS Applied Nano Materials**, [*s. l.*], v. 6, p. 7948-7959, 2023.

21 ANTÔNIO, R. S. *et al.* Application of graphene nanosheet oxide for atrazine adsorption in aqueous solution: synthesis, material characterization, and comprehension of the adsorption mechanism. **Environmental Science and Pollution Research**, [*s. l.*], v. 28, p. 5731–5741, 2021.

22 WANG, Y.-F. *et al.* Nano-Zn 2 SnO 4 /reduced graphene oxide composites for enhanced photocatalytic performance. **Materials Chemistry and Physics Mater**, [*s. l.*], v. 254, p. 1-8, 2020.

23 PENG, X. *et al.* Z-scheme transfer pathway assisted photoelectrocatalyst Zn 2 SnO 4 /rGO/Ag/AgBr for organic pollutants treatment. **Colloids Surfaces A**: Physicochemical and Engineering Aspects, [*s. l.*], v. 657, part A, p. 1-9, 2023.

24 CLARK, S. J. *et al.* First principles methods using CASTEP. **Zeitschrift für Krist-Cryst Mater**, [*s. l.*], v. 220, p. 567–570, 2005.

25 PERDEW, J. P.; BURKE, K.; ERNZERHOF, M. Generalized Gradient Approximation Made Simple. **Physical Review Letters**, [*s. l.*], v. 77, p. 3865–3868, 1997.

26 PACK, J. D.; MONKHORST, H. J. "Special points for Brillouin-zone integrations": a reply. **Physical Review B**, [*s. l.*], v. 16, p. 1748-1749, 1977.

27 FLETCHER, R. **Practical Methods of Optimization**. 2nd ed. New York: John Wiley & Sons, 1987.

28 USMAN, M. *et al.* First-principles calculations to investigate Structural, Electronic, optical and mechanical properties of Cu-based fluoroperovskite XCuF3 (X = K, Ru). **Computational and Theoretical Chemistry**, [*s. l.*], v. 1124, p. 1-5, 2023.

ANEXO A - SUPPLEMENTARY MATERIAL

Fig. S1 – Zoom in band structure only the rGO (1 0 0) surface

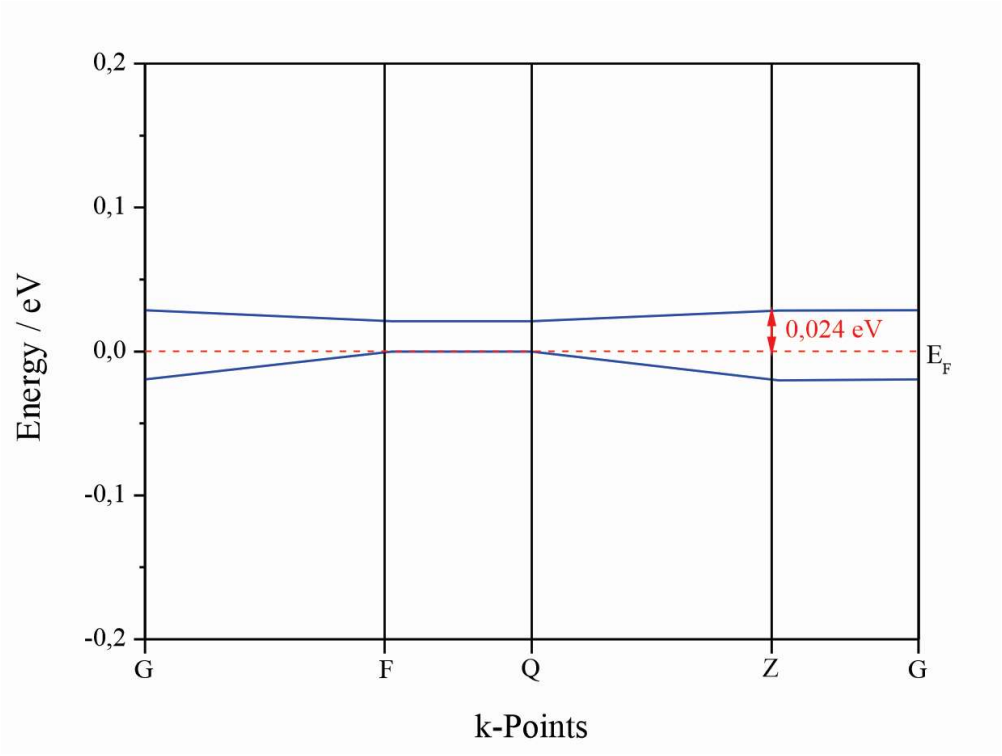

Fonte: Artigo submetido ao periódico Chemical Papers (Anexo B).

5 CONCLUSÕES

O Zn_2SnO_4 foi sintetizado, caracterizado e aplicado ineditamente com êxito no desenvolvimento de um sensor eletroquímico para determinação de OFL, por meio da VOQ. Ante o exposto, ficou claro o sinergismo entre os componentes do compósito (Zn_2SnO_4 e OGr) frente à detecção do OFL em amostras de fármacos. Evidenciou-se também eficiência no uso das informações obtidas por meio do diagrama de especiação do OFL para a compreensão da relação entre as espécies presentes no equilíbrio ($OFL^{\square}$, OFL^{+}, $OFL^{\square}$), a superfície eletródica modificada e otimização do eletrólito de suporte e pH. A espécie protonada (OFL^{+}) apresentou maior interação eletroquímica ao ECV/Zn_2SnO_4-OGr, exibindo ainda um comportamento eletroquímico anódico, irreversível, bieletrônico e de controle misto (difusional e adsortivo). O sistema desenvolvido (ECV/Zn_2SnO_4-OGr) demonstrou elevada sensibilidade, precisão e exatidão; ótima repetibilidade; e taxa média de recuperação aceitáveis para as amostras avaliadas. Os resultados apontaram que a metodologia eletroanalítica desenvolvida pode propiciamente ser utilizada como ferramenta alternativa na determinação de OFL em formulação farmacêutica comercial. Os estudos químico-teóricos apontaram que o processo de adsorção do OFL na superfície com Zn_2SnO_4 (E_{ads} = □21,03 eV) é mais espontâneo quando comparado a superfície com OGr (E_{ads} = □1,90 eV); denotando a significativa importância do óxido misto sintetizado na estrutura do compósito desenvolvido, frente a proposta do sensor desenvolvido.

REFERÊNCIAS

ABRAMS, A. C. **Clinical Pharmacotherapy**: principles for nursing practice. 7th ed. [*S. l.*]: Guanabara Publisher, 2006.

AGADI, N. P. *et al*. Fabrication of NiSe 2 decorated graphene oxide nanocomposite modified electrode as a high performance electrochemical sensor for carbamazepine. **Electroanalysis**, [*s. l.*], v. 35, n. 12, p. 1-12, 2023.

AKKAPINYO, C. *et al*. Disposable electrochemical sensor for food colorants detection by reduced graphene oxide and methionine film modified screen printed carbon electrode. **Molecules**, [*s. l.*], v. 26, p. 1-18, 2021.

ALBRECHT, R. Development of antibacterial agents of the nalidixic acid type. *In:* JUCKER, E. (ed.). **Progress in Drug Research**. [*S. l.*]: Birkhäuser Verlag Basel, 1977. v. 21, p. 11-104.

AL-RIFAI, J. H.; KHABBAZ, H.; SCHÄFER, A. I. Removal of pharmaceuticals and endocrine disrupting compounds in a water recycling process using reverse osmosis systems. **Separation and Purification Technology**, [*s. l.*], v. 77, p. 60–67, 2011.

ANDREU, V.; BLASCO, C.; PICO, Y. Analytical strategies to determine quinolone residues in food and the environment. **TrAC Trends in Analytical Chemistry**, [*s. l.*], v. 26, p. 534-556, 2007.

ANTONELLI, R. *et al.* Hybrid process of adsorption and electrochemically based green regeneration of bentonite clay for ofloxacin and ciprofloxacin removal. **Environmental Science and Pollution Research**, [*s. l.*], v. 30, p. 53648-53661, 2023.

ANTONELLI, R. *et al.* Ofloxacin adsorption by calcined Verde-lodo bentonite clay: batch and fixed bed system evaluation. **Journal of Molecular Liquids**, [*s. l.*], v. 315, p. 1-13, 2020.

ANTÔNIO, R. S. *et al.* Application of graphene nanosheet oxide for atrazine adsorption in aqueous solution: synthesis, material characterization, and comprehension of the adsorption mechanism. **Environmental Science and Pollution Research**, [*s. l.*], v. 28, p. 5731–5741, 2021.

ANVISA. Farmacopeia brasileira. 6. ed. Brasília, DF: Anvisa, 2019. Disponível em: https://www.gov.br/anvisa/pt-br/assuntos/farmacopeia/farmacopeia-brasileira/insumos-farmaceuticos-e-especialidades-ate-2a-errata-p-pdf-com-capa.pdf. Acesso em: 19 April 2023.

ANVISA. **Resolução da Diretoria Colegiada - RDC nº 166, de 24 de julho de 2017**. Dispõe sobre a validação de métodos analíticos e dá outras providências. [Brasília, DF]: Anvisa, 2017. Disponível em: http://antigo.anvisa.gov.br/documents/10181/2721567/RDC_166_2017_COMP.pdf/d5fb92b3-6c6b-4130-8670-4e3263763401. Acesso em: 14 March 2023.

ARAFAT, M. M.; ONG, J. Y.; HASEEB, A. S. M. A. Selectivity shifting behavior of Pd nanoparticles loaded zinc stannate/zinc oxide (Zn 2 SnO 4 /ZnO) nanowires sensors. **Applied Surface Science**, [*s. l.*], v. 435, p. 928-936, 2018.

BAGHERI, H. *et al*. Composite of Cu metal nanoparticles-multiwall carbon nanotubes-reduced graphene oxide as a novel and high performance platform of the electrochemical sensor for simultaneous determination of nitrite and nitrate. **Journal of Hazardous Materials**, [*s. l.*], v. 324, p. 762-772, 2017.

BARANWAL J. *et al.* Electrochemical sensors and their applications: a review. **Chemosensors**, [*s. l.*], v. 10, p. 363-375, 2022.

BARD, A. J.; FAULKNER, L. R.; WHITE, H. S. E**lectrochemical methods**: fundamentals and applications. 3rd ed. [*S. l.*]: John Wiley & Sons, 2022.

BARD, A. J.; FAULKNER, L. R. **Electrochemical Methodos Fundamentals and Applications**. 1st ed. New York: Wiley, 2001.

BARTH, T. F. W.; POSNJAK, E. Spinel structures: with and without variate atom equipoints. **Zeitschrift fur Kristallographie**: Crystalline Materials, [*s. l.*], v. 82, p. 325-341, 1932.

BAYABIL, H. K.; TESHOME, F. T.; YUNCONG, C. L. Emerging contaminants in soil and water. **Frontiers in Environmental Science**, [*s. l.*], v. 10, p. 1-8, 2022.

BELLIARD, F.; CONNOR, P. A.; IRVINE, J. T. S. Novel tin oxide-based anodes for Li-íon batteries. **Solid State Ionics**, [*s. l.*], v. 135, p. 163-167, 2000.

BILAL, M. *et al*. Hydrogen-based catalyst assisted advanced oxidation processes to mitigate emerging pharmaceutical contaminants. **International Journal Hydrogen Energy**, [*s. l.*], v. 47, n. 45, p. 19555-19569, 2022.

BOCKRIS, J. **Modern electrochemistry**: an introduction to an interdisciplinary area. [*S. l.*]: Springer Science, 2012.

BREDAR, A. R. C. *et al.* Electrochemical impedance spectroscopy of metal oxide electrodes for energy applications. **ACS Applied Energy Materials**, [*s. l.*], v. 3, p. 66-88, 2020.

CDC. A**ntibiotic use in the United States, 2018**. Atlanta, GA: US Department of Health and Human Services, 2019. Disponível em: https://www.cdc.gov/antibiotic-use/stewardship-report/pdf/stewardship-report-2018-508.pdf. Acesso em: 01 out. 2023.

CHABOT, V. *et al*. A review of graphene and graphene oxide sponge: material synthesis and applications to energy and the environment. **Energy & Environment Science**, [*s. l.*], v. 5, p. 1564-1596, 2014.

CHANG, F. *et al.* Selective adsorption of emerging contaminants from aqueous solution using Cu-based composite by solvothermal. **International Journal of Environmental Science and Technology**, [*s. l.*], v. 19, p. 11161–11168, 2022.

CHLANDA, A. *et al.* Investigation into morphological and electromechanical surface properties of reduced-graphene-oxide-loaded composite fibers for bone tissue engineering applications: a comprehensive nanoscale study using atomic force microscopy approach. **Micron**, [*s. l.*], 146, 2021.

CHU, D. T.; FERNANDES, P. B. Structure-activity relationships of the fluoroquinolones. **Antimicrobial Agents and Chemotherapy**, [*s. l.*], v. 33, n. 2, p.131-135, 1989.
CLARAMUNT, S. *et al.* The importance of interbands on the interpretation of the raman spectrum of graphene oxide. **Journal of Physics Chemistry C**, [*s. l.*], v. 119, p. 10123-10129, 2015.

CLARK, S. J. *et al.* First principles methods using CASTEP. **Zeitschrift für Krist-Cryst Mater**, [*s. l.*], v. 220, p. 567–570, 2005.

COCCIA, M.; BONTEMPI, E. New trajectories of technologies for the removal of pollutants and emerging contaminants in the environment. **Environmental Research**, [*s. l.*], v. 229, p. 1-10, 2023.

COFFEEN, W. W. Ceramic and dielectric properties of the stannates. **Journal of the American Ceramic Society**, [*s. l.*], v. 36, p. 207-214, 1953.

DAVYDOV, N. *et al*. Determination of fluoroquinolone antibiotics through the fluorescent response of Eu (III) based nanoparticles fabricated by layer-by-layer technique. **Analytica Chimica Acta**, [*s. l.*], v. 784, p. 65-71, 2013.

DENG, Y. *et al*. Effects of ofloxacin on the structure and function of freshwater microbial communities. **Aquatic Toxicology**, [*s. l.*], v. 244, p. 1-9, 2022.

DIAZ-CRUZ, M. S.; ALDA, M. J. L.; BARCELÓ, D. Environmental behavior and analysis of veterinary and human drugs in soils, sediments and sludge. **TrAC Trends in Analytical Chemistry**, [*s. l.*], v. 22, p. 340-351, 2003.

DILXAT, D. *et al.* Insights into the interaction mechanism of ofloxacin and functionalized nano-polystyrene. **Spectrochimica Acta Part A**: Molecular and Biomolecular Spectroscopy, [*s. l.*], v. 284, p. 1-10, 2023.

DOU, J.; CHEN, Q. Zinc stannate nanostructures for energy conversion. **Chinese Journal of. Chemistry**, [*s. l.*], v. 39, n. 2, p. 367-380, 2021.

DRAKOPOULOS, A. I.; IOANNOU, P. C. Spectrofluorimetric study of the acid–base equilibria and complexation behavior of the fluoroquinolone antibiotics ofloxacin, norfloxacin, ciprofloxacin and pefloxacin in aqueous solution. **Analytica Chimica Acta**, [*s. l.*], v. 354, p. 197-204, 1997.

DU, H.; XIE, Y.; WANG, J. Nanomaterial-sensors for herbicides detection using electrochemical techniques and prospect applications. **Trends in Analytical Chemistry**, [*s. l.*], v. 135, p.1-9, 2021.

ECR. Commission Regulation (EU) nº 37/2019 of 22 December 2009 on pharmacologically active substances and their classification regarding maximum residue limits in foodstuffs of animal origin. **Official Journal of the European Union**, [*s. l.*], 20 January, 2010.

EDA, G.; CHHOWALLA, M. Chemically derived graphene oxide: Towards large-area thin-film electronics and optoelectronics. **Advanced Materials**, [*s. l.*], v. 22, n. 22, p. 2392-2415, 2010.

EFSA. Perfluoroalkylated substances in food: occurrence and dietary exposure. **EFSA Journal**, [*s. l.*], v. 10, 2012.

EFSA. Scientific opinion on the risks to public health related to the presence of bisphenol A (BPA) in foodstuffs. **EFSA Journal**, [*s. l.*], v. 13, 2015.

EL-SAYED, D. S. Electronic band structure and density of state modulation of amphetamine and ABW type–zeolite adsorption system: DFT-CASTEP analysis. J**ournal of Molecular Modeling**, [*s. l.*], v. 29, n. 96, p. 1-11, 2023.

EMA. **ICH Guideline Q2 (R2) on Validation of Analytical Procedures**: step 2b. TheNetherlands: EMA, 2022. Disponível em: https://pink.pharmaintelligence.informa.com/-/media/supporting-documents/pink-sheet/2022/04/p0422ema_21.pdf/, 2022. Acesso em: 01 May 2023.

EROGUL, S. *et al.* A new electrochemical sensor based on Fe 3 O 4 functionalized graphene oxide–gold nanoparticle composite film for simultaneous determination of catechol and hydroquinone. **Electrochimica Acta**, [*s. l.*], v. 186, p. 302–313, 2015.

FARIA, L. V. D. *et al*. Adsorptive stripping voltammetric determination of chloramphenicol residues in milk samples using reduced graphene oxide sensor. **Analytical Methods**, [*s. l.*], v. 13, p. 5711-5718, 2021.

FENT, K.; WESTON, A. A.; CAMINADA, D. Ecotoxicology of human pharmaceuticals. **Aquatic Toxicology**, [*s. l.*], v. 76, n. 2, p. 122-159, 2006.
FLETCHER, R. **Practical Methods of Optimization**. 2nd ed. New York: John Wiley & Sons, 1987.

GAN, T. *et al*. Morphology-dependent electrochemical sensing properties of manganese dioxide-graphene oxide hybrid for guaiacol and vanillin. **Electrochimica Acta**, [*s. l.*], v. 147, p. 157–166, 2014.

GEIM, A. K.; NOVOSELOV, K. S. The rise of graphene, nanoscience and technology: a collection of reviews from nature journals. **Nanoscience and Technology**, [*s. l.*], p. 11–19, 2009.

GEISSEN, V. *et al.* Emerging pollutants in the environment: a challenge for water resource management. **International Soil and Water Conservation Research**, [*s. l.*], v. 3, p. 57-65, 2015.

GHAFAR, H. H. A.; RADWAN, E.K.; EL-WAKEEL S. T. Removal of Hazardous Contaminants from Water by Natural and Zwitterionic Surfactant-modified Clay. **ACS Omega**, [*s. l.*], v. 5, p. 6834-6845, 2020.

GHANBARI, M. H. *et al*. An electrochemical sensor based on poly (l-cysteine)-AuNPs reduced graphene oxide nanocomposite for determination of levofloxacin. **Microchemical Journal**, [*s. l.*], v. 147, p. 198-206, 2019.

GOMES, R. N. *et al*. Understanding the dipyrone oxidation allying electrochemical and computational approaches. **Analytica Chimica Acta**, [*s. l.*], v. 105, p. 49-57, 2019.

GOSSER JR., D. K. **Cyclic voltammetry**: simulation and analysis of reaction mechanisms. New York: UCH Publishers, 1993.

HAN, H.; LI, J.-Z.; PANG, X.-Z. Electrochemical sensor using glassy carbon electrode modified with HPMαFP/Ppy/GCE composite film for determination of ofloxacin. **International Journal of Electrochemical Science**, [*s. l.*], v. 8, p. 9060-9070, 2013.

HANSEN, M. *et al.* Fate and antibacterial potency of anticoccidial drugs and their main abiotic degradation products. **Environmental Pollution**, [*s. l.*], v. 157, n. 2, p. 474-480, 2009.

HOHENBERG, P.; KOHN, W. Inhomogeneous Electron Gas. **Physical Review**, [*s. l.*], v. 136, p. B864–B871, 1964.

HUANG, K.-J. *et al.* Voltammetric behavior of ofloxacin and its determination using a multi-walled carbon nanotubes-nafion film coated electrode. **Microchimica Acta**, [*s. l.*], v. 162 p. 227-233, 2008.

INDICE.EU. **Medicamentos**: Princípios ativos: Ofloxacina. [*S. l.*]: Indice.eu, c2023. Disponível em: https://www.indice.eu/pt/medicamentos/DCI/ofloxacina/informacao-cientifica. Acesso em: 04 mai. 2023.

IUPAC. **Nomenclature**. [*S. l.*]: IUPAC, c2023. Disponível em: https://iupac.org/what-we-do/nomenclature/. Acesso em: 04 mai. 2023.

JIA, T. *et al.* Synthesis, characterization and enhanced visible-light photocatalytic activity of Zn 2 SnO 4 /C nanocomposites with truncated octahedron morphology. **Ceramics International**, [*s. l.*], v. 42, p. 13893-13899, 2016.

JIANG, Z.; LI, G.; ZHANG, M. A novel electrochemical sensor based on SH-β-cyclodextrin functionalized gold nanoparticles/reduced-graphene oxide nanohybrids for ultrasensitive electrochemical sensing of acetaminophen and ofloxacin. **International Journal of Electrochemical Science**, [*s. l.*], v. 12, p. 5157-5173, 2017.

JIANG, Z. *et al.* Electrochemical sensor based on a novel Pt-Au bimetallic nanoclusters decorated on reduced graphene oxide for sensitive detection of ofloxacin. **Electroanalysis**, [*s. l.*], v. 29, p. 602-608, 2017.

JUNG, J. C.; BAEK, S.; PARK, O. S. Synthesis and antibacterial activity of 2-substituted 6-fluoro-1, 4-dihydro-4-oxo-3-quinolinecarboxylic acids. **II Farmaco**, [*s. l.*], v. 56, n. 9, p. 665-675, 2001.

KASHYAP, A. *et al.* Selective and Sensitive Detection of Formaldehyde at Room Temperature by Tin Oxide Nanoparticles/Reduced Graphene Oxide Composite. **ACS Applied Nano Materials**, [*s. l.*], v. 6, p. 7948-7959, 2023.

KEMPER, N. Veterinary antibiotics in the aquatic and terrestrial environment. **Ecological Indicators**, [*s. l.*], v. 8, p. 1-13, 2008.

KHAN, Z. U. *et al*. A review of graphene oxide, graphene buckypaper, and polymer/graphene composites: properties and fabrication techniques. **Journal of Plastic Film and Sheeting**, [*s. l.*], v. 32, p. 336-379, 2016.

KIMMEL, D. W. *et al*. Electrochemical sensors and biosensors. **Analytical Chemistry**, [*s. l.*], v. 84, n. 2, p. 685-707, 2012.

KOMORSKY-LOVRIC, S.; LOVRIC, M. Theory of square-wave stripping voltammetry with adsorptive accumulation. **Electrochemical Acta**, [*s. l.*], v. 335, p. 289-294, 1989.

KOSOWSKA, K. *et al.* Chitosan and graphene oxide/reduced graphene oxide hybrid nanocomposites: evaluation of physicochemical properties. **Materials Chemistry and Physics**, [*s. l.*], v. 216, p. 28-36, 2018.

KRASUCKA, P. *et al.* Adsorption and desorption of antiviral drugs (ritonavir and lopinavir) on sewage sludges as a potential environmental risk. **Journal of Hazardous Materials**, [*s. l.],* v. 425, p. 1-10, 2022.

KÜMMERER, K. Antibiotics in the aquatic environment: a review: part I. **Chemosphere**, [*s. l.*], v. 75, p. 417-434, 2009.

LANANAN, F. *et al*. Symbiotic bioremediation of aquaculture wastewater in reducing ammonia and phosphorus utilizing effective microorganism (EM-1) and microalgae (Chlorella sp.). **International Biodeterioration and Biodegradation**, [*s. l.*], v. 95, p. 127-134, 2014.

LARSON, A. C.; VON DREELE, R. B. **GSAS**: General structure analysis system. New Mexico: Los Alamos National Laboratory Report LAUR 86-748, 2004.

LIANG, H. *et al.* Adsorption behavior of molecules on Zn 2 SnO 4 (1 1 1) crystal plane and its effect on electrical conductivity. **Inorganic Chemistry Communications**, [*s. l.*], v. 144, p. 1-11, 2022.

LIAO, X. *et al*. An antifouling electrochemical sensor based on multiwalled carbon nanotubes functionalized black phosphorus for highly sensitive detection of carbendazim and corresponding response mechanisms analyses. **Microchemical Journal**, [*s. l.*], v. 190, p. 1-12, 2023.

LIU, G. *et al*. Electrochemical approach toward reduced graphene oxide-based electrodes for environmental applications: a review. **Science of the Total Environment**, [*s. l.*], v. 778, p. 1-14, 2021.

LIU, N. *et al*. Gold nanoparticles-decorated peptide hydrogel for antifouling electrochemical dopamine determination. **Microchimica Acta**, [*s. l.*], v. 190, p. 2-10, 2023.

LIU, T. *et al.* New insights into the effect of pH on the mechanism of ofloxacin electrochemical detection in aqueous solution. **Physical Chemistry Chemical Physics**, [*s. l.*], v. 21, p. 16282-16287, 2019.

LÓPEZ-DÍAZ, D. Towards understanding the raman spectrum of graphene oxide: the effect of the chemical composition. **Coatings**, [*s. l.*], v. 10, n. 6, p. 1-12, 2020.

LUO, T. *et al.* Sub-20nm-Fe 3 O 4 square and circular nanoplates: synthesis and facet-dependent magnetic and electrochemical properties. **ChemComm**, [*s. l.*], v. 50, p. 15952-15955, 2014.

MADURAIVEERAN, G.; JIN, W. Nanomaterials based electrochemical sensor and biosensor platforms for environmental applications. **Trends in Environmental Analytical Chemistry**, [*s. l.*], v. 13, p. 10-23, 2017.

MALI, S. S.; SHIM, C. S.; HONG, C. K. Highly porous zinc stannate (Zn 2 SnO 4) nanofibers scaffold photoelectrodes for efficient methyl ammonium halide perovskite solar cells. **Scientific Reports**, [*s. l.*], v. 5, p. 1-14, 2015.

MATOS, S. P. **Técnicas de análise química**: métodos clássicos e instrumentais. 1. ed. São Paulo: Saraiva, 2015.

MCCREERY, R. L. Advanced Carbon Electrode Materials for Molecular Electrochemistry. **Chemical Reviews**, [*s. l.*], v. 108, n. 7, p. 2646-2687, 2008.

MILLER, J. N.; MILLER, J. C. **Statistics and chemometrics for analytical chemistry**. 4th ed. England: Prentice Hall, 2005.

MIRCESKI, V.; KOMORSKY-LOVRIC, S.; LOVRIC, M. **Square-Wave Voltammetry**: theory and application. República da Macedônia: Springer, 2007.

MIRI, P. S. *et al*. MOF-biomolecule nanocomposites for electrosensing. **Nanochemistry Research**, [*s. l.*], v. 6, p. 213-222, 2021.

MITSCHER, L. A. Bacterial topoisomerase inhibitors: quinolone and pyridone antibacterial agents. **Chemical Reviews**, [*s. l.*], v. 105, p. 559-592, 2005.

MORIN-CRINI, N. *et al.* Worldwide cases of water pollution by emerging contaminants: a review. **Environmental Chemistry Letters**, [*s. l.*], v. 20, p. 2311-2338, 2022.

MUTHU D. *et al*. Reduced graphene oxide supported monoclinic bismuth vanadate nanoparticles as an electrocatalyst for selective determination of dopamine in human urine samples. **Materials Chemistry and Physics**, [*s. l.*], v. 297, p. 1-10, 2023.

MUZYKA, R. *et al.* Characterization of graphite oxide and reduced graphene oxide obtained from different graphite precursors and oxidized by different methods using raman spectroscopy. **Materials (Basel)**, [*s. l.*], v. 11, n. 7, 2018

NAGLES, E.; CERONI, M.; HURTADO, J. Simultaneous etection of tartrazine-sunset yellow in food samples using bioxide/carbon paste microcomposite with lanthanum and titanium. **Journal of Electrochemical Science and Technology**, [*s. l.*], v. 11, p. 421-429, 2020.

NAGLES, E. *et al*. Simultaneous electrochemical determination of paracetamol and allura red in pharmaceutical doses and food using a Mo(VI) oxide-carbon paste microcomposite. **Electroanalysis**, [*s. l.*], v. 33, n. 11, p. 2335-2344, 2021.

NGUYEN, T.-D. *et al*. Chronic ecotoxicology and statistical investigation of ciprofloxacin and ofloxacin to Daphnia magna under extendedly long-term exposure. **Environmental Pollution**, [*s. l.*], v. 291, 118095, 2021.

NIETO, J. *et al*. Photocatalyzed degradation of flumequine by doped TiO 2 and simulated solar light. **Journal of Hazardous Materials**, [*s. l.*], v. 155, p. 45-50, 2008.

NIKOLIĆ, M. V. *et al.* Far infrared properties of bulk sintered and thin film Zn 2 SnO 4, **Materials Science and Engineering**: B, [*s. l.*], v. 138, n. 1, p. 7-11, 2007.

NOFFKE, A. L. *et al*. Designing organometallic compounds for catalysis and therapy. **Chemical Communications**, [*s. l.*], v. 48, p. 5219, 2012.

OHTA, M.; KOGA, H. Three-dimensional structure-activity relationships and receptor mapping of N1-substituents of quinolone antibacterials. **Journal of Medicinal Chemistry**, [*s. l.*], v. 34, p. 131-139, 1991.

ONWUDIWE, D. C.; OYEWO, O. A. Facile synthesis and structural characterization of zinc stannate/tin oxide and zinc stannate/tin composites for the removal of methylene blue from water. **Materials Research Express**, [*s. l.*], v. 6, n. 1, 2019.

OPAS. **Novo relatório da OMS revela diferenças no uso de antibióticos entre 65 países**. [*S. l.*], 12 nov. 2018. Disponível em: https://www.paho.org/pt/noticias/12-11-2018-novo-relatorio-da-oms-revela-diferencas-no-uso-antibioticos-entre-65-paises. Acesso em: 01 out. 2023.

OVERTON, O. C. *et al*. Wetland removal mechanisms for emerging contaminants. **Land**, [*s. l.*], v. 12, n. 2, p. 472, 2023.

PACK, J. D.; MONKHORST, H. J. “Special points for Brillouin-zone integrations”: a reply. **Physical Review B**, [*s. l.*], v. 16, p. 1748-1749, 1977.

PARK, H.-R.; KIM, T. H.; BARK, K.-M. Physicochemical properties of quinolone antibiotics in various environments. **European Journal of Medicinal Chemistry**, [*s. l.*], v. 37, n. 1-3, p. 443-460, 2002.

PARR, R. G. Density Functional Theory of Atoms and Molecules. *In*: FUKUI, K.; PULLMAN, B. (ed.). **Horizons of Quantum Chemistry**. Dordrecht: Springer Netherlands, 1980. p 5–15.

PAVIA, D. L. *et al*. **Introduction to spectroscopy**. [*S. l.*]: Cengage Learning, 2014.

PENG, X. *et al.* Z-scheme transfer pathway assisted photoelectrocatalyst Zn 2 SnO 4 /rGO/Ag/AgBr for organic pollutants treatment. **Colloids Surfaces A**: Physicochemical and Engineering Aspects, [*s. l.*], v. 657, part A, p. 1-9, 2023.

PERDEW, J. P.; BURKE, K.; ERNZERHOF, M. Generalized Gradient Approximation Made Simple. **Physical Review Letters**, [*s. l.*], v. 77, p. 3865–3868, 1997.

PERLES, C. E. Physicochemical properties related to the development of Nafion membranes for application in fuel cells. **Polymers**, São Carlos, v. 18, n. 4, p. 281-288, 2008.

PETRIE, B.; BARDEN, R.; KASPRZYK-HORDERN, B. A review on emerging contaminants in wastewaters and the environment: current knowledge, understudied areas and recommendations for future monitoring. **Water Research**, [*s. l.*], v. 72, p. 3-27, 2015.

PINACHO, D. G.; SANCHEZ-BAEZA, F.; MARCO, M. P. Molecular modeling assisted hapten design to produce broad selectivity antibodies for fluoroquinolone antibiotics. **Analytical Chemistry**, [*s. l.*], v. 84, p. 4527-4534, 2012.

PLETCHER, D. *et al.* **Instrumental methods in electrochemistry**. New York: John Wiley & Sons, 1985.

POIX, P. On some crystallographic and magnetic determinations of oxygen. Compounds having spinel structure, containing tin, titanium, magnesium, zinc and cobalt. **Annali di Chimica**, [*s. l.*], v. 10, p. 49-79, 1965.

PRAJAPATI, D. *et al*. A critical review on emerging contaminants:origin, discernment, and remedies. **Sustainable Water Resources Management**, [*s. l.*], v. 9, p. 1-11, 2023.

PRICHARD, E.; BARWICK, V. **Quality assurance in analytical chemistry**. 1st ed. New York: Wiley, 2007.

PURI, M.; GANDHI, K.; KUMAR, M. S. Emerging environmental contaminants: a global perspective on policies and regulations. **Journal of Environmental Management**, [*s. l.*], v. 332, p. 1-13, 2023.

QIAO, J. X.; LUO, H. Q.; LI, N. B. Electrochemical behavior of uric acid and epinephrine at an electrochemically activated glassy carbon electrode. **Colloids Surf B Biointerfaces**, [*s. l.*], v. 62, n. 1, p. 31-35, 2008.

RADWAN, E. K. *et al.* Recent trends in treatment technologies of emerging contaminants. **Environmental Quality Management,** [*s. l.*], v. 32, n. 3, p. 7-25, 2023.

RAHMATI, Z.; ROUSHANI, M.; HOSSEINI, H. MOF-derived Ni-P bundle-like nanorods as high-performance substrate for design of electrochemical aptasensor toward cortisol detection. **IEEE Sensors Journal**, [*s. l.*], v. 23, p. 1770-1777, 2023.

RAO, A. *et al.* Adsorption of five emerging contaminants on activated carbon from aqueous medium: kinetic characteristics and computational modeling for plausible mechanism. **Environmental Science and Pollution Research**, [*s. l.*], v. 28, p. 21347–21358, 2021.

RAWAL, I. Facial synthesis of hexagonal metal oxide nanoparticles for low temperature ammonia gas sensing applications. **RSC Advances,** [*s. l.*], v. 5, p. 4135-4142, 2015.

RAZAQ, A. *et al*. Review on graphene, graphene oxide, reduced graphene oxide-based flexible composites: from fabrication to applications. **Materials**, [*s. l.*], v. 15, n. 3, p. 1-17, 2022.

RIBEIRO, F. W. P. *et al.* Analytical determination of nimesulide and ofloxacin in pharmaceutical preparations using square-wave voltammetry. **Journal of Analytical Chemistry**, [*s. l.*], v. 69, p. 62-71, 2014.

RIETVELD, H. M. Line profiles of neutron powder-diffraction peaks for structure refinement. **Acta Crystallographica**, [*s. l.*], v. 22, p. 151-152, 1967.

SHEN, X. *et al.* Phase transition of Zn 2 SnO 4 nanowires under high pressure. **Journal of Applied Physics**, [*s. l.*], v. 106, n. 11, p. 1-5, 2009.

SHOMAKHOV, Z. V. *et al.* Zinc stannate nanostructures for fast response gas sensors. **Russian Reviewed Scientific Edition**, [*s. l.*], v. 14, p. 726-735, 2022.

SI, X. *et al.* A sensitive electrochemical sensor for ofloxacin based on a graphene/zinc oxide composite film. **Analytical Methods**, [*s. l.*], v. 17, p. 1961-1967, 2018.

SI, X. *et al.* Detection of ofloxacin by differential pulse voltammetry in drugs based on a novel p-aminobenzene sulfonic acid/graphene. **International Journal Electrochemical Science**, [*s. l.*], v. 15, p. 8883-8891, 2020.

SKOOG, D. A.; HOLLER, F. J.; CROUCH, S. R. **Principles of instrumental analysis**. [*S. l.*]: Cengage Learning, 2017.

SONG, W. *et al.* Graphene-induced confined crystal growth of octahedral Zn 2 SnO 4 and its improved Li-storage properties. **Journal of Materials Research**, [*s. l.*], v. 27, p. 3096-3102, 2012.

SOUZA, D.; MACHADO, S. A. S.; AVACA, L. A. **Voltametria de onda quadrada**. Primeira parte: aspectos teóricos. Química Nova, São Paulo, v. 26, p. 81-89, 2003.

SPALTRO, A. *et al.* Removal of paracetamol from aqueous solution by activated carbon and silica. Experimental and computational study. **Journal of Contaminant Hydrology**, [*s. l.*], v. 236, p. 1-10, 2021.

SPAOLONZI, M. P.; SILVA, M. G. C.; VIEIRA, M. G. A. Adsorption of antibiotic cefazolin in organoclay fixed-bed column: characterization, mathematical modeling, and DFT-based calculations. **Environmental Science and Pollution Research**, [*s. l.*], v. 29, p. 31646–31658, 2022.

SPAOLONZI, M. P. *et al*. Green-functionalized carbon nanotubes as adsorbents for the removal of emerging contaminants from aqueous media. **Journal of Cleaner Production**, [*s. l.*], v. 373, p. 1-14, 2022.

STEPHENS, P. J. *et al*. Ab Initio Calculation of Vibrational Absorption and Circular Dichroism Spectra Using Density Functional Force Fields. **The Journal of Physical Chemistry**, [*s. l.*], v. 98, p. 11623–11627, 1994.

TANG, X. *et al.* Construction of rose flower-like NiCo-LDH electrode derived from bimetallic MOF for highly sensitive electrochemical sensing of hydrazine in food samples. **Food Chemistry**, [*s. l.*], v. 427, p. 1-8, 2023.

THOMPSON, M. *et al.* Harmonized guidelines for the use of recovery information in analytical measurement. **Pure and Applied Chemistry**, [*s. l.*], v. 71, n. 2, p. 337-348, 1999.

TIAN, X. *et al.* Nonenzymatic electrochemical sensor based on CuO–TiO 2 for sensitive and selective detection of methyl parathion pesticide in ground water. **Sensors and Actuators B**: Chemical, [*s. l.*], v. 256, p. 135-142, 2018.

TKACZYK, A.; MITROWSKA, K.; POSYNIAK, A. Synthetic organic dyes as contaminants of the aquatic environment and their implications for ecosystems: a review. **Science of The Total Environment**, [*s. l.*], v. 717, p. 1-19, 2020.

TOBY, B. H. EXPGUI, a graphical user interface for GSAS. **Journal of Applied Crystallography**, [*s. l.*], v. 34, p. 210-213, 2001.

TOLEDO, R. A. *et al.* Estudo eletroquímico e químico-quântico da oxidação do antidepressivo tricíclico amitriptilina. **Química Nova**, São Paulo, v. 28, n. 3, p. 456-461, 2005.

TUAN LE, H. *et al*. Mo and Zn-Dual doped Cu x O nanocrystals confined High-Conductive Cu arrays as novel sensitive sensor for neurotransmitter detection. **Journal of Colloid and Interface Science**, [*s. l.*], v. 606, p. 1031-1041, 2022.

TUINSTRA, F.; KOENIG, J. L. Raman spectrum of graphite. **The Journal of Chemistry Physics**, [*s. l.*], v. 53, n. 3, p. 1126-1130, 1970.

TUNIOLI, F. *et al*. Adsorption of emerging contaminants by graphene related materials and their alginate composite hydrogels. **Journal of Environmental Chemical Engineering**, [*s. l.*], v. 11, n. 2, p. 1-11, 2023.

U. S. EPA. **Aquatic life criteria for contaminants of emerging concern**: Part I: General guidelines and recommendations. [*S. l.*]: EPA, 2008.

USMAN, M. *et al.* First-principles calculations to investigate Structural, Electronic, optical and mechanical properties of Cu-based fluoroperovskite XCuF3 (X = K, Ru). **Computational and Theoretical Chemistry**, [*s. l.*], v. 1124, p. 1-5, 2023.

VANDERMEERSCH, G. *et al*. Environmental contaminants of emerging concern in seafood–European database on contaminant levels. **Environmental Research**, [*s. l.*], v. 143, part. B, p. 29-45, 2015.

WANG, J. **Analytical electrochemistry**. New York: Wiley VCH, 2001.

WANG, P.; HE, Y.-L.; HUANG, C.-H. Oxidation of fluoroquinolone antibiotics and structurally related amines by chlorine dioxide: reaction kinetics, product and pathway evaluation. **Water Research**, [*s. l.*], v. 44, p. 5989-5998, 2010.

WANG, S. *et al.* Influence of inorganic admixtures on the 11 Å-tobermorite formation prepared from steel slags: XRD and FTIR analysis. **Construction and Building Materials**, [*s. l.*], v. 60, p. 42-47, 2014.

WANG, Y.-F. *et al.* Nano-Zn 2 SnO 4 /reduced graphene oxide composites for enhanced photocatalytic performance. **Materials Chemistry and Physics Mater**, [*s. l.*], v. 254, p. 1-8, 2020.

WANG, Y.-F. *et al.* Nano-Zn 2 SnO 4 /reduced graphene oxide composites for enhanced photocatalytic performance. **Materials Chemistry and Physics Mater**, [*s. l.*], v. 254, p. 1-8, 2020.

WEBBER, A.; SHAH, M.; OSTERYOUNG, J. Electrochemical reduction and determination of cimetidine at nanomolar to micromolar levels of concentration. **Analytica Chimica Acta**, [*s. l.*], v. 154, p. 105-109, 1983.

WOJDYR, M. Fityk: a general-purpose peak fitting program. **Journal of Applied Crystallography**, [*s. l.*], v. 43, part 5, p. 1126-1128, 2010.

WONG, A. *et al.* Electrochemical sensor based on graphene oxide and ionic liquid for ofloxacin determination at nanomolar levels. **Talanta**, [*s. l.*], v. 161, p. 333-341, 2016.

WU, P. *et al*. Self-assembled multilayer Nb 2 C MXene/MnFe 2 O 4 electrochemical sensor with Schottky junctions for the detection of acetaminophen and dopamine. **Colloids and Surfaces A**: Physicochemical and Engineering Aspects, [*s. l.*], v. 667, p. 1-10, 2023.

XI, C. *et al.* Prevalence of antibiotic resistance in drinking water treatment and distribution system. **Applied and Environmental Microbiology Journal**, [*s. l.*], v. 75, p. 5714-5722, 2009.

XIE, J. *et al*. Synthesis of zincn stannate and zinc stannate coated ano-CaCO 3 by homogeneous precipitation. **Journal of Chemical Research**, [*s. l.*], v. 35, p. 109-111, 2011.

YI, Y. *et al.* Electrochemical corrosion of a glassy carbon electrode. **Catalysis Today**, [*s. l.*], v. 295, p. 32-40, 2017.

YOUNG, G. M.; LURIE, I. S. Recent forensic applications of enhanced chromatographic separation methods. **Journal of Separation Science**, [*s. l.*], v. 45, p. 369-381, 2022.

YOUNG, R. A.; MACKIE, P. E.; VON DREELE, R. B. Application of the pattern-fitting structure-refinement method of X-ray powder diffractometer patterns. **Journal of Applied Crystallography**, [*s. l.*], v. 10, p. 262-269, 1977.

YOUNG, R. A. **The Rietveld Method**. 4th ed. United States of American: Oxford University Press, 1996.

YU, J. H.; CHOI, G. M. Selective CO gas detection of Zn 2 SnO 4 gas sensor. **Journal of Electroceramics**, [*s. l.*], v. 8, p. 249-255, 2002.

ZANCHETTA, P. G.; PENA, A.; GONÇALVES, R. Development and validation of an analytical method for the simultaneous quantification of ofloxacin, norfloxacin and ciprofloxacin in human urine. **Sanitary and Environmental Engineering**, Rio de Janeiro, v. 20, p. 307-314, 2015.

ZHANG, F. *et al.* Simultaneous determination of ofloxacin and gatifloxacin on cysteic acid modified electrode in the presence of sodium dodecyl benzene sulfonate. **Bioelectrochemistry**, [*s. l.*], v. 89 p. 42-49, 2013.

ZHANG, Y. *et al*. Crystal growth of undoped ZnO films on Si substrates under different sputtering conditions. **Journal of Crystal Growth**, [*s. l.*], v. 243, p. 439-443, 2002.

ZHU, C. *et al.* A flexible electrochemical biosensor based on functionalized poly (3,4-ethylenedioxythiophene) film to detect lactate in sweat of the human body. **Journal of Colloid and Interface Science**, [*s. l.*], v. 617, p. 454-462, 2022.

ZUCCATO, E.; CASTIGLIONI, S.; FANELLI, R. Identification of the pharmaceuticals forhuman use contaminating the Italian aquatic environment. **Journal of Hazardous Materials**, [*s. l.*], v. 122, n. 3, p. 205-209, 2005.

ANEXO A - MANUSCRITO 1

Journal of The Electrochemical Society

ACCEPTED MANUSCRIPT

Electrocatalytic Amplified Sensor for Determination of Ofloxacin Using Zn2SnO4/Reduced Graphene Oxide Composite as Surface-Modifying Agent

Janevane de Castro[1], Anderson Valerio[1], Pierre Fechine[1], Raissa de Oliveira[1], Francisco Ribeiro[2], Pedro de Lima-Neto[3], Dieric Abreu[4], Cristiani de Oliveira[5] and ADRIANA CORREIA[6]

Accepted Manuscript online 15 December 2023

DOI 10.1149/1945-7111/ad1633

Author e-mails

adriana@ufc.br

Author affiliations

[1] Federal University of Ceara, Bloco 940, Fortaleza, CE, 60440900, BRAZIL

[2] Federal University of Ceara, Bloco 940, Fortaleza, CE, 60400900, BRAZIL

[3] A, Federal University of Ceara, Campus do Pici bloco 940, Fortaleza, CE, 60455-760, BRAZIL

[4] Federal University of Ceara, Departamento de Química Analítica e Físico-Química, Fortaleza, CE, 60440-900, BRAZIL

[5] Federal University of Ceara, Departamento de Farmácia, Fortaleza, CE, 60430372, BRAZIL

[6] Federal University of Ceara, Bloco 940, Fortaleza, CE, 60440-900, BRAZIL

ORCID iDs

ADRIANA CORREIA https://orcid.org/0000-0002-3357-0160

Dates

1. Received 22 September 2023
2. Revised 8 December 2023
3. Accepted 15 December 2023
4. Accepted Manuscript online 15 December 2023

Journal of The Electrochemical Society, 2024 **171** 017501
1945-7111/2024/171(1)/017501/16/$40.00 © 2024 The Electrochemical Society ("ECS"). Published on behalf of ECS by IOP Publishing Limited

Electrocatalytic Amplified Sensor For Determination of Ofloxacin Using Zn_2SnO_4/Reduced Graphene Oxide Composite As Surface-Modifying Agent

Janevane S. de Castro,[1,2] Anderson V. Chaves,[2] Pierre B. A. Fechine,[2] Raíssa C. de Oliveira,[2] Francisco W. P. Ribeiro,[3] Pedro de Lima-Neto,[2] Dieric S. Abreu,[4] Cristiani L. C. G. de Oliveira,[5] and Adriana N. Correia[2,z]

[1]*Departamento de Engenharia de Alimentos, Universidade Federal do Ceará, Campus do Pici, 60440-900, Fortaleza, CE, Brazil*
[2]*Departamento de Química Analítica e Físico-Química, Universidade Federal do Ceará, Campus do Pici, 60440-900, Fortaleza, CE, Brazil*
[3]*Instituto de Ciências Exatas e da Natureza, Universidade da Integração Internacional da Lusofonia Afro-Brasileira, Campus das Auroras, 62790-970, Redenção, CE, Brazil*
[4]*Laboratório de Materiais e Dispositivos, Departamento de Química Analítica e Físico-Química, Centro de Ciências, Universidade Federal do Ceará, Campus do Pici, Fortaleza, CE 60440-900, Brazil*
[5]*Departamento de Farmácia, Universidade Federal do Ceará, Campus do Porangabussu, 60430-372, Fortaleza, CE, Brazil*

This study describes an electroanalytical approach for the quantification of ofloxacin (OFL) through an electrochemical sensor based on a glassy carbon electrode modified with composite material (Zn_2SnO_4-rGO/GCE) using square wave voltammetry. Zn_2SnO_4 was synthesized by hydrothermal treatment and characterized by X-ray diffraction, Fourier-transform infrared and Raman spectroscopy and scanning electron microscopy. The analysis suggests a synergistic effect between the composite material, indicating irreversible oxidation of OFL in its protonated form (OFL^+), involving two electrons. The electroanalytical methodology was successfully applied to determine OFL in ophthalmic solutions samples, achieving recovery rates ranging from 98.03% to 104.91%. Furthermore, it demonstrated high stability in both repeatability (RSD = 3.20%, n = 12) and reproducibility (RSD = 4.64%, n = 7), with no observed interference when additional substances were added. These results suggest the potential electroanalytical application of Zn_2SnO_4 and recommend the developed methodology as an alternative tool for OFL determination in commercial pharmaceutical samples.
 [DOI: 10.1149/1945-7111/ad1633]

Manuscript submitted September 22, 2023; revised manuscript received December 8, 2023. Published January 8, 2024.

Supplementary material for this article is available online

Ofloxacin (OFL, IUPAC name: (RS)−7-fluoro-2-methyl-6-(4-methylpiperazin-1-yl)−10-oxo-4-oxa-1-azatricyclo [7.3.1.0^{5,13}] trideca-5(13),6,8,11-tetraene-11-carboxylic acid[1] is a broad spectrum quinolone antibiotic, belonging to the second generation of fluoroquinolones.[2] Fluoroquinolones possess at least one fluorine substituent group (−F) in its quinoline ring, promoting higher efficiency in the antimicrobial activity of the drug against gram-negative and gram-positive bacteria. This class of bactericides also possess clinical applications in both humans and veterinary medicine (cattle, equines, canines, and felines), being specially used in ophthalmic and urinary tract infections, while it also shows efficacy against respiratory and gastrointestinal tract infections.[2]

Fluoroquinolone's mechanism of action is highly affected by its physicochemical properties, especially due to its ionization in the function of the medium pH and its capacity for complexation with metallic ions.[3] OFL has two ionizable functional groups, which confers to it two dissociation constants, corresponding to the carboxyl (pKa_1 of 5.89 to 6.05) and amino group (pKa_2 of 7.9 to 8.2).[4,5] Therefore, it is highlighted that the protonation of the analyte is dependent on the relation between the medium pH and the values of pKa, as shown in Fig. 1A.

Literature describes numerous successful applications of simple oxide-based composites on development of electrochemical sensors, such as Fe_3O_4 and rGO applied in catechol and hydroquinone detection,[6] CuO and TiO_2 in methyl parathion detection,[7] MnO_2 and graphene oxide (GO) to determine guaiacol and vaniline,[8] usage of ZnO and Gr to detect OFL,[9] and other applications.

Despite records of the use of the ZnO-Gr nanocomposite in the development of an electrochemical sensor for OFL detection, the linearity range obtained was at relatively high concentrations (1–100 μmol l^{-1}), presenting a value of LOD equal to 0.33 μmol l^{-1} and very low sensitivity to the drug (0.089 A mol^{-1} l); compromising its use in samples with low concentrations of OFL.[9]

Mixed oxides have raised much of the scientific community´s interest due to their numerous technological applications. Some oxides are based on zinc and tin (Zn_2SnO_4, $ZnSnO_2$ e $ZnSnO_3$), known generically as zinc stannates.[10] Its majority is synthesized from ZnO and SnO_2 reactions at high temperatures (above 1000 °C) or from reactions between $Zn(CH_3COO)_2$ and $SnCl_4$ in alkaline medium, although the synthesis cannot promote complete conversion of ZnO and SnO_2 in zinc stannate.[10] The literature reports the development of the Zn_2SnO_4/graphene composite, prepared using a hydrothermal route, where the octahedral Zn_2SnO_4 crystals remained firmly confined by the graphene sheets, forming a unique hybrid structure, enhancing Li storage performance.[11]

Zn_2SnO_4 has diamagnetic and semiconductor properties[12] and is specially applied in toxic gas sensing.[13] However, no records were found in the literature of applications of Zn_2SnO_4 in developing electrochemical sensors for any drugs, making its use for such purposes unprecedented. Some studies are reported in the literature concerning using simple/mixed oxide-based composites and rGO in the development of electrochemical sensors.[14–16] rGO presents good dispersion in polar mediums and possesses numerous reactive sites (epoxy, hydroxyl, and carboxyl) in its basal structure, qualifying this material as an excellent material for electrochemical sensors, considering sensibility, limit of detection (LOD) and limit of quantification (LOQ).[16,17]

Most of the drugs (among them the OFL) have official methodologies of detection based on chromatographic techniques, which often make the determination process more difficult due to the high cost of analysis. In that regard, electroanalytical methodologies have been presented as an alternative for drug detection, especially due to their ease of operation, high sensitivity, selectivity, low cost of instrumentation and absence of organic solvents.[18]

[z]E-mail: adriana@ufc.br

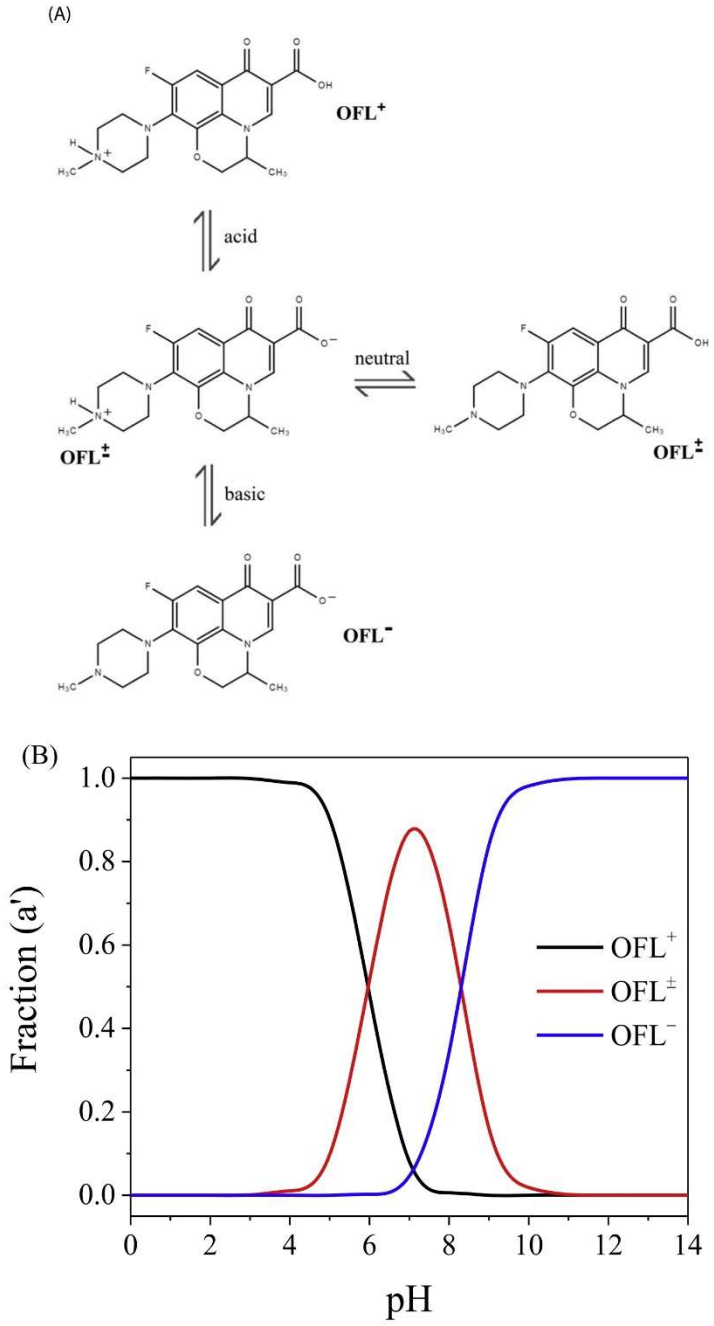

Figure 1. (A) Species present in the OFL acid-base balance. (B) Distribution (α') of the OFL species with the pH using the acid-base equilibrium and mass-balance equations.

Therefore, the objective of this investigation is to propose a simple electroanalytical methodology to determine and quantify OFL in pharmaceutical samples using an electrochemical sensor based on the modification of the glassy carbon surface with the composite Zn_2SnO_4-rGO (Zn_2SnO_4-rGO/GCE) and using square-wave voltammetry (SWV) as an electroanalytical technique; also envisioning the possibility of tests and applications in more complex samples (such as water matrices), which could become an alternative tool for controlling and supervising the drug in waters. The study also addresses the relevant relationship between the OFL speciation diagram and the electrostatic nature of the modified electrode surface.

Material and Methods

Chemicals and reagents.—OFL (⩾99.9%), Nafion® (⩾95.0%), and rGO were acquired from Sigma-Aldrich®. Pharmaceutical samples containing OFL (sterile ophthalmic solution, OFLOX®) were purchased from Allergan (Brazil). OFL standards were produced by dissolving a determined quantity in ethanol (96%). Zn_2SnO_4 was synthesized using $SnCl_2.2H_2O$ (⩾98.0%) and $Zn(CH_3COO)_2.2H_2O$ (⩾98.0%), both acquired from Dinâmica®. H_2SO_4 solutions in 5.0×10^{-3} mol l^{-1}, 5.0×10^{-2} mol l^{-1} and 5.0×10^{-1} mol l^{-1} were prepared. Britton-Robinson (BR), Sörensen, and Clark-Lubs buffer solutions were prepared with an adjusted pH of 2.0, and phosphate buffer solution (PBS) was prepared with an adjusted pH of 7.4. $K_4[Fe(CN)_6]$ / $K_3[Fe(CN)_6]$ 1.0×10^{-3} mol l^{-1} solution was prepared in KCl 1.0×10^{-1} mol l^{-1}. All reagents were of analytical grade. Ultra-purified water (18.2 MΩ cm) was used in the glassware cleaning and the preparation of the solutions, obtained through the Milli-Q® (Millipore, Inc.) system.

Apparatus.—A Micronal® pHmeter (model B474A) was used to measure the solutions' pH. A Quimis® (model Q335D) ultrasonic bath was used to homogenize the composite suspension and perform the GCE cleaning post-polishment procedure. To homogenize the solution in the electrochemical cell and to clean the procedure of the modified GCE surface, a Gehaka® (model AA-840) magnetic stirrer was used, along with a magnetic bar. A PGSTAT 101 Metrohm® (Eco Chemie) potentiostat/galvanostat was connected to a computer with Nova software (version 2.1.3) was used. A conventional three-electrode system was carried out with a GCE (BASi®, 3mm diameter) as the working electrode, a platinum plate as the counter electrode (1.03 cm^2) and an $Ag_{(s)}/AgCl_{(s)}/Cl^-_{(aq)}$ (saturated KCl) as the reference electrode. Chromatographic analysis was performed using a Waters® (model Alliance 2695) HPLC, coupled to a UV-Vis detector (diode array adjusted at 294 nm) and a reverse phase C18 column Eclipse plus from Agilent (250 mm × 4.6 mm, 5 μm particle size), using isocratic elution with a mobile phase consisting of 60% acetonitrile and 40% acetic acid 1% (pH 7,0), injection volumes of 20 μl, 1.0 ml min^{-1} flow, while the column was kept at 35 °C.

Synthesis of Zn_2SnO_4.—Zn_2SnO_4 was synthesized using the hydrothermal method. Briefly, separate solutions of tin chloride dehydrate ($SnCl_2.2H_2O$) and zinc acetate dehydrate ($Zn(CH_3COO)_2.2H_2O$) were prepared separately with a 1:2 molar ratio, respectively. After stirring the mixture for 10 min, the pH was adjusted by adding 0.75 g NaOH, and the solution was left to settle for 15 min. The solution was transferred into a Teflon-lined steel autoclave and heated at 200 °C for 22 h. After the reaction was complete, the autoclave was cooled, and the resulting precipitate was separated by centrifugation and then washed several times with deionized water and ethanol to remove any residual ions in the solution. Finally, the sample was dried at 80 °C for 12 h. The chemical reaction that represents the formation of Zn_2SnO_4 particles in an alkaline medium via the hydrothermal route is shown in Eq. 1:[11]

$$2Zn^{2+}_{(aq)} + Sn^{4+}_{(aq)} + 8OH^-_{(aq)} \rightarrow Zn_2SnO_{4(s)} + 4H_2O_{(l)} \quad [1]$$

Characterization of Zn_2SnO_4.—X-ray diffraction (XRD) measurements were conducted at room temperature using a Bruker diffractometer (D8 Advance) with CuKα tube (λ = 1.5418 Å), equipped with a LynxEye linear detector. The instrumental parameters were a voltage of 40 kV and a current of 40 mA, scanning in the 2θ range of 10°–90° with a step of 0.02. For Fourier transform infrared spectroscopy (FTIR) spectra, a Perkin-Elmer (model 2000 FT-IR) spectrophotometer was used with a scan range from 4000 to 400 cm^{-1}. To obtain the pellets, the sample was previously dried to remove water absorption and dispersed in KBr in a 1:10 ratio, which was molded with a hydraulic press. Raman spectroscopy of powder and thin film samples was conducted using the LabRam HR Raman Spectrometer (Horiba) equipped with a microscope (BX41, Nikon). A 100× objective lens (UMPlanFl, Olympus) with a numerical aperture (NA) of 0.90 was employed to focus a He-Ne laser (Melles Griot) with a wavelength of 632.8 nm on the surface of the thin film sample for excitation. The Raman scattered light was dispersed using a 600 gr/mm diffraction grating and then projected onto a Peltier cooling charge-coupled device (CCD) detector. Raman spectra were acquired at multiple points across the thin films, with an acquisition time of 10 s at each point, and each spectrum represented an average of 5 readings. The resulting Raman spectra were processed using the Fityk program[19] employing a nonlinear deconvolution algorithm known as the Levenberg-Marquardt method. Spectrum fits were performed assuming a linear baseline, and all deconvoluted curves exhibited a Lorentzian distribution shape. The micrograph images of the samples were obtained by scanning electron microscopy (SEM, Quanta® 450 FEG electron microscope and FEI Ambiental) with an acceleration of up to 20 kV. The samples were fixed onto carbon strips, air-dried, and covered with a thin gold layer to ensure good conductivity.

Sensor preparation.—The individual suspensions of Zn_2SnO_4 and rGO were prepared both at 1.0 mg ml^{-1} in dimethylformamide (DMF), while the composite suspension (Zn_2SnO_4-rGO) was prepared by mixing 1.0 mg of both Zn_2SnO_4 and rGO in 1.0 ml (DMF) with 0.5% Nafion®. All prepared suspensions were homogenized in an ultrasonic bath for 120 min. Before modification, the GCE surface was polished using 3 μm diamond paste, being cleaned in an ultrasonic bath in ethanol (96%) and ultrapure water, respectively, for 3 min each. Afterward, the GCE was modified with Zn_2SnO_4-rGO composite suspension using a 1.5 μl aliquot, being dried shortly after in a drying oven at ±60 °C for 15 min.

Electrochemical experiments.—Electrochemical experiments were conducted at 25 °C using 10 ml of supporting electrolyte in the electrochemical cell. Evaluations of the electrochemical properties of the sensor were performed with cyclic voltammetry (CV) between 0.0 and 1.5 V in 5.0×10^{-1} mol l^{-1} H_2SO_4, varying the scan rate (ν) from 10 up to 200 mV s^{-1}.

To study the charge transfer process in the electrode surface, electrochemical impedance spectroscopy (EIS) was carried out in presence of 1.0×10^{-3} mol l^{-1} $K_4[Fe(CN)_6]/K_3[Fe(CN)_6]$, with a molar ratio 1:1 (Fe^{2+}/Fe^{3+}) in 1.0×10^{-1} mol l^{-1} KCl, ranging from 60 kHz to 100 mHz, with a amplitude perturbation of 5 mV.

SWV measurements were carried out from 0.0 up to 1.5 V, with experimental conditions optimization being evaluated in different buffer solutions: Britton-Robinson (BR) pH 2.0; Sörensen pH 2.0; Clark-Lubs pH 2.0; PBS pH 7.4) and H_2SO_4 (0.005–0.5 mol l^{-1}) and voltammetric parameters: f (10 to 150 s^{-1}), a (10 to 50 mV) and ΔE_s (1 to 5 mV). Between the consecutive SWV measurements, solutions were kept under stirring for 3 min and rested, followed by a resting time of at least 30 s. After optimizing the initial parameters, an ideal cleaning procedure was evaluated for the modified electrode surface submerged in solution through mechanical stirring for 60, 120, 180 and 240 s to assure OFL desorption out of the electrode surface.

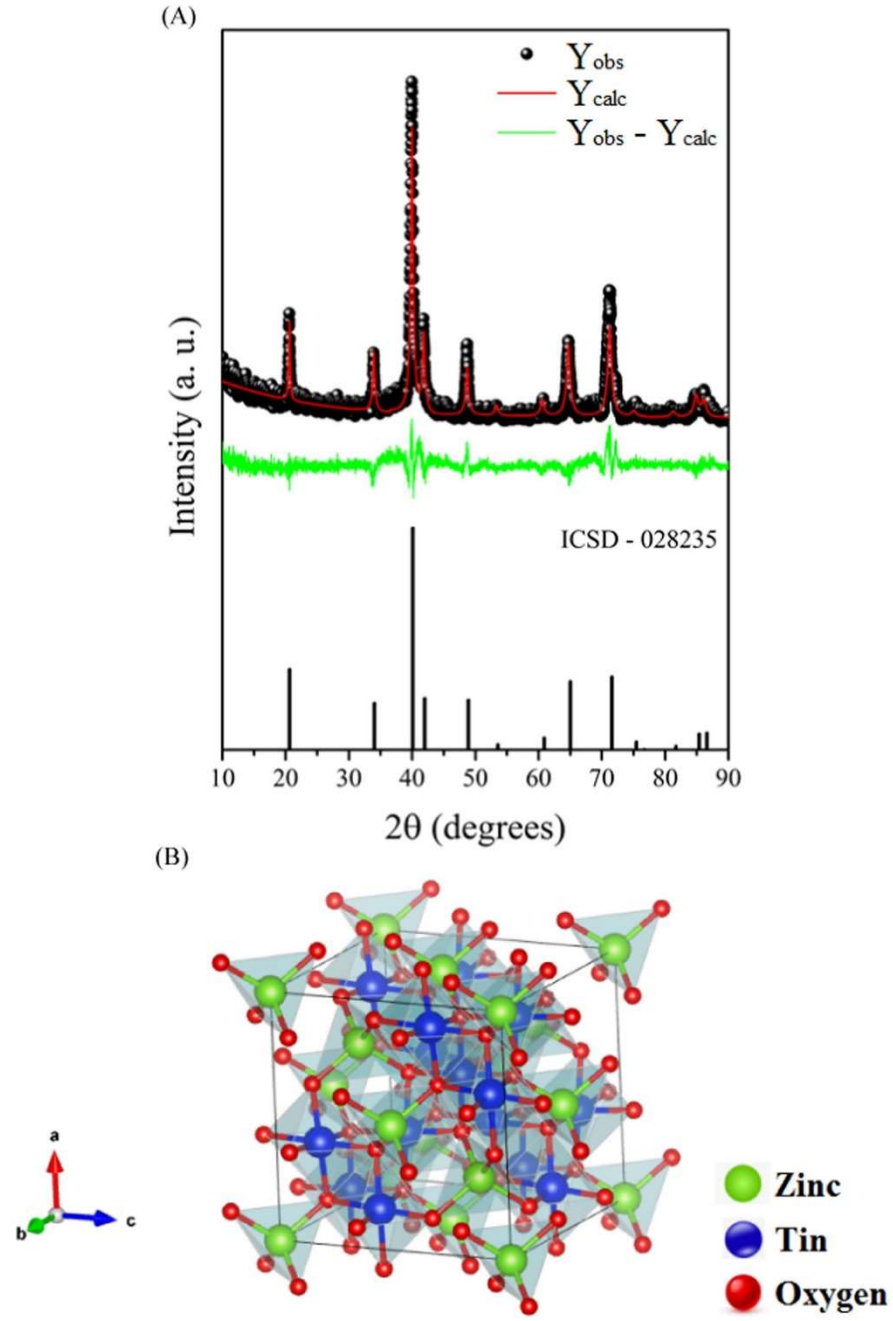

Figure 2. (A) Diffraction pattern obtained from Zn_2SnO_4 sample (B) Crystal structure of Zn_2SnO_4.

Table I. Pattern structural results refined by Rietveld method of the Zn_2SnO_4 sample.

		Lattice parameters				
Crystalline phase	Mass (%)	a (Å)	b (Å)	c (Å)	Density (g cm^{-3})	Diameter (nm)
Zn_2SnO_4	100	86.93	86.93	86.93	11.08	22.96

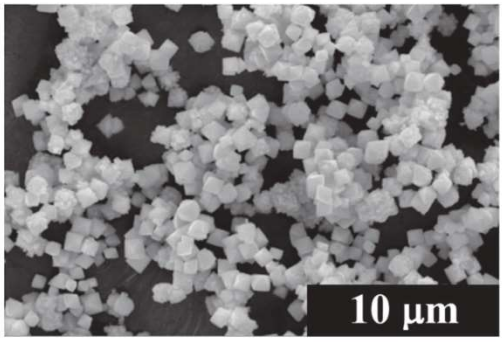

Figure 3. SEM image obtained for surface with Zn_2SnO_4 at 10.000× magnification.

Electroanalytical methodology.—After the optimization of the voltammetric parameters, analytical curves were obtained using the standard addition method. Analytical parameters such as linearity range, LOD, LOQ, correlation coefficient (r), sensitivity, confidence intervals, precision (repeatability and reproducibility), accuracy (recovery percentage), BIAS% and relative standard deviation (RSD%) were determined according to described in the literature.[20–24] The LOD and LOQ were calculated using Eqs. 2 and 3:[20,24]

$$\text{LOD} = \frac{3.3\sigma}{S} \quad [2]$$

$$\text{LOQ} = \frac{10\sigma}{S} \quad [3]$$

where:

σ = standard deviation of the linear coefficient (intercept) of the analytical curve;

S = the slope of the analytical curve.

Values of LOD and LOQ calculated for OFL on Zn_2SnO_4-rGO/GCE were compared with values obtained for HPLC methods.

Application of methodology in commercial pharmaceutical formulation.—The efficiency of the electrochemical methodology developed to determine OFL was assessed through recovery tests in commercial pharmaceutical samples (sterile ophthalmic solution) utilizing the proposed sensor (Zn_2SnO_4-rGO/GCE). The obtained results were compared with values obtained from HPLC (official methodology recommended by the Brazilian Pharmacopoeia).[25] Comparisons between concentration averages of recovered OFL obtained from the two methodologies were conducted through *t*-test, with its variances being evaluated by *F*-test.[20,21]

Results and Discussion

Characterization of the Zn_2SnO_4.—An electrochemical sensor performance is affected by the electrode surface modifiers.[26] Aspects such as its morphology, chemical bonds, molecular structure, and geometry are topics that must be known to obtain detailed information about the surface modifier material. With that in mind, synthesized Zn_2SnO_4 was characterized through XRD, FTIR, RS and SEM.

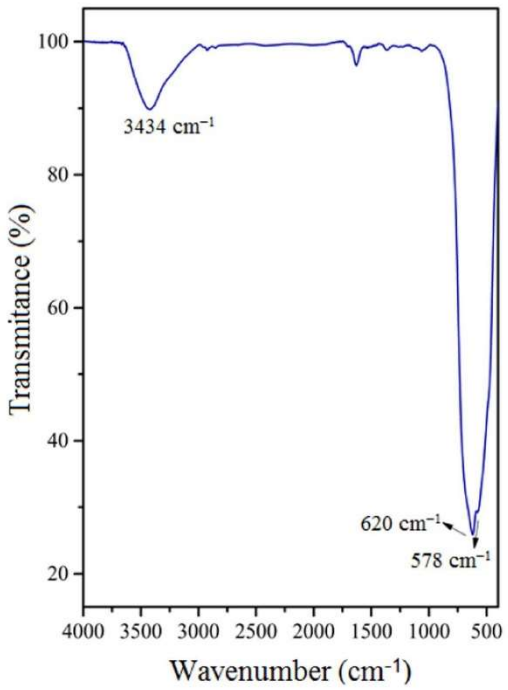

Figure 4. FTIR spectra for Zn_2SnO_4.

XRD was used to study the crystallinity of the material. As seen, the sample presented a single phase of zinc stannate compound (Zn_2SnO_4), which presented a cubic inverse spinel crystalline structure with a Fd3m spatial group, No. 028235, according to the crystallographic database (Inorganic Crystal Structure Database, ICSD), Fig. 2A.[27,28] The crystallite unit cell showed tetrahedral sites occupied by Zn^{2+} ions (ZnO_4) and octahedral sites occupied by zinc and tin ions (ZnO_6 and SnO_6), respectively. (Figure 2B) The results obtained provide relevant information for a more detailed physical characterization of the spatial structure of the Zn_2SnO_4 crystallite, including presenting the basic physical measurements of the crystallite structure.

Table I shows the results of the refinement and lattice parameters of the sample through Rietveld method using GSAS/EXPGUI software,[29,30] indicating a value of *S* (goodness of fit) of 1.23 and weighted profile *R*-value (R_{wp}) of the 26.07%, indicating a good agreement with data obtained in the literature.[31] The crystallite average diameter size for the Zn_2SnO_4 sample was 22.96 (±0.51) nm through the Scherrer equation.[28,32] Figure 3 shows SEM image of the Zn_2SnO_4. It can be found that the material presents a truncated

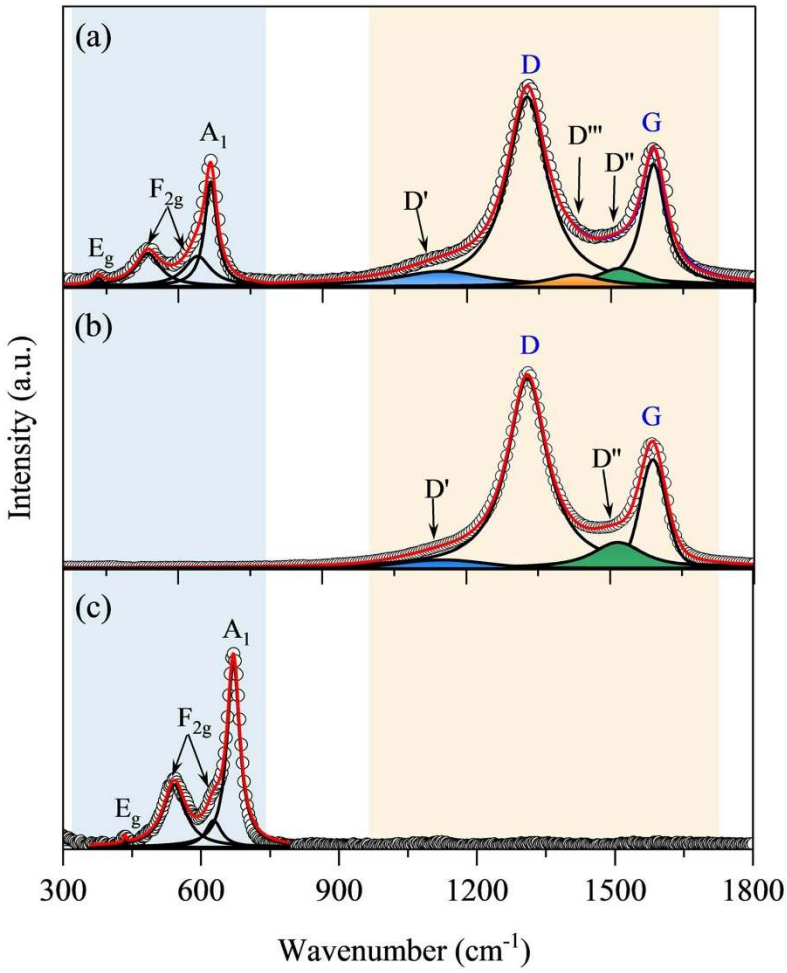

Figure 5. Raman spectra of gold-coated films for (a) Zn_2SnO_4-rGO composite, (b) rGO, and (c) Zn_2SnO_4, within the range of 300–1800 cm^{-1}. The white circles (○) represent the experimental Raman spectra, the solid red lines (–) indicate the fitted spectra, and the solid black lines (—) depict the best Lorentzian fitting curves.

octahedron morphology. This geometry was also found by other authors who used the same synthetic route (hydrothermal method) used in the present work.[33,34] The average particle size of octahedrons was 1.16 (±0.24) μm.

FTIR spectrum obtained for Zn_2SnO_4 (Fig. 4) points towards 620 cm^{-1} and 578 cm^{-1} absorption band, which, according to literature, corresponds to natural oxygen bonds vibrations (Sn–O) and (Zn–O); such results back up the XRD crystallographic structure presented in this work.[35] FTIR spectrum for Zn_2SnO_4 described a broad band around 3434 cm^{-1} from O–H intermolecular hydrogen bonds, 620 cm^{-1} and 578 cm^{-1} bands can be attributed to Sn–O and Zn–O vibrations, respectively, due to the occurrence of water molecules in the interlamellar space of numerous crystallite types, which are resultant of its own structural organization.[35,36]

Raman spectroscopy was utilized to assess the stretching vibrations of the chemical bonds present in the as-prepared powder of Zn_2SnO_4. Figure 1S (Supplementary Material) shows the Raman spectrum of Zn_2SnO_4 powder, displaying characteristic peaks at 667 cm^{-1}, 534 cm^{-1}, and 434 cm^{-1}. According to group theory, the inverse spinel Zn_2SnO_4 exhibits a total number of vibration modes: $\Gamma = 1A_{1g} + 1E_g + 3F_{2g} + 7F_{1u}$, where $1A_{1g}$, $1E_g$, and $3F_{2g}$ are active Raman modes.[37–39] The data obtained confirm a cubic inverse spinel crystal structure for Zn_2SnO_4, supporting the results obtained in this work using XRD and FTIR techniques.

In addition, Raman spectroscopy was used to characterize the composite thin film Zn_2SnO_4-rGO and to elucidate the role of Zn_2SnO_4 in influencing the structural and electronic properties of rGO within the composite, including defects and disorder. To eliminate the effect of the background Raman modes from the glassy carbon electrode, thin films of Zn_2SnO_4, rGO, and the composite Zn_2SnO_4-rGO were prepared on gold substrates following the procedure outlined in Characterization of Zn_2SnO_4 section. The Raman spectra of the rGO and Zn_2SnO_4-rGO (Figs. 5b and 5c respectively) show the two main feature D and G bands centered at 1327 cm^{-1} and 1589 cm^{-1} respectively.[40] Besides

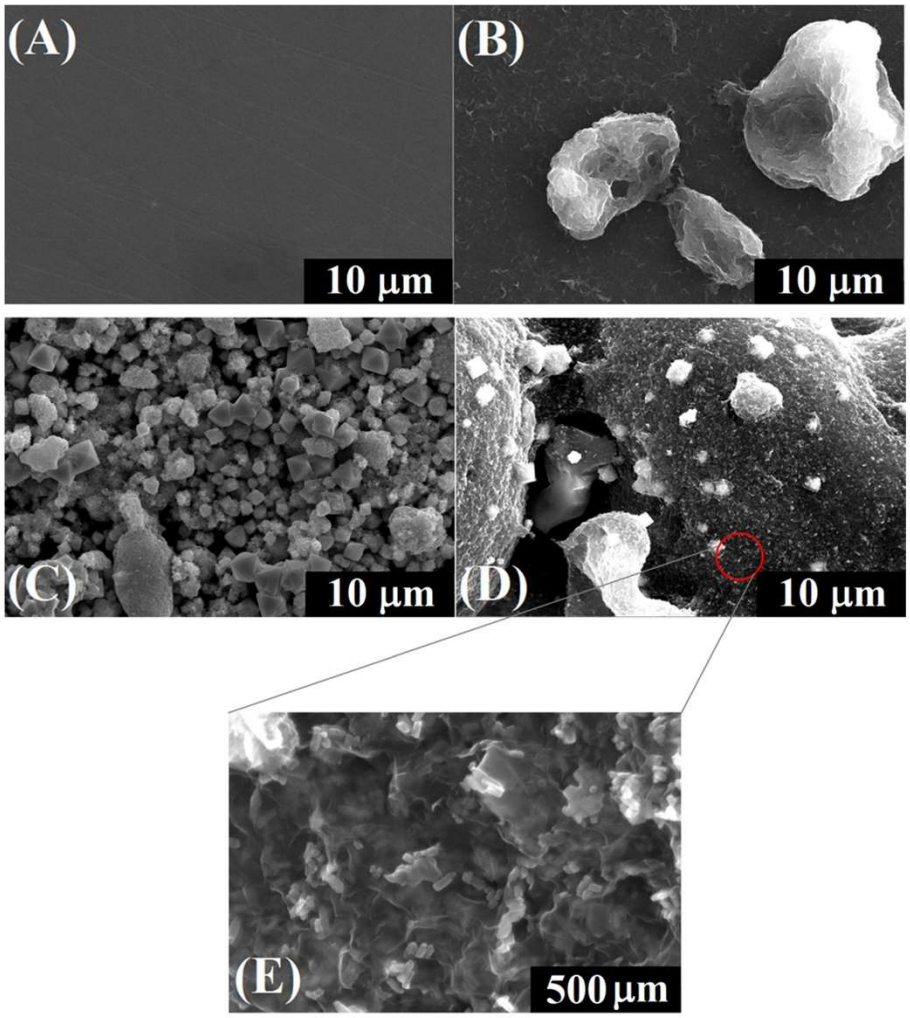

Figure 6. SEM images obtained for the surfaces of GCE (A), rGO/GCE (B) and Zn_2SnO_4/GCE (C) at 10.000× magnification; and Zn_2SnO_4-rGO/GCE (D) and (E) respectively with magnifications of 10.000× and 150.000×.

the typical D and G bands, the Raman spectrum of rGO exhibits additional bands centered at 1150 cm^{-1} (D´ band) and 1516 cm^{-1} (D″ band). Conversely, the Raman spectrum of the Zn_2SnO_4-rGO composite shows similar peaks slightly shifted to 1148 cm^{-1} (D′ band), 1519 cm^{-1} (D″ band) and 1426 cm^{-1} (D‴ band) also appeared. The appearance of new D bands in the Raman spectrum is linked to defects that interrupt the regular graphene lattice.[41] These defects stem from the disordered graphitic structure induced by the presence of sp^3 bonds and are also connected to the existence of amorphous phases.[40–42] The structural defects and imperfections on the nanosheet basal plane of graphene were commonly identified using the intensity ratio of the D and G bands (Tuinstra–Koenig correlation, I_D/I_G).[40,43] In the gold-coated film of the Zn_2SnO_4-rGO composite, an I_D/I_G ratio of 1.56 shows a decrease compared to the I_D/I_G ratio of 1.75 for the gold-coated film of pristine rGO, revealing an increase in the crystallinity of the rGO in the composite.[41] Although this behavior indicates an increase in crystallinity, the presence of other featured bands (observed additional D bands) exhibits an opposite trend.

Notably, there is an increase in the D′ band in the Raman spectrum of the Zn_2SnO_4-rGO composite (Fig. 5a) compared to that in rGO (Fig. 5b). This behavior is linked to the oxidation level of the rGO sheets, where the intensity rises, and the peak position shifts to lower wavenumber values as the oxygen content increases.[41] This aligns with the presence and interaction of oxides from Zn_2SnO_4 near rGO. A comparison between Raman spectra of gold-coated film Zn_2SnO_4 (Fig. 5c) and Zn_2SnO_4-rGO composite (Fig. 5c) show evidence of the interaction between Zn_2SnO_4 and reduced graphene oxide. The Raman spectrum of the gold-coated film of pristine Zn_2SnO_4 displays characteristic peaks at 670 cm^{-1} (A_{1g}), attributed to the symmetric stretching of the Zn–O bonds in ZnO_4 tetrahedra; 541 cm^{-1} and 627 cm^{-1} (F_{2g}), and 434 cm^{-1} (E_g) representative of

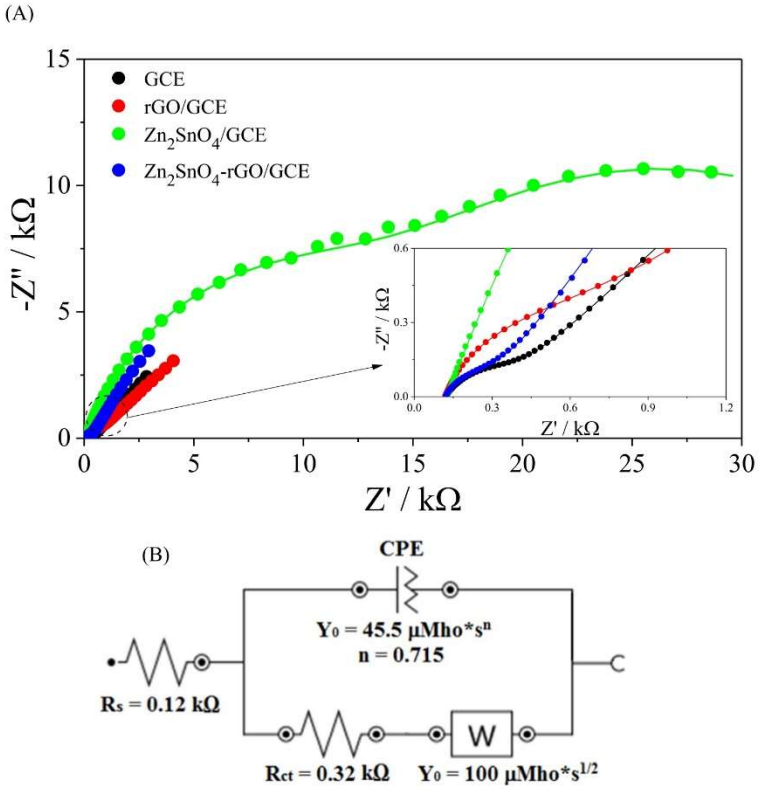

Figure 7. (A) Nyquist plots for GCE, rGO/GCE, Zn_2SnO_4/GCE and Zn_2SnO_4-rGO/GCE in 1.0×10^{-3} mol l^{-1} $K_4[Fe(CN)_6]/K_3[Fe(CN)_6]$ (1:1) and 1.0×10^{-1} mol l^{-1} KCl. The insert corresponds to the Nyquist plots in the region of high frequencies. (B) Fitting of equivalent electrical circuit obtained for Zn_2SnO_4-rGO/GCE.

the vibrations of Zn–O and Sn–O in octahedral sites.[44] Meanwhile, in the gold-coated film of the Zn_2SnO_4-rGO composite (Fig. 5c), the Raman spectra within the Zn_2SnO_4 modes region (400–760 cm^{-1}) exhibit a slight downshift in the A_{1g} band (667 cm^{-1}) and an opposite trend in the F_{2g} bands: a slight downshift to 536 cm^{-1} and an upward shift to 640 cm^{-1}. We attribute this behavior to the anisotropic interaction of Zn–O and Sn–O in octahedral sites with the rGO, causing the shift of the F_{2g} bands towards lower and higher wavenumbers, respectively, due to changes in the chemical bond length. The shorter bond length results in a shift to higher wavenumbers, an ordinary phenomenon in vibrational spectroscopy.

Characterization of modified electrode surfaces.—SEM images (Figs. 6A–6E) for GCE, Zn_2SnO_4/GCE, rGO/GCE and Zn_2SnO_4-rGO/GCE surfaces were obtained to evaluate the surface morphology.

GCE (Fig. 6A) presented a regular and uniform electrochemical surface, while in rGO/GCE (Fig. 6B) compact layers were observed, possibly explained by the stability granted by (π-π) interactions that are present in rGO structure.[45,46] Zn_2SnO_4/GCE surface (Fig. 6C) showed a structure formed primarily by isolated crystals, confirming once more the cubical structure formed by ZnO_4 tetrahedrons and ZnO_6/SnO_6 octahedrons.[47] Zn_2SnO_4-rGO/GCE image (Figs. 6D and 6E) illustrates the proposed composite's morphology, showing both the components' aggregation and synergism amidst the dispersion of the material.

Electrochemical performance of the modified GCE in the ferrocyanide/ferricyanide system.—EIS provides data on electrolyte resistance (R_Ω), also known as solution resistance (R_S); and on the charge transfer resistance (R_{ct}). The diameter of the arc (semicircle) observed is related to the resistance that the electrode surface offers to the charge transfer process so high R_{ct} values indicate greater difficulty in the occurrence of redox processes.

Values of charge transfer resistance (R_{ct}) for GCE, Zn_2SnO_4/GCE, rGO/GCE and Zn_2SnO_4-rGO/GCE were evaluated through EIS in $K_4[Fe(CN)_6]/K_3[Fe(CN)_6]$ + KCl, as shown in the Nyquist diagrams (Fig. 7A).

When considering the Nyquist diagrams, it was observed that the Zn_2SnO_4/GCE surface showed two arcs in separate R_{ct} values, the highest being 23.24 kΩ and the absence of the Warburg's diffusion line. This indicates that Zn_2SnO_4 individual usage during GCE's modification did not favor the charge transfer process in the electrode's surface. Several articles report the presence of two arcs in a Nyquist diagram and Warburg's diffusion line absence, including tin oxides (SnO_2, SnO_4 and SnO_6).[47,48] However, there's no consensus about such behavior, which is attributed to the passivation layer formation or the rapid oxide recombination in the electrode's surface.[47,48]

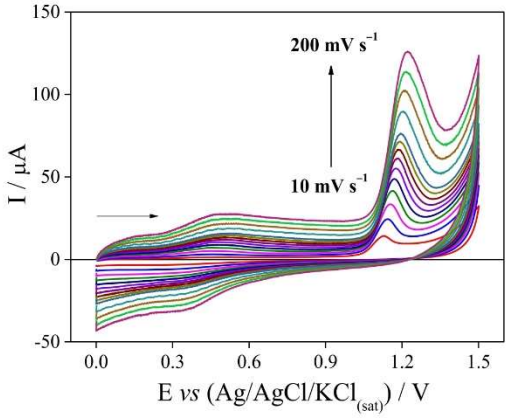

Figure 8. Cyclic voltammograms of 2.95×10^{-5} mol l^{-1} OFL in 5.0×10^{-1} mol l^{-1} H_2SO_4, using Zn_2SnO_4-rGO/GCE, with scan rates between 10 and 200 mV s^{-1}.

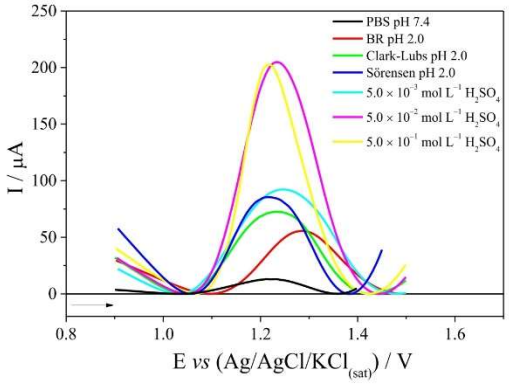

Figure 9. Square-wave voltammograms on different supporting electrolytes and pH values for 2.95×10^{-5} mol l^{-1} OFL using Zn_2SnO_4-rGO/GCE at $f = 100$ s^{-1}, $a = 50$ mV and $\Delta E_s = 2$ mV.

Nevertheless, the Zn_2SnO_4-rGO/GCE surface presented the lowest R_{ct} value (0.32 kΩ) of those that were evaluated, inferring that there was a relevant synergism between materials (Zn_2SnO_4 and rGO) and by such, the developed composite (Zn_2SnO_4-rGO) favored the charge transfer process at the electrode surface, with an equivalent circuit represented in Fig. 7B. It was also observed that although Nafion® contributes to physical aggregation of the composite materials (Zn_2SnO_4-rGO), it also promotes relative difficulty during the charge transfer process in the electrode surface ($K_4[Fe(CN)_6]/K_3[Fe(CN)_6]$) due to its sulfonate groups ($-SO_3^-$) present in its structure, generating electrostatic repulsion.[49]

Evaluation of the electrochemical behavior of OFL in GCE/Zn_2SnO_4-rGO through CV.—CV experiments were carried out to evaluate scan rate influence between 10 and 200 mV s^{-1} in the presence of 2.95×10^{-5} mol l^{-1} OFL in 5.0×10^{-1} mol l^{-1} H_2SO_4 using Zn_2SnO_4-rGO/GCE between 0.0 and 1.5 V. Its electrochemical behavior is shown in Fig. 8.

OFL voltammetric profiles clearly indicate that OFL suffered an oxidation process when using Zn_2SnO_4-rGO/GCE. Moreover, it can be noted that the reverse peak is absent and that the increase of the scan rate (ν) promoted both the enhancement of I_p values and the dislocating peak potential (E_p) towards more positive values, confirming the irreversible process for OFL in Zn_2SnO_4-rGO/GCE.[50–52] In addition, a discrete reversible process was noted in approximately 0.5 V. According to the literature, this fact can be attributed to oxide formations due to interactions between H_2SO_4 and carbonaceous materials, such as GC and rGO.[53–55]

A linear relation between I_p and the scan rate square root ($\nu^{1/2}$), as expressed in the equation: I_p (μA) $= -1.09 \times 10^{-5} \pm 4.24 \times 10^{-7} + 1.90 \times 10^{-4} \pm 1.45 \times 10^{-6} \nu^{1/2}$ (V s^{-1}) with r = 0.999, suggests that OFL oxidation process is primarily diffusion controlled.[56] Relation between log I_p and log ν was also established: log I_p (μA) $= -5.73 \pm 0.04 + 0.71 \pm 0.02$ log ν (mV s^{-1}) with r = 0.995. Since its angular coefficient is 0.71, it was concluded that the OFL oxidation process has mixed control (both diffusional and adsorptive), although its inclination points out that it is mostly controlled by diffusion (closer to 0.5).[56]

It was also estimated the number of electrons involved in OFL oxidation, through E_p and log ν relation, as expressed in the equation: E_p (V) $= 1.05 \pm 2.0 \times 10^{-3} + 0.07 \pm 1.0 \times 10^{-3}$ log ν (mV s^{-1}) with r = 0.996. For irreversible and anodic reactions, there's a linear relation between E_p and log ν, which has its inclination expressed in Eq. 4:[56]

$$\frac{\Delta E_p}{\Delta \log \nu} = \frac{2.303RT}{\alpha n F} \quad [4]$$

where R is the universal gas constant (J K^{-1} mol^{-1}), temperature is T (K), F is Faraday's constant (C), α is the electrons' transfer coefficient and n is the number of electrons transferred.

Through the line equation obtained, E_p (V) $= 1.05 \pm 2.0 \times 10^{-3} + 0.07 \pm 1.0 \times 10^{-3}$ log ν (mV s^{-1}) with r = 0.996, and its proper substitutions (8.314 J $K^{-1}$$mol^{-1}$, 298.15 K and 96,480 C mol^{-1}, αn was determined to be 0.86. For systems with organic molecules in aqueous medium, $\alpha = 0.5$[57] which concludes that the number of electrons involved in the rate- determining step is 2, as previously reported in the literature.[4,5]

Electrochemical behavior of OFL in modified electrodes, through SWV.— *Evaluation of OFL species distribution and optimization of the supporting electrolyte and pH.*—As previously seen (Fig. 1A), OFL protonation is dependent on the solvation medium pH and pKa values, which directly influences the number of species.[4,5] To understand better the behavior of the OFL species concentrations in the function of the pH, a species distribution study was carried out through the construction of a species distribution curve, calculated by acid-base equilibrium and mass balance, as seen in Fig. 1B.

As observed, three OFL species can exist in an aqueous medium. Protonated OFL species (OFL^+) are predominant in pH values below 2.0; neutral OFL species ($OFL^\pm$) are common in the 6.0 to 8.5 pH range; meanwhile, deprotonated OFL species (OFL^-) predominate in pH values above 10.0. The crossover point in their distribution curves ($\alpha' = 0.5$) happens when pH is equal to pKa, according to literature ($pKa_1 = 5.9$ and $pKa_2 = 8.2$).[4,5] It is fundamental to know the analyte species in the function of pH to correlate which pH condition favors the formation of chemical and electrostatic interactions at the modified electrode surface.[58]

Zn_2SnO_4-rGO promotes the formation of a negatively charged electrode surface due to the chemical structure of its components. Zn_2SnO_4 has neutral molecular structure;[12,47] rGO has in its basal structure epoxy (–COC–), hydroxyl (–OH) and carboxyl (–COOH) functional groups, which are charged negatively and provide excellent reaction sites to a protonated analyte (such as OFL^+);[17] Nafion® has sulfonate groups ($-SO_3^-$) in its structure, also negatively charged, and equally reactive to a protonated analyte.[49] With such analysis, it's been concluded that the composite-modified electrode surface (with the composite proposed in this work,

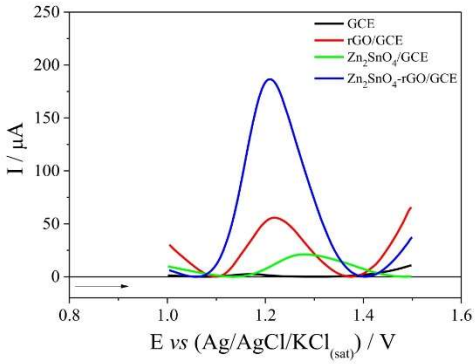

Figure 10. Square-wave voltammograms on different electrode surfaces for 2.39×10^{-5} mol l^{-1} OFL in 5.0×10^{-1} mol l^{-1} H_2SO_4 at $f = 100$ s^{-1}, $a = 50$ mV e $\Delta E_s = 2$ mV.

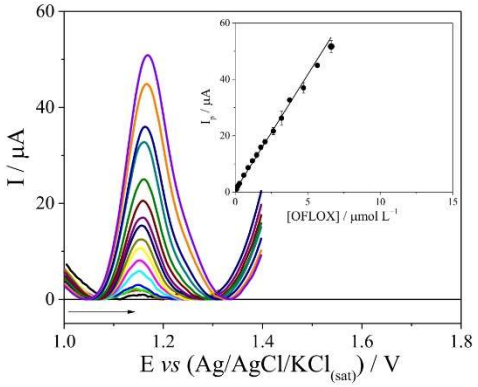

Figure 11. Square-wave voltammograms for OFL concentrations from 9.99×10^{-8} to 6.62×10^{-6} mol l^{-1} in 5.0×10^{-1} mol l^{-1} H_2SO_4 using Zn_2SnO_4-rGO/GCE at $f = 60$ s^{-1}, $a = 30$ mV, and $\Delta E_s = 3$ mV. The insert shows the mean calibration curve of three independent curves.

Zn_2SnO_4-rGO/GCE) has great electrostatic interaction with protonated species, such as OFL^+ in this work. These results corroborate with Liu et al.[58] concerning OFL oxidation under different pH conditions. According to Fig. 1B, supporting electrolyte and pH optimization studies were restricted to pH conditions below 2.0 because the preferred species (OFL^+) was primarily present. Based on the discussion above, the importance of understanding the relationship between the OFL speciation diagram and the electrostatic nature of the modified electrode surface can be seen, including theoretically evaluating the possible optimized pH conditions of the studied system.[58]

Due to the limited number of buffer solutions available in the determined range (0 to 2.0), it was chosen BR, Clark-Lubs and Sörensen buffers, 5.0×10^{-3} mol l^{-1} H_2SO_4; 5.0×10^{-2} mol l^{-1} H_2SO_4 and 5.0×10^{-1} mol l^{-1} H_2SO_4. To evaluate the proposed optimization procedure and verify the low electrochemical interaction between the composite-modified electrode surface (Zn_2SnO_4-rGO) and both the neutral and deprotonated analyte species ($OFL^{\pm}$ e OFL^-), pH 7.4 PBS was assessed to reproduce physiological medium. Supporting electrolyte and pH influence was evaluated through SWV, using 2.95×10^{-5} mol l^{-1} OFL in Zn_2SnO_4-rGO/GCE, using standard parameters $f = 100$ s^{-1}, $a = 50$ mV and $\Delta E_s = 2$ mV, as shown in Fig. 9.

At first, SWV experiments showed an OFL irreversible ($I_{di}/I_{rev} > 1$) oxidation process ($I_p > 0$) in all analyzed electrolytes in the 1.0 to 1.5 V potential range.[59] It was observed that the pH 7.4 PBS buffer solution was the least effective in OFL detection when using the Zn_2SnO_4-rGO/GCE sensor, confirming what was proposed based on the OFL species fraction distribution diagram (Fig. 1B) and in the general behavior of the composite components (Zn_2SnO_4, rGO and Nafion®). With the voltammetric profiles as a basis, both the supporting electrolyte and pH-optimized conditions were 5.0×10^{-1} mol l^{-1} H_2SO_4, having presented both higher sensitivity ($I_p = 2.29 \times 10^{-4}$ A) and selectivity ($\Delta E_{p/2} = 131$ mV) to OFL.

Evaluation of electrochemical synergism between modifying agents and optimization of the electrode surface cleaning process and SWV parameters.—Electrochemical synergism between the developed composite components (Zn_2SnO_4 and rGO) when used for OFL oxidation was evaluated using 2.39×10^{-5} mol l^{-1} OFL and optimized supporting electrolyte and pH (5.0×10^{-1} mol l^{-1} H_2SO_4) in the following conditions: bare GCE, rGO/GCE, Zn_2SnO_4/GCE and Zn_2SnO_4-rGO/GCE; through SWV at $f = 100$ s^{-1}, $a = 50$ mV and $\Delta E_s = 2$ mV (Fig. 10).

By Fig. 10, it was observed that all modifications were more effective than bare GCE. A clear chemical synergism between Zn_2SnO_4 and rGO when used to detect OFL was noted, as it amplified significantly the I_p signal, justifying Zn_2SnO_4-rGO as the optimized modification for this work.

Table II. Analytical parameters calculated from calibration curves for the determination of OFL at Zn_2SnO_4-rGO/GCE using SWV and HPLC.

Parameter	SWV	HPLC
Linearity range (mol l^{-1})	9.99×10^{-8} to 6.62×10^{-6}	3.19×10^{-6} to 2.21×10^{-4}
Intercept	6.49×10^{-7} A	11520 (u.a.)
Slope	8.21 A mol^{-1} l	8.43×10^{9} (u.a.) mol^{-1} l
Confidence interval of intercept	$\pm 6.48 \times 10^{-8}$	±210
Confidence interval of slope	$\pm 1.30 \times 10^{-1}$	$\pm 3.74 \times 10^{8}$
Correlation coefficient (R)	0.998	0.997
Standard deviation of intercept (S_a)	2.06×10^{-7} A	236 (u.a.)
Standard deviation of slope (S_b)	2.28×10^{-1} mol^{-1} l	9.07×10^{7}(u.a.) mol^{-1} l
LOD (mol l^{-1})	8.28×10^{-8}	8.65×10^{-8}
LOD (μg l^{-1})	29.92	31.26
LOQ (mol l^{-1})	2.76×10^{-7}	2.88×10^{-7}
LOQ (μg l^{-1})	99.63	104.09
% RSD Repeatability (n = 12)	3.20	—
% RSD Reproducibility (n = 7)	4.64	—

Table III. Analytical characteristics for determination of OFL applied electrochemical devices.

Electrode	Linearity range (μmol l^{-1})	LOD (μmol l^{-1})	Sensitivity (A mol^{-1} l)	Real sample	References
rGO/Pt-Au/GCE	0.08 to 100	0.05	2.40	Tablets and human urine	64
rGO/AuNPs/SH-βCD/GCE	0.01 to 10	0.008	0.28	Tablets and human urine	65
Ppy/HPMc/FP/GCE	2 to 100	0.065	0.076	Ophthalmic solution	66
Gr/pABSA/GCE	0.1 to 40	0.03	0.2425	Ophthalmic solution	67
Gr/ZnO/GCE	1 to 100	0.33	0.089	Tablets and saline solution	9
CA/CPE	0.06 to 10	0.02	0.80	Tablets and saline solution	68
/MWCNT/GCE	0.5 to 100	0.01	0.3064	Tablets, capsules and injection	69
IL-rGO/GCE	0.007 to 0.7	0.00028	7.70	Ophthalmic solution and human urine	70
Zn_2SnO_4-rGO/GCE	0.09 to 6.62	0.0828	8.21	Ophthalmic solution	This work

CA (Cystein acid); AuNPs (Gold nanoparticles); GCE (Glass carbono electrode); CPE (Carbon past electrode); Gr (Graphene); HPMc-FP (1-phenyl-3-methyl-4-(o-furoyl)-pyrazolone-5); IL (Ionic liquid); rGO (Reduced graphene oxide); pABSA (p-aminobenzene sulfonic acid); Ppy (Polypyrrole); Pt-Au (Platinum and gold); SH-β-CD (Beta-cyclodextrin); ZnO (Zinc oxide); Zn_2SnO_4 (Zinc stannate).

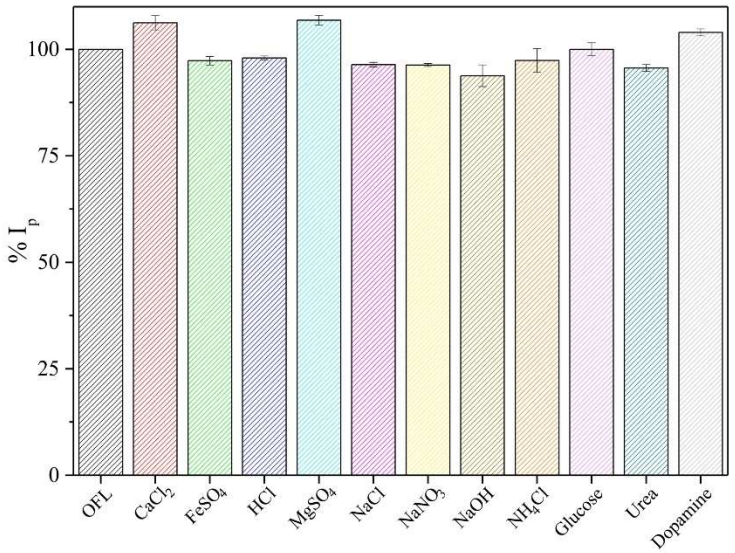

Figure 12. Effect of inorganic and organic species on the reduction signal of OFL in 5.0×10^{-1} mol l^{-1} H_2SO_4 on Zn_2SnO_4-rGO/GCE.

In sequence, an experimental cleaning procedure based on simple mechanical stirring of the solution containing OFL was tested, using 60, 120, 180 and 240 s as stirring times. The most effective sensor cleaning condition was 180 s, being chosen as the optimized procedure.

SWV optimization parameters were carried out at 2.95×10^{-5} mol l^{-1} OFL in 5.0×10^{-1} mol l^{-1} H_2SO_4, using Zn_2SnO_4-rGO/GCE. f, a and ΔE_s values were evaluated in 10 to 100 s^{-1}, 10 to 50 mV, and 1 to 5 mV ranges, respectively. Linear dependency between f and I_p values in the 10 to 60 s^{-1} was observed: I_p (μA) = $1.62 \times 10^{-5} \pm 2.45 \times 10^{-6} + 1.57 \times 10^{-6} \pm 6.28 \times 10^{-8}$ f (s^{-1}), with r = 0.992; it was also noted that I_p values were proportional to f increments, which confirmed through SWV the irreversible nature of the OFL oxidation process in the proposed system, which corroborates to the CV results obtained in this work.[50,60,61]

Frequency optimization study was also used to estimate the value of n, through the relation between E_p and log f, according to: E_p (V) = $1.01 \pm 4.0 \times 10^{-3} + 0.08 \pm 2.0 \times 10^{-3}$ log f (s^{-1}); with r = 0.995. For irreversible and anodic reactions, there is a linear relation between E_p and log f, following Eq. 5:[61,62]

$$\frac{\Delta E_p}{\Delta \log f} = \frac{2.303RT}{\alpha n F} \quad [5]$$

Substituting in the equation above inclination (0.08) and other values (R, T and F), it was estimated that n was equal to 2, corroborating with the previously reported.[4,5,61–63]

Values of a presented linear dependency with I_p from 10 up to 30 mV: I_p (μA) = $1.33 \times 10^{-5} \pm 8.64 \times 10^{-7} + 2.99 \times 10^{-6} \pm 4.65 \times 10^{-8}$ a (mV) with r = 0.999. The linearity range observed between I_p and a is in agreement with the SWV theory for the theoretical optimized amplitude determination in irreversible systems, which follows the 50/n ratio, where n is the number of electrons involved.[60–62] That way, the theoretical optimized amplitude value was equal to 25 mV, which was very close to the experimentally obtained value (30 mV).

ΔE_s values presented linearity with I_p from 1 up to 3 mV: I_p (μA) = $5.03 \times 10^{-5} \pm 1.78 \times 10^{-7} + 5.13 \times 10^{-5} \pm 1.27 \times 10^{-7}$ ΔE_s (mV) with r = 0.999. As such, for the developed electrochemical methodology, the optimized parameters were f = 60 s^{-1}, a = 30 mV and ΔE_s = 3 mV.

Analytical curves for OFL and evaluation of interferents.— After optimizing SWV values, OFL analytical curves were constructed using Zn_2SnO_4-rGO/GCE in 5.0×10^{-1} mol l^{-1} H_2SO_4 with f = 60 s^{-1}, a = 30 mV and ΔE_s = 3mV. Figure 11 shows the SWV voltammetric profiles obtained, with the insertion of an average analytical curve, including error bars.

Results show a linear relation between I_p and OFL concentration ([OFL]) from 9.99×10^{-8} up to 6.62×10^{-6} mol l^{-1}: I_p (μA) = $6.49 \times 10^{-7} \pm 6.48 \times 10^{-8} + 8.21 \pm 0.13$ [OFL] (μmol l^{-1}) with r = 0.998 and n = 16. Calculated values of LOD and LOQ were 8.28×10^{-8} and 2.76×10^{-7} mol^{-1} L, respectively; these values were inferior to those obtained through HPLC (Table II), evidencing a satisfactory sensitivity of the developed sensor.

The precision of the methodology was confirmed through intraday (repeatability; n = 12) and interday (reproducibility; n = 7), showing in both tests RSD lower than 5%, which demonstrated the efficiency and reliability of the proposed sensor being compared to other published articles, as seen in Table III.

Zn_2SnO_4-rGO/GCE showed that it was the most sensitive (8,21 A mol^{-1} L) among the sensors cataloged in Table III, presenting comparable and adequate characteristics for OFL detection. An interference study for OFL detection using Zn_2SnO_4-rGO/GCE was carried out adding various chemical species in fixed OFL quantities (Fig. 12) in the 100:1 ratio ([interferent]:[OFL]).

Results pointed that Fe^{2+}, Na^+, NH_4^+, H^+, SO_4^{2-}, NO_3^-, Cl^-, glucose, urea and dopamine species in 100 times higher concentrations than OFL exhibited interferences lower than ±5%. To compare the mean I_p obtained for each of the interferers with the mean I_p obtained for the system with only the OFL, the t-test was applied. For all the interferers evaluated, the $t_{calculated}$ was lower than $t_{critical}$ (4.30), indicating that none of them promoted a significant difference

Table IV. Recovery of OFL in commercial pharmaceutical formulation (n = 3), at different concentrations, through the Zn_2SnO_4-rGO/GCE, using SWV in the optimized parameters; f = 60 s^{-1}, a = 30 mV e ΔE_s = 3 mV.

		Zn_2SnO_4-rGO/GCE					
	$[OFL]_{added}$ (mol l^{-1})	2.99×10^{-7}	5.96×10^{-7}	1.19×10^{-6}	1.48×10^{-6}	2.92×10^{-6}	3.20×10^{-6}
	$[OFL]_{found}$ (mol l^{-1})	2.98×10^{-7}	6.26×10^{-7}	1.22×10^{-6}	1.46×10^{-6}	2.90×10^{-6}	3.13×10^{-6}
Ophthalmic solution	Confidence interval (mol l^{-1})	±1.12 × 10^{-7}	±4.07 × 10^{-7}	±8.59 × 10^{-7}	±7.71 × 10^{-7}	±1.37 × 10^{-7}	±3.46 × 10^{-7}
	Recovery (%)	99.74	104.91	102.77	98.88	99.18	98.03
	RSD (%)	0.89	2.54	1.49	1.63	0.81	0.53
	BIAS (%)	−0.26	4.91	2.78	−1.12	−0.82	−1.97

Table V. Recovery of OFL in commercial pharmaceutical formulation (n = 3), through SWV using Zn_2SnO_4-rGO/GCE and HPLC with UV-Vis detector.

		SWV	HPLC (UV-Vis)
Ophthalmic solution	$[OFL]_{added}$ (mol l^{-1})	3.19×10^{-6}	3.19×10^{-6}
	$[OFL]_{found}$ (mol l^{-1})	3.13×10^{-6}	3.17×10^{-6}
	Confidence interval (mol l^{-1})	$\pm 3.46 \times 10^{-7}$	$\pm 3.92 \times 10^{-7}$
	Recovery (%)	98.03	99.18
	RSD (%)	0.53	0.86
	BIAS (%)	−1.97	−0.81

at the 5% level (p-value > 0.05) in the OFL detection I_p, highlighting that the developed sensor (Zn_2SnO_4-rGO/GCE) has good anti-interference capacity.

Sensor application in commercial pharmaceutical formulation.—Zn_2SnO_4-rGO/GCE was applied in ophthalmic solution samples containing OFL. Recovery studies were performed through analysis of six different concentration points in triplicate, distributed in three concentration ranges (low, medium, and high) in the linearity range of the calibration curve,[24] meanwhile calculating REC%, RSD% and BIAS% (Table IV).[22,23]

The slopes of the lines obtained through linear regressions of the standard analytical curve and the analytical curve of the commercial pharmaceutical formulation (ophthalmic solution) were compared, considering the same [OFL] points in each of the conditions, presenting slope values equal to 8.21 ± 0.13 and 8.02 ± 0.08 A mol^{-1} L, respectively; making it possible to verify the parallelism between the lines.[20,24] To confirm this observation, the *F* and *t*-tests were used to evaluate a possible significant difference between the average slope values obtained for each of the curves. The $F_{calculated}$ (3.0) and $t_{calculated}$ (0.48) values found were lower than the $F_{critical}$ (19.0) and $t_{critical}$ (4.30) values, indicating that there was no significant difference (p-value > 0.05) between the slopes of the curves; and that, therefore, there was no occurrence of the matrix effect in the commercial pharmaceutical formulation samples.[20,24]

Using the International Conference for Harmonization (ICH) as a basis, it was possible to affirm that the proposed analytical method showed satisfactory REC%, with recovery percentages of 70 to 130%.[20] The %REC obtained is also within the tolerance limit (80% and 110%), in accordance with the standards of the Brazilian National Health Surveillance Agency (ANVISA-Brazil) for analyte recovery studies at the concentrations evaluated in this research.[24] The developed methodology presented $REC\%_{average} = 100.58\%$, while having high precision (average RSD% = 1.31%) and accuracy (BIAS% < ±5%) for OFL determination in ophthalmic solution, demonstrating high sensitivity and selectivity in a complex matrix. Thereafter, it was possible to conclude that the proposed procedure using Zn_2SnO_4-rGO/GCE is adequate to determine OFL in pharmaceutical formulation.

SWV results were compared to those obtained through HPLC coupled to a UV-Vis detector (Table V) to evaluate the efficiency of the proposed sensor, as suggested by the Brazilian Pharmacopoeia for OFL detection.[25]

Recovery results found in both methods (SWV and HPLC) were evaluated through the *F*-test. A result of $F_{calculated} = 1.96$ was obtained, below the theoretical value ($F_{critical} = 19.0$), indicating that there was no significant difference between the obtained results, and as such, the two methodologies do not differ in precision.

Conclusions

A novel sensor based on metallic ternary oxides (Zn_2SnO_4) allied with rGO was successfully developed for OFL determination. The good electrochemical performance of the modified electrode was attributed to the synergistic effects between Zn_2SnO_4/rGO. OFL on Zn_2SnO_4-rGO/GCE exhibited only an irreversible oxidation process involving two electrons; OFL protonated species were responsible for higher electroactivity and a typical mixed diffusion-adsorption controlled process. The newly developed electrochemical sensor showed analytical data with excellent wide linearity, sensitivity, accuracy, precision (repeatability and reproducibility) and anti-interference ability. The LOD and LOQ values obtained with the proposed sensor were lower than the data obtained by HPLC methods. In addition, the electroanalytical methodology developed was successfully applied for OFL determination in pharmaceutical formulation. Therefore, the sensor based on Zn_2SnO_4-rGO can be considered an excellent alternative tool to OFL analysis.

Acknowledgments

This study was financed in part by the Coordenação de Aperfeiçoamento de Pessoal de Nível Superior - Brasil (CAPES)—Finance Code 001 (PROEX 23038.000509/2020–82). The authors thank the financial support given by the following Brazilian funding agencies: Coordenação de Aperfeiçoamento de Pessoal de Nível Superior (CAPES), Conselho Nacional de Desenvolvimento Científico e Tecnológico (CNPq) and Fundação Cearense de Apoio ao Desenvolvimento Científico e Tecnológica (FUNCAP). P.B.A. Fechine thanks CNPq (proc. 308452/2022–4) and Funcap (proc. PNE-0112–00048.01.00/16). F.W.P. Ribeiro acknowledges the funding provided by FUNCAP-BPI (proc. BP5–0197–00017.01.00/22). P. de Lima-Neto thanks CNPq (proc. 302825/2022–3). D. S. Abreu thanks FINEP (CV. 01.22.0174.00 BIONANO SPR) and CNPq (proc. 407954/2022–8) for financial support. A.N. Correia gratefully acknowledges the funding provided by CNPq (proc. 305136/2018–6 and proc. 305103/2022–9). The authors would like to thank the Central Analítica-UFC/CT-INFRA/MCTI-SISANO/Pró-Equipamentos CAPES for their support.

ORCID

Adriana N. Correia https://orcid.org/0000-0002-3357-0160

References

1. IUPAC (ed.), International Union of Pure and Applied Chemistry (2023), https://iupac.org/what-we-do/nomenclature/ (accessed 04 May 2023).
2. P. G. Zanchetta, A. Pena, and R. F. Gonçalves, "Development and validation of an analytical method for the simultaneous quantification of ofloxacin, norfloxacin and ciprofloxacin in human urine." *Sanit. Environ. Eng.*, **20**, 307 (2015).
3. A. I. Drakopoulos and P. C. Ioannou, "Spectrofluorimetric study of the acid–base equilibria and complexation behavior of the fluoroquinolone antibiotics ofloxacin, norfloxacin, ciprofloxacin and pefloxacisn in aqueous solution." *Anal. Chim. Acta*, **354**, 197 (1997).
4. N. Davydov, R. Zairov, A. Mustafina, V. Syakayev, D. Tatarinov, V. Mironovet, and S. Ereminal, "Determination of fluoroquinolone antibiotics through the fluorescent response of Eu (III) based nanoparticles fabricated by layer-by-layer technique." *Anal. Chim. Acta*, **784**, 65 (2013).
5. D. G. Pinacho, F. Sanchez-Baeza, and M. P. Marco, "Molecular modeling assisted hapten design to produce broad selectivity antibodies for fluoroquinolone antibiotics." *Anal. Chem.*, **84**, 4527 (2015).
6. S. Erogul, S. Z. Bas, M. Ozmen, and S. Yildiz, "A new electrochemical sensor based on Fe_3O_4 functionalized graphene oxide–gold nanoparticle composite film for simultaneous determination of catechol and hydroquinone." *Electrochim. Acta*, **186**, 302 (2015).
7. X. Tian, L. Liu, Y. Li, C. Yang, Z. Zhou, Y. Nie, and Y. Wang, "Nonenzymatic electrochemical sensor based on CuO-TiO_2 for sensitive and selective detection of methyl parathion pesticide in ground water." *Sens. Actuators B Chem.*, **256**, 135 (2018).

8. T. Gan, Z. Shi, Y. Deng, J. Sun, and H. Wang, "Morphology-dependent electrochemical sensing properties of manganese dioxide-graphene oxide hybrid for guaiacol and vanillin." *Electrochim. Acta*, **147**, 157 (2014).
9. X. Si, Y. Wei, C. Wang, L. Li, and Y. Ding, "A sensitive electrochemical sensor for ofloxacin based on a graphene/zinc oxide composite film." *Anal. Methods*, **10**, 1961 (2018).
10. J. Xie, Y. Jiao, J. Xu, and H. Sun, "Synthesis of zinc stannate and zinc stannate coated nano-$CaCO_3$ by homogeneous precipitation." *J. Chem. Res.*, **35**, 109 (2011).
11. W. Song, J. Xie, S. Liu, G. Cao, T. Zhu, and X. Zhao, "Graphene-induced confined crystal growth of octahedral Zn_2SnO_4 and its improved Li-storage properties." *J. Mater. Res.*, **27**, 3096 (2012).
12. W. W. Coffeen, "Ceramic and dielectric properties of the stannates." *J. Am. Ceram. Soc.*, **36**, 207 (1953).
13. Z. V. Shomakhov, S. S. Nalimova, B. Z. Shurdumov, A. I. Maximov, and V. A. Moshnikov, "Zinc stannate nanostructures for fast response gas sensors." *Phys. Chem. Aspects ST.*, **14**, 726 (2022).
14. C. Akkapinyo, K. Subannajui, Y. Poo-Arporn, and R. P. Poo-Arporn, "Disposable electrochemical sensor for food colorants detection by reduced graphene oxide and methionine film modified screen printed carbon electrode." *Molecules.*, **26**, 2312 (2021).
15. G. Liu, Z. Xiong, L. Yang, H. Shi, D. Fang, M. Wang, P. Shao, and X. Luo, "Electrochemical approach toward reduced graphene oxide-based electrodes for environmental applications: a review." *Sci. Total Environ.*, **778**, 146301 (2021).
16. A. Razaq, F. Bibi, X. Zheng, R. Papadakis, S. H. M. Jafri, and H. Li, "Review on graphene, graphene oxide, reduced graphene oxide-based flexible composites: from fabrication to applications." *Materials.*, **15**, 1012 (2022).
17. G. Eda and M. Chhowalla, "Chemically derived graphene oxide: Towards large-area thin-film electronics and optoelectronics." *Adv. Mater.*, **22**, 2392 (2010).
18. C. Zhu, Y. Xu, Q. Chen, H. Zhao, B. Gao, and T. Zhang, "A flexible electrochemical biosensor based on functionalized poly (3,4-ethylenedioxythiophene) film to detect lactate in sweat of the human body." *J. Colloid Interface Sci.*, **617**, 454 (2022).
19. M. Wojdyr, "Fityk: a general-purpose peak fitting program." *J. Appl. Crystallogr.*, **43**, 1126 (2010).
20. European Medicines Agency, ICH Guideline Q2 (R2) on Validation of Analytical Procedures, (2022) https://pink.pharmaintelligence.informa.com/-/media/supporting-documents/pink-sheet/2022/04/p0422ema_21.pdf/ (accessed 01 May 2023).
21. J. N. Miller and J. C. Miller, *Statistics and Chemometrics for Analytical Chemistry* 4th ed. (Prentice Hall, England) (2005).
22. M. Thompson, S. L. R. Ellison, A. Fajgelj, P. Willetts, and R. Wood, "Harmonized guidelines for the use of recovery information in analytical measurement." *Pure Appl. Chem.*, **71**, 337 (1999).
23. E. Prichard and V. Barwick, *Quality Assurance in Analytical Chemistry* 1st ed. (Wiley, New York) (2007).
24. ANVISA, National Health Surveillance Agency, RCB nº 166/2017: Provides for the validation of analytical methods and other measures, Brasília, Brazil (2017), http://antigo.anvisa.gov.br/documents/10181/2721567/RDC_166_2017_COMP.pdf/d5fb92b3-6c6b-4130-8670-4e3263763401/ (accessed 14 March 2023).
25. ANVISA, *National Health Surveillance Agency* 6th ed.(Brazilian Pharmacopoeia, Brasilia, Brazil) (2019), https://gov.br/anvisa/pt-br/assuntos/farmacopeia/farmacopeia-brasileira/insumos-farmaceuticos-e-especialidades-ate-2a-errata-p-pdf-com-capa.pdf/ (accessed: 19 April 2023).
26. T. Luo, Q. Q. Meng, C. Gao, X. Y. Yu, Y. Jia, B. Sun, Z. Jin, Q. X. Li, J. H. Liu, and X. J. Huang, "Sub-20nm-Fe_3O_4 square and circular nanoplates: synthesis and facet-dependent magnetic and electrochemical properties." *ChemComm.*, **50**, 15952 (2014).
27. R. A. Young, P. E. Mackie, and R. B. Von Dreele, "Application of the pattern-fitting structure-refinement method of X-ray powder diffractometer patterns." *J. Appl. Crystallogr.*, **10**, 262 (1977).
28. R. A. Young, *The Rietveld Method* (Oxford University Press/IUCr, United States of American) 4th ed. (1996).
29. B. H. Toby, "EXPGUI, a graphical user interface for GSAS." *J. Appl. Crystallogr.*, **34**, 210 (2001).
30. A. C. Larson and R. B. Von Dreele, *General structure analysis system (GSAS), Los Alamos National Laboratory Report LAUR* (University of California, USA) p. 86 (2004).
31. H. M. Rietveld, "Line profiles of neutron powder-diffraction peaks for structure refinement." *Acta Crystallogr.*, **22**, 151 (1967).
32. S. S. Mali, C. S. Shim, and C. K. Hong, "Highly porous zinc stannate (Zn_2SnO_4) nanofibers scaffold photoelectrodes for efficient methyl ammonium halide perovskite solar cells." *Sci. Rep.*, **5**, 11424 (2015).
33. T. Jia, F. Fu, F. Long, Z. Min, J. Zhao, J. Chen, and J. Li, "Synthesis, characterization and enhanced visible-light photocatalytic activity of Zn_2SnO_4/C nanocomposites with truncated octahedron morphology." *Ceram. Int.*, **42**, 13893 (2016).
34. J. Dou and Q. Chen, "Zinc stannate nanostructures for energy conversion." *Chin. J. Chem.*, **39**, 367 (2021).
35. I. Rawal, "Facial synthesis of hexagonal metal oxide nanoparticles for low temperature ammonia gas sensing applications." *RSC Adv.*, **5**, 4135 (2015).
36. S. Wang, X. Peng, L. Tang, L. Zeng, and C. Lan, "Influence of inorganic admixtures on the 11 Å-tobermorite formation prepared from steel slags: XRD and FTIR analysis." *Constr. Build. Mater.*, **60**, 42 (2014).
37. M. V. Nikolić, T. Ivetić, D. L. Young, K. M. Paraskevopoulos, T. T. Zorba, V. Blagojević, P. M. Nikolić, D. Vasiljević-Radović, and M. M. Ristić, "Far infrared properties of bulk sintered and thin film Zn_2SnO_4." *Mater. Sci. Eng. B*, **138**, 7 (2007).
38. Y.-F. Wang, F.-F. Xin, Y.-R. Deng, D.-J. Li, and X.-F. Li, "Nano-Zn_2SnO_4/reduced graphene oxide composites for enhanced photocatalytic performance." *Mater. Chem. Phys.*, **254**, 123505 (2020).
39. X. Shen et al., "Phase transition of Zn_2SnO_4 nanowires under high pressure." *J. Appl. Phys.*, **106**, 113523 (2009).
40. F. Tuinstra and J. L. Koenig, "Raman spectrum of graphite." *J. Chem. Phys.*, **53**, 1126 (1970).
41. S. Claramunt, A. Varea, D. López-Díaz, M. M. Velázquez, A. Cornet, and A. Cirera, "The importance of interbands on the interpretation of the raman spectrum of graphene oxide." *J. Phys. Chem. C*, **119**, 10123 (2015).
42. R. Muzyka, S. Drewniak, T. Pustelny, M. Chrubasik, and G. Gryglewicz, "Characterization of graphite oxide and reduced graphene oxide obtained from different graphite precursors and oxidized by different methods using raman spectroscopy." *Materials (Basel).*, **11**, 1050 (2018).
43. D. López-Díaz, J. A. Delgado-Notario, V. Clericò, E. Diez, M. D. Merchán, and M. M. Velázquez, "Towards understanding the raman spectrum of graphene oxide: the effect of the chemical composition." *Coatings.*, **10**, 524 (2020).
44. S. S. Mali, C. Su Shim, and C. Kook Hong, "Highly porous zinc stannate (Zn_2SnO_4) nanofibers scaffold photoelectrodes for efficient methyl ammonium halide perovskite solar cells." *Sci. Rep.*, **5**, 11424 (2015).
45. K. Kosowska, P. Domalik-Pyzik, M. Nocuń, and J. Chłopek, "Chitosan and graphene oxide/reduced graphene oxide hybrid nanocomposites—evaluation of physicochemical properties." *Mater. Chem. Phys.*, **216**, 28 (2018).
46. A. Chlanda, E. Walejewska, K. Kowiorski, M. Heljak, W. Swieszkowski, and L. Lipińska, "Investigation into morphological and electromechanical surface properties of reduced-graphene-oxide-loaded composite fibers for bone tissue engineering applications: a comprehensive nanoscale study using atomic force microscopy approach." *Micron*, **146**, 103072 (2021).
47. D. C. Onwudiwe and O. A. Oyewo, "Facile synthesis and structural characterization of zinc stannate/tin oxide and zinc stannate/tin composites for the removal of methylene blue from water." *Mater. Res. Express*, **6**, 125025 (2019).
48. A. R. C. Bredar, A. L. Chown, A. R. Burton, and B. H. Farnum, "Electrochemical impedance spectroscopy of metal oxide electrodes for energy applications." *ACS Appl. Energy Mater.*, **3**, 66 (2020).
49. C. E. Perles, "Physicochemical properties related to the development of Nafion® membranes for application in fuel cells." *Polymers.*, **18**, 281 (2008).
50. A. J. Bard and L. R. Faulkner, *Electrochemical Methodos Fundamentals and Applications* 1st ed.(Wiley, New York) (2001).
51. R. Greff, R. Peat, L. M. Peter, D. Pletcher, and J. Robinson, *Instrumental Methods in Electrochemistry* (Wiley, New York) 1st ed. (1985).
52. R. A. Toledo, L. H. Mazo, M. C. Santos, K. M. Honório, A. B. F. Silva, and E. T. G. Cavalheiro, "Electrochemical and quantum-chemical study of the oxidation of the tricyclic antidepressant amitriptyline." *New J. Chem.*, **28**, 456 (2005).
53. R. L. Mccreery, "Advanced carbon electrode materials for molecular electrochemistry." *Chem. Rev.*, **108**, 2646 (2008).
54. J. X. Qiao, H. Q. Luo, and N. B. Li, "Electrochemical behavior of uric acid and epinephrine at an electrochemically activated glassy carbon electrode." *Colloids Surf. B*, **62**, 31 (2008).
55. Y. Yi, G. Weinberg, M. Prenzel, M. Greiner, S. Heumann, S. Becker, and R. Schlögl, "Electrochemical corrosion of a glassy carbon electrode." *Catal. Today*, **295**, 32 (2017).
56. D. K. Gosser Jr, *Cyclic voltammetry: simulation and analysis of reaction mechanisms* 1st ed. (UCH Publishers, New York) (1993).
57. J. Wang, *Analytical Electrochemistry* 2nd ed. (Wiley VCH, New York) (2001).
58. T. Liu, Q. Xue, J. B. Jia, F. Liu, S. Z. Zou, R. S. Tang, T. Chen, J. W. Li, and Y. M. Qian, "New insights into the effect of pH on the mechanism of ofloxacin electrochemical detection in aqueous solution." *Phys. Chem. Chem. Phys.*, **21**, 16282 (2019).
59. M. Lovric′, S. Komorsky-Lovric′, and R. W. Murray, "Theory of square-wave stripping voltammetry with adsorptive accumulation." *Electrochim. Acta*, **335**, 289 (1989).
60. A. Webber, M. Shah, and J. Osteryoung, "Electrochemical reduction and determination of cimetidine at nanomolar to micromolar levels of concentration." *Anal. Chim. Acta*, **154**, 105 (1983).
61. V. Mirceski, S. Komorsky-Lovric, and M. Lovric, *Square Wave Voltammetry Theory and Application* (Springer Science & Business Media, Republic of Macedonia) (2007).
62. D. D. Souza, S. A. S. Machado, and L. A. Avaca, "Square wave voltammetry. First part: theoretical aspects." *New J. Chem.*, **26**, 81 (2003).
63. F. W. P. Ribeiro, T. R. V. Soares, S. D. Oliveira, L. C. Melo, J. E. Soares, H. Becker, D. De Souza, P. de Lima-Neto, and A. N. Correia, "Analytical determination of nimesulide and ofloxacin in pharmaceutical preparations using square-wave voltammetry." *J. Anal. Chem.*, **69**, 62 (2014).
64. Z. M. Jiang, Q. Liu, Y. R. Tang, and M. X. Zhang, "Electrochemical sensor based on a novel Pt-Au bimetallic nanoclusters decorated on reduced graphene oxide for sensitive detection of ofloxacin." *Electroanalysis.*, **29**, 602 (2017).
65. Z. M. Jiang, G. Y. Li, and M. X. Zhang, "A novel electrochemical sensor based on SH-β-cyclodextrin functionalized gold nanoparticles/reduced-graphene oxide nanohybrids for ultrasensitive electrochemical sensing of acetaminophen and ofloxacin." *Int. J. Electrochem. Sci.*, **12**, 5157 (2017).
66. H. Han, J. Z. Li, and X. Z. Pang, "Electrochemical sensor using glassy carbon electrode modified with HPMoFP/Ppy/GCE composite film for determination of ofloxacin." *Int. J. Electrochem. Sci.*, **8**, 9060 (2013).

67. X. J. Si, C. Bai, X. Gong, J. T. Han, Z. C. Chen, and Y. P. Ding, "Detection of ofloxacin by differential pulse voltammetry in drugs based on a novel p-aminobenzene sulfonic acid/graphene." *Int. J. Electrochem. Sci.*, **15**, 8883 (2020).
68. F. F. Zhang, S. Q. Gu, Y. P. Ding, L. Li, and X. Liu, "Simultaneous determination of ofloxacin and gatifloxacin on cysteic acid modified electrode in the presence of sodium dodecyl benzene sulfonate." *Bioelectrochemistry.*, **89**, 42 (2013).
69. K. J. Huang, X. Liu, W. Z. Xie, and H. X. Yuan, "Voltammetric behavior of ofloxacin and its determination using a multi-walled carbon nanotubes-nafion film coated electrode." *Microchim. Acta*, **162**, 227 (2008).
70. A. Wong, T. A. Silva, F. C. Vicentini, and O. Fatibello-Filho, "Electrochemical sensor based on graphene oxide and ionic liquid for ofloxacin determination at nanomolar levels." *Talanta*, **161**, 333 (2016).

ANEXO B – MANUSCRITO 2

Chemical Papers

Theoretical insights from adsorption of ofloxacin using Zn2SnO4/reduced graphene oxide composite

--Manuscript Draft--

Manuscript Number:	
Full Title:	Theoretical insights from adsorption of ofloxacin using Zn2SnO4/reduced graphene oxide composite
Article Type:	Original Paper
Section/Category:	Biochemistry and Nanochemistry
Funding Information:	
Abstract:	Emerging Contaminants (ECs), such as pesticides, steroid hormones, antibiotics growth accelerators, and inhibitors of pathogenic microorganisms, among others, have become an increasingly severe and worrying problem to ecosystems and human health, including the contamination of water bodies. Therefore, it is imperative to seek ways to measure and evaluate the current conditions of various environmental matrices so that urgent strategies can be planned and designed to mitigate the spread of these contaminants. Ofloxacin, a widely prescribed antibiotic, is resistant to biological degradation and promotes bacteria resistance, being considered environmentally maleficent. In this sense, this work arises to theoretically study the adsorption of ofloxacin (OFL) on two surfaces (zinc stannate (Zn2SnO4) and reduced graphene oxide (rGO)), considering that OFL is classified as a toxic organic EC and, therefore, it is imperative to develop analytical methodologies for their removal. Furthermore, all theoretical calculations were carried out in the CASTEP software using Density Functional Theory (DFT) and the GGA functional, obtaining results for adsorption energy, band structure and Total Density of States (TDOS). The results showed that adsorption occurs more effectively with Zn2SnO4 (1 0 0), with an adsorption energy of -21.03 eV, compared to -1.90 eV in the rGO surface (1 0 0), and that the metallic character of this compound did not change after OFL adsorption. However, the OFL-Zn2SnO4 complex had more states to be occupied. Furthermore, it was observed that the OFL-rGO complex presented a greater semiconductor character.
Corresponding Author:	Norberto Monteiro Federal University of Ceara: Universidade Federal do Ceara BRAZIL
Corresponding Author Secondary Information:	
Corresponding Author's Institution:	Federal University of Ceara: Universidade Federal do Ceara
Corresponding Author's Secondary Institution:	
First Author:	Janevane S. de Castro
First Author Secondary Information:	
Order of Authors:	Janevane S. de Castro
	Renato V. de Oliveira
	Lucas L. Bezerra
	José O. de Souza-Júnior
	Anderson V. Chaves
	Pierre B. A. Fechine
	Pedro de Lima-Neto
	Adriana N. Correia

	Norberto Monteiro
Order of Authors Secondary Information:	
Author Comments:	On behalf of all the authors, we are very happy to publish our manuscript in your journal.
Suggested Reviewers:	Davi Vieira, * davi.vieira@ufrn.br This researcher has expertise in the area of theoretical chemistry.
	Hosiberto Batista hbs@ufc.br This researcher has expertise in the area of chemical catalysis.
	André Henrique andrehbo@ufc.br This researcher has expertise in the area of environmental chemistry.

CO

CHPA- Editorial Office <em@editorialmanager.com>
Para: Você

Ter, 14/11/2023 16:23

Re: "Theoretical insights from adsorption of ofloxacin using Zn2SnO4/reduced graphene oxide composite"
Full author list: Janevane S. de Castro; Renato V. de Oliveira; Lucas L. Bezerra; José O. de Souza-Júnior; Anderson V. Chaves; Pierre B. A. Fechine; Pedro de Lima-Neto; Adriana N. Correia; Norberto Monteiro

Dear de Castro,

We have received the submission entitled: "Theoretical insights from adsorption of ofloxacin using Zn2SnO4/reduced graphene oxide composite" for possible publication in Chemical Papers, and you are listed as one of the co-authors.

The manuscript has been submitted to the journal by Dr. Professor Norberto Monteiro who will be able to track the status of the paper through his/her login.
If you have any objections, please contact the editorial office as soon as possible. If we do not hear back from you, we will assume you agree with your co-authorship.

Thank you very much.

With kind regards,

Springer Journals Editorial Office
Chemical Papers